Perivascular Cell Differentiation in Tissue Remodeling and Fibrosis.

Riley Thomas Hannan

Charlottesville, VA

Bachelor of Science, Georgia Institute of Technology, 2014

A Dissertation presented to the Graduate Faculty of the University of Virginia in Candidacy for the Degree of Doctor of Philosophy

Department of Pathology

University of Virginia

May 2021

Acknowledgements

Over the course of my thesis work, many have poked fun at the hassle of scheduling meetings between two PIs and the sometimes excessively crowded joint lab meetings. They said, “It takes a village to graduate a Riley”.

This sentiment is completely, absolutely, irrefutably, unimpeachably true, and I wish to take some space here to acknowledge the many, many members of my village. From my immediate lab families, to other families in the village, to village elders, and even those from other towns far away who provide counsel and insight. Excuse the extended metaphor.

To my PIs, Dr. Shayn Peirce-Cottler and Dr. Thomas Barker: Thank you, truly, for allowing me to find my own path and discover a project that I could become personally invested in. It is a rare privilege to be given the autonomy afforded to me, and I have come to cherish the ownership and agency over my work product which you cultivated. I want to thank you for your patience and understanding as I have stumbled, and your kindness in helping me back up every time. I appreciate the opportunities to author and contribute to grants and publications, and know the quality and speed of my scientific writing has improved tremendously under your example. And lastly, thank you both for fully including me in both of your groups. None of my work would have been possible without a full commitment from both labs.

To the members of my thesis committee, thank you for your constant input and critique. I appreciate your willingness to reign in my often overambitious plans with a dose of kind pragmatism. Dr. Brant Isakson, Dr. Anjelica Gonzalez, Dr. Steven Caliari, and Dr. Janet Cross, my committee chair. Thank you all so much.

Dr. Cross, thank you for your constant guidance and wearing of multiple hats. An admissions counselor, an educator, my committee chair, and the head of my department and subsequently dean of my graduate program. You have worn all those hats and more, always with the goal of bettering student outcomes. Additional thanks to Dr. James Zimring, who has been kind and thoughtful while wearing a brand new hat. Thank you.

Many thanks to staff at the Flow Cytometry Core Facility, who brought me up from a flow novice to a fiend for high-dimensional flow cytometry. Thanks to Lesa Campbell, Mike Solga, Claude Chew, and Alex Wendling for constant suggestions, advice, problem solving, and always being wonderful, fun, and smiling.

To members of Barker and Peirce-Cottler labs, past and present. Thank you so much for your constant good humor, expert advice, and humoring of my (sometimes) scientific rants about microscopy. I have not once felt alone or unsupported thanks to you all. I will miss the lab outings and even the long lab meetings. Special thanks to Anthony Bruce for

never-ending patience and snarky good humor. Thanks to the many undergrads I have worked with over the years, especially Claire Hung and Catherine Sano.

In the greater graduate student community, thanks to my home department of Pathology for creating an intimate and welcoming research environment. I would like to thank my adoptive department of BME for welcoming me into the fold, even if I couldn't write a PDE solver.

I cannot possibly list all my wonderful friends and peers, but am so grateful and glad for all your company and support over the years. I would like to especially acknowledge Lee Talman, Katie Gorick, Stephanie Melchor, Leandro Moretti, Michaela Rikard, Julie Leonard-Duke, Pedro Costa-Pinheiro, Tori Osinski, and Jeremy Shaw for being gracious, kind, and supportive. To my more distant friends Derreck, Lily, Connor, Randal, Frank, Danielle, Caleb, Joel, Stephen, and everyone else – thank you for countless hours of games and fun.

I would like to take a step back and acknowledge several role models and educators. Justin Howell and DeAnn Peterson, my 9th and 11th grade biology teachers – thank you so much for your humanity and enthusiasm. I have nothing but fond memories and effusive praise for you and your teaching. To Dr. Shana Kerr, thank you for going above and beyond and allowing me to adopt you as my advisor, and providing guidance in my final years of undergrad. Dr. Ashley Brown – thank you for years of meaningful and enjoyable work and tutelage, I would not have discovered my abiding love for research without the opportunity you provided.

Thanks to my family for putting up with my long hours and uncertain timelines, and allowing me a place away from graduate school whenever I needed it. I couldn't do any of this without your support.

Thanks to my wonderful pup Nym, you are joy and kindness and curiosity molded into canine form, and you have made my life infinitely better. To Samy, you are what I look forward to most every day. You never fail to make me smile, even when I don't want to. I love you, and am so excited to see where our lives will go in the future.

This work was supported by The Hartwell Foundation, NIH R01HL127283 and U01AR069393, and the UVA Engineering in Medicine Seed Grant.

Abstract

Perivascular cells, or pericytes, are microvascular support cells which can be found in capillary beds in all tissues of the body. Pericytes are essential for vascular homeostasis, development, and wound healing. These cells maintain their local extracellular matrix (ECM) environment, ensuring the continuity of tissue form and thus tissue function. Given the right stimuli, pericytes can transdifferentiate into a variety of cell types both *in vitro* and *in vivo*, leading some to argue for their inclusion into a growing repertoire of stromal or mesenchymal stem cells. Several studies over the past decade have explored the possibility of perivascular contributions to myofibroblasts in fibrotic disease, but are limited by the difficulty in positively identifying a perivascular cell as it transitions from a quiescent to pro-fibrotic tissue remodeling phenotype.

Here we investigated the effector cells of fibrotic disease, the myofibroblast, and ascertain the degree to which pericytes participate in myofibroblastic behaviors in a murine model of pulmonary fibrosis. A novel application of a murine pericyte lineage model allowed for the thorough quantitation and characterization of pericyte-derived myofibroblasts. We observed significant, substantial increases in contractile and matrix-secreting phenotypes, as well as the upregulation of tissue-remodeling gene families. Further analysis reveals a possible integrin-mediated mechanism for perivascular activation through active αvβ3 heterodimer.

Exploration of pericyte response to bleomycin insult resulted in the discovery of several unique pericyte behaviors. A substantial population of pericytes express endothelial surface protein and mRNA, indicating a possible pericyte-endothelial transitional phenotype both in quiescent tissue and in tissue-remodeling disease. We also characterized the impact of stem cell factor KLF4 on perivascular cell transcript responses to lung injury, and found a large differential in expression profiles between KLF4 naïve and KLF4 knockout pericytes.

In total, this work represents advances in our ability to study the pulmonary pericyte through the novel application of the reporter mouse in the bleomycin disease model, and significant improvements in our understanding of the mechanisms by which pericytes interact with fibroproliferative injury models.

Table of Contents

List of Figures

List of Tables

Abbreviations

AEC – alveolar epithelial cell

ASC – adipose-derived stem cell

BP – biological process

CC – cellular component

Col1a1 – collagen type 1 alpha 1

cRAD – cyclic RAD peptide

cRGD – cyclic RGD peptide

DDR2 – discoidin domain receptor 2

DP – double positive pericyte

ECM – extracellular matrix

EMT – epithelial-to-mesenchymal transition

EndoMT – endothelial-to-mesenchymal transition

ES – enrichment score

FA – focal adhesion

FACS – fluorescence activated cell sorting

FGF – fibroblast growth factor

FMO – fluorescence-minus-one

FOX – forkhead box (gene group)

FSP1 – fibroblast-specific protein 1

FWER – family-wise error rate

GO – gene ontology

GSEA – GeneSet Enrichment Analysis

H&E – hematoxylin and eosin (histologic staining process)

IF – immunofluorescence / intermediate filament

ILD – interstitial lung disease

Il-1α - interleukin 1 alpha

Il-1β – interleukin 1 beta

IPF – idiopathic pulmonary fibrosis

LC-MS liquid chromatography-mass spectrometry

MF – molecular function

MFI – mean fluorescence intensity

MMP – matrix metalloproteinase

MRTF – myocardin-related transcription factor

MSC – mesenchymal stem/stromal cell

Myh11 – myosin heavy chain 11 or smooth muscle myosin heavy chain (synonyms)

NES – normalized enrichment score

NOM p-val – nominal p-value

PC – perivascular cell, pericyte

PDGF – platelet derived growth factor

PDGFR – platelet derived growth factor receptor

PECAM – platelet endothelial cell adhesion molecule

PFA – paraformaldehyde

RAD – arginine, alanine, aspartate (peptide)

RGD – arginine, glycine, aspartate (peptide)

RNA-seq – ribonucleic acid sequencing

SMC – smooth muscle cell

SRF – serum response factor

TGF-β– transforming growth factor beta

TNFα - tumor necrosis factor alpha

VEC – vascular endothelial cell

VEGF – vascular endothelial growth factor

VEGFR – vascular endothelial growth factor receptor

VSMC – vascular smooth muscle cell

αSMA – alpha smooth muscle actin

Chapter 1 General Introduction

Abstract

The lung is a highly specialized gas exchange structure which constantly faces insult due to its exposure to particulate and pathogen through respiration. A constant baseline of immune activation and regenerative healing must be maintained, and disruption of that balance can result in infection or fibrosis, with loss of respiratory function as a consequence. In this chapter we outline the structure of the alveolus, discuss the cellular populations therein, describe the current understanding of fibrotic disease etiology in the lung, and introduce models used to study the disease in a laboratory setting.

Physiology of the Alveolus

The lung is a beautiful example of tissue form being dictated by the physical requirements of function. Gas exchange systems all derive their structure from fundamental considerations of mass transfer. Minimizing linear distances to reduce series resistance, maximizing surface area for gas exchange, minimizing diffusion distance, and maximizing the differential in partial pressures between gas exchange media are all vital functional parameters that form the boundary conditions of respiratory organ design[1]. These considerations have selected for organs with massive numbers of parallel, tiny, and highly vascularized gas exchange units. In all mammals and most vertebrates (excepting birds and fish) this functional unit is the alveolus. Alveoli are remarkably consistent: alveolar diameter can vary by a factor of five between species[2] while lung volume can vary by seven orders of magnitude, or a factor of at least one million, between species [3,4].

Understanding the composition of this fundamental unit of respiration is vital to understanding its function in health and pathophysiology of dysfunction in disease.

The alveolar unit is typically described as four distinct components: alveolar epithelium, capillary endothelium, a shared thin basement membrane, and an interstitial or stromal region containing pericytes, fibroblasts, and a variety of other tissue-resident cells[5,6]. All these layers are exceptionally thin, with distances between atmosphere and erythrocytes in alveolar microcirculation as low as hundreds of nanometers.

Alveolar epithelium consists of Type I and Type II alveolar epithelial cells (AECs). Type I AECs are the more numerous of the two and maintain epithelial barrier function while minimizing the distance between alveolar airspace. Type I AECs are the primary cytokine producing cells in lung injury, activating immune and tissue remodeling processes. Type I AECs maintain fluid homeostasis on the epithelial surface and are equipped with a variety of channels and ion pumps to achieve this function[7]. This behavior from Type I AECs is one half of an essential balancing act with Type II AECs. Type II AECs cells prevent collapse of the alveolus by secreting a surfactant which lies on top of the water layer. This surfactant layer prevents the generation of large surface-tension forces, which is a phenomenon where water on wetted surfaces will minimize its surface area. This will cause collapse of the alveolar interior surface without surfactant, resulting in loss of function. Type II AECs also secrete immune factors into the surfactant, providing an antimicrobial function at the air interface. Type II AECs have been shown to self-renew and differentiate, and will generate *de novo* alveolar structures

when cultured in appropriate conditions [8]. Epithelial-to-mesenchymal transition (EMT) has been shown in both Type I and Type II AECs [7,8].

Physiology of Pulmonary Microcirculation

Each alveolus is supplied by the pulmonary, or lesser, circulation. The circulation facilitates gas exchange by providing constant deoxygenated blood to alveoli via the pulmonary artery. Successive branchings of the pulmonary artery form a capillary plexus, a dense and highly distensible network of microvessels, notable for its minimal vascular smooth muscle cell (VSMC) content relative to capillaries in systemic circulation and its highly branched morphology[9–11].

Capillary branching from pre-capillary arteries is highly heterogeneous, in contrast to the relatively ordered branching of the precapillary pulmonary artery tree. Capillaries can branch at right angles from parent arteries, small arteries immediately transition to capillary networks, and even large arteries (>100 micron in diameter) can dead-end into capillary networks[12,13]. The ratio of precapillary supply arteries to alveolar circulation is dependent on the size of the lung, with a positive coefficient of organ and organism volume. Ratios of artery:alveolus from humans, cats, and rats are 17-24, 4.1, and 0.3, respectively[14–16]. These ratios are necessarily related to the number of successive branches in the pulmonary arterial tree, which are measured a number of ways (Strahler, diameter modified Strahler, Weibel, and Horsfield). However, consensus across these methods is that the number of branches increases with organism mass [15,17–19].

Characterizing alveolar capillary network perfusion has been a difficult task; the network density and vessel distensibility in three dimensions leave some ambiguity in the direction and magnitude of perfusion in the network, and observations thereof are highly sensitive to the conditions of their acquisition. The two primary models used to describe alveolar capillary circulation are the interconnected sheet/post model, or the short tube model. The sheet-post model posits that the level of interconnectedness in the alveolar capillary network is so high, the individual vessel length so short, that alveoli can be approximated as 'posts' in a 'sheet' of perfused space which spans from precapillary arterial circulation to the postcapillary venular circulation [20]. In contrast, the short-tube model attempts to model highly branched and independent circulation in the alveolar capillary network via many short tubes. These two models have been debated since the 1970s[21,22], but slowly the short tube model has become the standard model, in no small part due to the available computational resources which obviate the need for the simplifications of the sheet-post model[10].

A capillary segment is comprised of sparse and thin squamous endothelial cells and surrounded by basement membrane, which encompasses some interstitial layer, which is finally bounded by the alveolar epithelium. Endothelial cells make many intercellular contacts between themselves and other interstitial cells, with tight junctions observed between vascular endothelial cells, pericytes, and interstitial fibroblasts[11]. These contacts allow for juxtacrine signaling between endothelial cells and their neighbors both within and across the basement membrane[23,24]. Basement membrane is a sheet of extracellular

matrix (ECM), a mesh network of fibrillar proteins which provides structural cues and physical organization to cells and tissues. Pulmonary basement membrane is exceptionally thin, and is often shared between the alveolar epithelium and capillary endothelium, while epithelial and endothelial basement membranes are not typically shared in other organs. Basement membranes are composed of roughly equal amounts of collagen IV and laminin, with smaller contributions from fibronectin and other proteoglycans [25,26]. Clinically, loss of pulmonary basement membrane is considered a hallmark of non-recoverable lung injury[27], as the interstitium defined by basement membrane has remodeled to the point of replacing healthy structure with fibroproliferative scar.

Lung Interstitial Cells

In addition to pulmonary epithelium and endothelium, several other cells exist in the interstitium which do not provide endothelial or epithelial barrier function. These stromal cells are defined as cells apart from apically/basally or lumenally organized cellular structures. Some stromal cells are sourced from circulation while other stromal cells are tissue resident and self-renewing. Fibroblasts, pericytes, and immune cells make up the majority of pulmonary stromal cells [28–30].

Pulmonary interstitial fibroblasts are found in thicker regions of interstitium: alveolar septal interfaces or junctions and in capillary branches. These cells have extensions which are thin and lie between the endothelial and epithelial cell layers. It is unknown if

these processes fully intercalate into basement membrane or exist in an independent interstitial space[13]. Resident fibroblasts maintain and remodel the extracellular matrix of the lung. Up to half of these cells contain lipid droplets, and are thought to interact with surfactant production of type II AECs[31]. Attempts to characterize these interstitial fibroblasts have shown they are highly heterogeneous and plastic, with lipofibroblasts and myofibroblasts being hallmark cells of healthy tissue and disease, respectively[32]. These fibroblasts derive from a variety of developmental lineages and maintain a diversity in phenotype as interstitial fibroblasts in adult lungs, as elucidated by single-cell RNA sequencing (scRNASeq) and transposase-accessible chromatin sequencing (ATACSeq) on human and murine models[33–39]. The specific mechanisms by which fibroblasts become pathologically activated and their behaviors will be elaborated on in Chapter 2 of this dissertation.

Perivascular cells, or pericytes, are a class of interstitial or stromal cells embedded within vascular basement membrane abluminal to capillary endothelium. Pericytes stabilize capillary vessels, regulating tone, permeability, and angiogenesis and neovascularization[40]. As proof-positive identification of pericytes relies on ultrastructural analysis of a shared basement membrane between pericytes and vascular basement membrane, most pericyte researchers instead use a combination of surface protein or gene expression, location, and morphology to define their perivascular population. None of these methods are perfect; there are no surface markers which perfectly separate pericytes from vascular smooth muscle cells (VSMCs) or other stromal cells, nor are

there morphologic or locational characteristics found in pericytes to the exclusion of all other endothelial-proximal cells. Indeed, it is becoming accepted that VSMCs and pericytes belong to the same developmental lineage of vascular mural cells. These compromise definitions are not standardized and there are large differences in how peer-reviewed pericyte literature defines pericytes[40–44].

Pericytes engage in bidirectional signaling with endothelial cells through various junctions, adhesion plaques, and paracrine signaling along platelet-derived growth factor (PDGF) and Ang-Tie2 axes, among others[42,44]. Pericytes additionally express toll-like receptors (TLRs) and are sentinels which can quickly respond to circulating or extracirculatory danger associated molecular patterns (DAMPs). Pericytes have been shown to facilitate the extravasation of circulating immune cells through the endothelial basement membrane[40]. Pericyte dropout or dysfunction are correlated with a variety of vascular pathologies outside the lung, including diabetic retinopathy and neuropathy, ischemic injury and scarring, and cancer metastasis. Within the lung, pericyte-mediated disease is less studied, but pericytes have been shown to control the metastatic microenvironment in cancer and participate in fibrotic disease[40,45,46]. Pericytes in these disease models demonstrate immense phenotypic plasticity, and fit criteria to be classified as stem cells. This plasticity will be discussed in Chapters 3 and 4 of this dissertation.

Finally, pulmonary immune cells provide a constant, active presence to facilitate both innate and adaptive immunities. T cells expressing T-cell antigen receptor (TCR) are

comprised of the thymic αβ and tissue-resident γδ cells, the latter of which are more commonly found in mucosa of the airways and may have a more conserved repertoire of antigen responsiveness[47–49]. It is thought that γδ T cells contribute to a more innate and immediate cytolytic immune response[49,50]. These cells modulate net T cell activity by balancing the balance between Th1 Th2 and Th17 polarization of T cells. Broadly, Th1 primes T cells for intracellular threats, Th2 primes cells for extracellular threats, and Th17 promotes tissue inflammation[51]. Th1, or type 1 responses, activate granulocytes and macrophages through their respective colony-stimulating factors. Th2, or Type 2 responses are associated with secretion of many interleukins (4, 5, 9, 10, and 13) which promote antigen presentation and adaptive immune response. Excessive Type 2 response is associated with fibrotic pathologies[29,52]. Lastly, Th17 polarization is characterized by secretion of interleukins 17, 6, and 22, as well as tumor necrosis factor alpha (TNFα), which in turn activate fibroblasts, macrophages, and endothelial and epithelial cells to secrete further cytokine. This cytokine release recruits granulocytes and results in tissue inflammation[51]. Beyond the antigen-dependent cytolytic T cells, NK and NK T cells respond to a lack of 'self' molecule class I MHC. This primes NK cells to respond to cell-hijacking viruses and some cancer cells. Additionally, NK cells respond to nucleic DAMPs via TLRs[53]. Immature dendritic cells await antigen in the airway epithelium and pulmonary vessels and proceed to lymph nodes for antigen presentation once activated by DAMPs or proinflammatory cytokine such as interferon alpha (IFN-α)[54]. These dendritic cells present antigen to naïve T cells, activating them, and begin the T cell polarization

process towards Th1, 2, or 17[55].The complexities of immune cell signaling and polarization continue to be studied and elaborated into increasingly nuanced relationships. Within this dissertation, we paint this immense and interconnected system with broad strokes, framing the immune response as a component of the myofibroblast activating, forward-feeding cycle of fibrotic disease.

Fibrotic Disease of the Lung

Fibrosis is defined as a pathologic accumulation or overproduction of ECM in tissues which results in stiffening, scarring, or other functionally deleterious changes in ECM properties. Fibrosis is thought to be initiated by repeated epithelial injury or insult, resulting in several processes which generate or recruit tissue-remodeling cells. Cell death, metabolic stress, epithelial-to-mesenchymal transition (EMT), latent transforming growth factor beta (TGFβ) activation, and immune responses all contribute to the pro-fibrotic milieu, which feeds forward into a self-perpetuating pathology. Many tissue-resident fibroblasts and stromal cells differentiate into myofibroblasts, the ECM remodeling, cytokine secreting effector cells of fibrotic disease[27,56,57]. An extensive review of myofibroblast biology will feature in the next chapter.

Fibrosis contributes to as much as 45% of all deaths in industrialized countries, and as such is the subject of intense study for pharmacologic intervention. Fibrotic pathologies of the lung are characterized by the fibrotic expansion of interstitial spaces and are termed interstitial lung diseases (ILDs). Collectively, ILD prevalence is roughly 75 cases

per 100,000 people in the United States. This umbrella includes sarcoidosis, connective tissue disorders, and idiopathic pulmonary fibrosis (IPF)[58]. IPF is a particularly relevant pathology for myofibroblast research, as its unknown etiology and fatal, progressive fibrosis focuses treatment efforts on controlling the fibrotic process. Out of dozens of clinical trials for all classes of therapeutics in the past three decades, there are only two FDA-approved treatments for IPF as of this writing, neither of which change long-term mortality rates of the disease [56,57].

This inability to meaningfully intervene in fibroproliferative pathologies has motivated the study of the fibrotic effector cell: the myofibroblast. While all cells in the alveolar niche are capable of some degree of myofibroblastic transdifferentiation, or an ability to adopt a tissue-remodeling phenotype, phenotypically plastic stromal populations contribute heavily to the activated myofibroblast population in various disease contexts[38,59–61] and behave as stem cells in healthy tissues[62,63]. Pericytes are one such plastic population which, in health, promote vascular homeostasis and angiogenesis in wound healing. In fibrotic diseases, pericytes have been shown to act as tissue-remodeling myofibroblasts[46,64,65].

Preclinical Models of Fibrosis

Animal models vary in their ability to recapitulate the physiology of human ILDs, especially IPF. Without understanding the initial mechanisms in the pathogenesis of IPF, models instead seek to recapitulate hallmarks of the human disease: progressive scarring

and expansion of the interstitial space by myofibroblasts. Dogs, cats, donkeys, and horses can spontaneously generate interstitial lung diseases. These diseases, associated with old age, are sometimes equated with human IPF due to homology in radiologic and histologic observations between human and animal[66]. As none of these models are inducible, they are rarely used for large, controlled studies and murine models comprise the near entirety of animal models for fibrosis research. Intratracheal bleomycin sulfate generates a patchy and initially robust fibrotic response thought to track with acute progressive phases of IPF in humans, but does not persist without repeat doses. Recent innovations, such as the addition of sphingosine analogue FTY720/Fingolimod to bleomycin result in a chronic and progressive fibrotic disease, which is thought to be a result of FTY720's disruption of vascular endothelial integrity during tissue remodeling and enhanced vascular permeability allowing for greater diffusion of bleomycin [67]. Silica, asbestos, fluorescent isothiocyanate (FITC), and radiation are all less commonly dosed into pulmonary tissue to generate fibrosis. Additionally, transgenic and viral vector-based murine systems to knock in or knock out specific cytokines or surface proteins exist and provide tools to answer discrete hypotheses, but are yet to be widely adopted in the field as standard models[66,68]. The American Thoracic Society recently held a workshop on preclinical animal models which reported: *"The consensus view is that use of the murine intratracheal bleomycin model in animals…is the best-characterized animal model available for preclinical testing."*[69].

Thus, single-dose intratracheal bleomycin is the murine model used for the animal experiments reported in this dissertation. At fourteen days post-bleomycin administration, an early inflammatory phase is resolved, and fibrotic remodeling is being potentiated by activated myofibroblasts[70]. It is this timepoint which is the most useful window for studying the activation and behavior of myofibroblasts which go on to generate scar, before they dedifferentiate into quiescence or apoptose[71,72].

Chapter 2 A Review of Fibroblast Biology and Heterogeneity

Publication Note

The text of this chapter has been adapted from Hannan RT, Peirce SM, Barker TH. Fibroblasts: Diverse Cells Critical to Biomaterials Integration. ACS Biomater Sci Eng. 2018;4(4):1223-1232. doi:10.1021/acsbiomaterials.7b00244

Abstract

Fibroblasts are key participants in wound healing and inflammation, and are capable of driving the progression of tissue repair to fully functional tissue or pathologic scar, or fibrosis, depending on the specific mechanical and biochemical cues with which they are presented. Thus, understanding and modulating the fibroblastic response to implanted materials is paramount to achieving desirable outcomes, such as long term implant function or tissue regeneration. However, fibroblasts are remarkably heterogeneous and can differ vastly in their contributions to regeneration and fibrosis. This heterogeneity exists between tissues and within tissues, down to the level of individual cells. This review will discuss the role of fibroblasts, the pitfalls of describing them as a collective, the specifics of their function, and potential future directions to better understand and organize their highly variable biology.

Wound healing response in biomaterials

The body's response to foreign material can be described as a modified process of wound healing. Insofar as the regenerative response is concerned, an implanted material is often treated as a chronic wound, with expectably deleterious consequences. A large focus of biomaterials science aims to develop strategies for integrating the material with the host, while avoiding the scarring and fibrotic response generated by recruited fibroblasts during wound healing.

The canonical process of wound healing is characterized by four progressing phases of hemostasis, inflammation, proliferation, and remodeling, as described in Figure 1. In the realm of biomaterials, this is collectively given the term, “foreign body response”. The process is a delicate orchestration of signaling by numerous cell types along a myriad of axes. Immune cells, platelets, endothelial and associated perivascular cells, epithelium and fibroblasts must all participate in the appropriate spatial and temporal arrangement to restore functional tissue and integrate with the material. An overloading, or imbalance, of these factors can cascade into fibrotic tissue. When a remodeling fibroblast, known as a myofibroblast, continues to receive activation cues long after it is no longer needed, or experiences epigenetic alterations that inhibit its normal programmed apoptosis or dedifferentiation, the result is fibrosis and loss of function of both host tissue and implant.

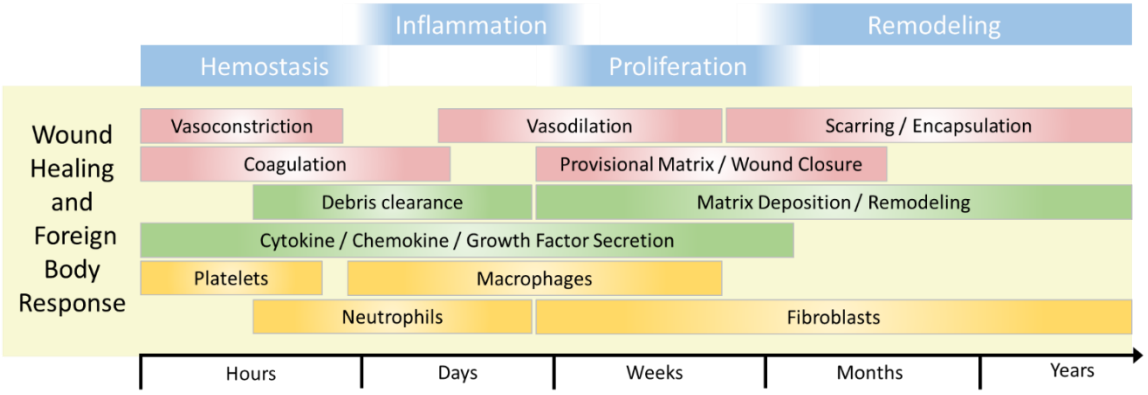

Figure 2.1: A timeline of wound healing and the foreign body response broken into stages progressing from the initial response to the years beyond. Red*: gross-scale tissue phenomena;* green*: cellular activity;* gold*: prominent cells.*

Disruption of vascular endothelial integrity begins the hemostasis phase. Exposed matrix and pooling vascular contents activate blood platelets, which begin to form a plug of rapidly polymerizing fibrin at the wound site. These activated platelets and mechanically deformed extracellular matrix (ECM) recruit inflammatory cells[73] and effect vasoconstriction[74,75]. The fibrin-platelet plug, referred to in matrix biology as the "early provisional matrix", leads to the cessation of bloodletting and maintains hemostasis. Concurrent with the resolution of the hemostatic phase is the inflammatory phase. This phase is characterized by massive cellular recruitment initiated by active platelets that release their contents from α-granules, damaged cells, and activation of the immune complement system[75].

Inflammatory cells include a variety of monocytes and neutrophils, which clear debris and invading pathogens. Monocytes also secrete a large variety of cytokines which activate fibroblasts. Interleukin 1 beta (IL-1β), platelet-derived growth factor (PDGF) transforming growth factor beta (TGF-β), vascular endothelial growth factor (VEGF), and others are released and propagate further recruitment, clearance, and remodeling[76,77]. This deluge of molecules activates both the canonical interstitial fibroblast as well as other fibroblast progenitors we will discuss below, and begins the 'repair' phase of wound healing. This effect is especially pronounced in the foreign body response, where macrophages condense into multinucleated giant cells, in an attempt to encircle, isolate, and destroy the foreign body. This mass accumulation of activated immune cells increases the levels of subsequent fibroblast recruitment [78]. Directing inflammation

toward pro-repair phenotypes and away from pro-inflammatory phenotypes remains a key scientific focus in biomaterials research, yet complete elimination of inflammation is not productive[78–80]. For example, an interesting consequence of the burst of pro-inflammatory cytokines from macrophages and neutrophils is the transient "activation" of resident, quiescent fibroblasts through shedding of Thy-1 from their cell surface[81]. The role of Thy-1 in fibroblast biology will be expanded later.

The proliferation (or repair) phase of wound healing is characterized by wound contraction, deposition of ECM, angiogenesis, and re-epithelialization where relevant. Recruited fibroblasts stimulated with key growth factors, such as TGF-β, undergo a necessary transition to an activated myofibroblast (named for their expression of certain muscle proteins including α smooth muscle actin or αSMA) and deposit the so-called "late provisional matrix", which provides a scaffold upon which revascularization and epithelialization occur. This late provisional matrix is rich in fibronectin[82] and serves as the template for more permanent ECM comprised of collagens[83]. Fibroblasts and other adherent cells migrate across and mechanically interact with fibronectin and other proteoglycans in the wound via integrins, which facilitate cellular interactions with ECM and are elaborated below. Fibroblasts preferentially deposit collagen I matrix as repair progresses[84].

Over the course of weeks to years, the processes of epithelization and angiogenesis conclude, but fibroblasts remain in the healed wound. The late provisional matrix, comprised primarily of fibronectin, is converted into a mature matrix comprised of

collagen III-rich ECM and is then slowly replaced during remodeling with collagen I. Collagen I comprises 80% of adult dermal collagen and is the most abundant molecular component of mature epithelial matrix[84]. A balance of degradation via matrix metalloproteinases (MMPs) and deposition of new collagen is required for healthy maturation of tissue and the avoidance of excessive scarring, characteristic of collagen I-rich ECM[85]. As the collagen turns over, the tensile strength of the regenerated dermis increases from 40% up to 70% of uninjured tissue[86]. The myofibroblasts in the healed tissue are meant to eventually reach an equilibrium with their local ECM, and will undergo apoptosis or dedifferentiate into a quiescent cell, as the net change in tissue composition trends towards zero[87].

In the context of an implanted device, the development of thick, acellular ECM around the implant site is a strong indicator of poor biomaterial integration with the host. This ‘terminal’ stage of biomaterial integration is characterized by a fibrotic capsule, which isolates implanted material from host tissue, save in certain contexts wherein it is desirable for the implant to become anchored and isolated, such as in implant-based breast reconstruction[78].

This fibrosis is not unique to implanted biomaterials; pathologic fibrosis is defined as an excessive, deleterious deposition of ECM, and is found wherever fibroblasts become ‘overenthusiastic’ remodelers and when myofibroblasts, the primary wound repair cell, are unable to undergo timely apoptosis or otherwise become inactive.

Biomaterial-associated fibrosis is similar to physiologic fibrosis in that the final 'scar' is a highly fibrous and acellular matrix composed of a collagen I/III ratio that characterizes physiologic fibrosis[88]. There is little comparative research on the two types of scar, which leaves an opening for both sides to collaborate using deliberately engineered biomaterial and pathologic contexts to explore and learn from unique yet congruent expertise. The exact progression that drives fibroblasts into a fibrotic state is unknown; multivariable systems such as these are difficult to tackle wholly. But we now know many ways by which the fibroblast is driven to a pro-fibrotic phenotype. Fibroblast reciprocity in signaling between the cell and its local chemo-mechanical environment can result in dangerous and pathologic signaling loops. Fibroblasts respond to cytokines released from immune cells and damaged tissue, including the interleukins, latent TGF-β and PDGF-β, by increasing α-SMA expression, focal adhesion (FA) assembly, internal contractility and synthesis of matrix proteins. The increase in contractile machinery and cell-matrix contact allows for more force to be generated on the matrix. The increased strain on local ECM releases further latent TGF-β, in addition to TGF-β being secreted by the fibroblast itself, and the activation can continue in a devastating positive feedback loop, which in concert with other factors, drives excessive deposition of ECM[89–92]. This alters the mechanical attributes of the tissue with consequences ranging from minor to fatal[93,94]. For a biomaterial, this fibrosis prevents the material from properly integrating into the host, which will at best negate any intended benefit in materials not designed to take advantage of this phenomena. In this way, fibroblasts are the final arbiter of success or failure in

biomaterial-host integration and understanding their biology and pathology is essential for biomaterials science.

This stiffness sensing is driving the biomaterials field away from stiff, smooth materials. Implants with textured or irregular topology[95], hydrogel or other soft materials[96], and displaying endogenous ECM epitopes[96–98] produce less severe fibrotic responses and integrate more thoroughly with tissue.

One thread of research dissecting the progression of fibrosis revolves around the outer leaflet glycoprotein Thy-1, introduced earlier. Thy-1 (also known as CD90), often used as a marker for mesenchymal stem cells, is a GPI-linked cell-surface protein found in a subset of fibroblasts. It was originally noted to differentiate fibroblast sensitivity towards PDGF-AA over PDGF-BB[99] and is found in an inverse proportion to myofibroblast markers[81,100]. The involvement of Thy-1 in fibroblast mechanobiology has since expanded and it is now considered a major factor driving fibrosis. It is thought to differentiate environmentally responsive fibroblasts from non-responsive cells through its involvement in integrin-mediated mechanotransduction[101]. Thy-1$^-$ cells are apoptotically resistant, and are found in fibrotic foci in diseased tissue, which are areas of active fibroblast proliferation and fibrosis[81,101–103]. The heterogeneity of Thy-1 expression in the fibrosing lung is caused by epigenetic silencing[102,104]. Thy-1 may also play a critical role in the necessary transient activation of fibroblasts at the initial stages of would repair. Specifically, inflammatory cytokines such as IL-1β and tumor necrosis factor α (TNFα) are known to induce a transient shedding of Thy-1 from the fibroblast surface through

exosomal shedding. This event results in only a short term loss of Thy-1, as opposed to its epigenetic silencing in fibrotic disorders, and could represent a mechanism linking inflammation to the triggering of fibroblast recruitment to the wound[81].

As fibroblasts determine the final outcome of implanted biomaterials, they must be a priority consideration in biomaterial development. Designing around this constant hazard requires understanding fibroblast function, their origins, and their heterogeneity.

What is a fibroblast?

The fibroblast in literature is a seemingly amorphous cell type, meeting a variety of indicative criteria. The most prevalent definition of a fibroblast is on based on in situ morphology. These fibroblasts are interstitial cells with ECM contacts. They are characteristically spindle-shaped with cellular processes extending from each tip [105], and are easily isolated in culture via several passages of most tissues on plastic. This definition is simple and workable, with an easily identifiable in situ phenotype and a no-questions-asked system for cell culture.

However, fibroblasts by this definition exhibit high degrees of heterogeneity in expression and phenotype between tissues [100,106,107] and even within the same tissue [100,108]. Collagen I, intermediate filament (IF) proteins, discoidin domain receptor 2 (DDR2), platelet-derived growth factor receptors (PDGFR-α and β), Fibroblast growth factors (FGF10), periostin, transcription factor 21 (Tcf21), Thy-1; the list of nonspecific

fibroblast markers is long. Many of these markers are expressed only transiently, or exclusively in the quiescent (or fibrotic) context.

Because of the remarkably heterogeneous nature of the fibroblast, there have been recent, directed efforts to find a universal, fibroblast-specific marker. Those efforts have met with difficulty, such as with fibroblast-specific protein 1 (FSP1). It labels interstitial fibroblasts in studies of renal [109] and pulmonary [110] tissues, and shows some involvement in late developmental epithelial to mesenchymal transition (EMT) [111], the putative source for most adult quiescent fibroblasts [112]. However, FSP1 in recent years has garnered controversy after being found in a variety of other cell contexts, including inflammatory macrophages [113] and vascular smooth muscle cells [114], among others [115,116].

There are many other endogenous and engineered targets used to identify putative fibroblasts, all of which have their caveats. See the review from Tallquist [117] for a more thorough exploration of genetic fibroblast-tracking tools and their controversies. The struggle to find a consistent fibroblast marker is summarized in her review in Table 2.

It is important to question the contributions of fibroblast heterogeneities at various scales. Understanding why one fibroblast displays one surface protein while another does not provides insight into basic biology, development, and contributions fibroblasts have towards both quiescent tissue health and pathologic fibrosis, including in response to biomaterials (and how those states differ between tissues).

For example, Thy-1, in addition to its biologic role in the progression of fibrosis, is an excellent example of the highly heterogeneous nature of a classically defined fibroblast. As discussed above, fibroblasts are Thy-1^+ and Thy-1^-, with demonstrated phenotypic differences known between the subtypes: proliferation, apoptosis, response to growth factors, mechanotransduction, ECM synthesis, etc. However, further heterogeneity also exists *within* the Thy-1^+ fibroblast population, as measured by liquid chromatography-mass spectrometry (LC-MS). Analysis of nuclear, cytoplasmic, and secreted protein fractions, gathered from quiescent primary, activated primary, and cancer-associated primary fibroblasts, showed extensive variability in expression. Thy-1 was just one of many proteins found to demonstrate differential expression profiles between tissues. Dermal fibroblasts expressed PDGFR-β in every tissue examined, as did myeloma-associated fibroblasts, while the remaining tissues showed inconsistent fibroblast PDGFR-β expression. Similar diversity was found with MMP-1, proteoglycan 4, EGFR pathway components, fibrillin, and CTGF, among others. An additional interesting finding was that the density of procollagens, Thy-1, and other peptides in nuclear, cytoplasmic, and secreted fractions varied based on tissue origin [100].

Moreover, even within a single tissue there exists additional sources of heterogeneity between fibroblasts. As an example, dermal fibroblast cDNA can be binned into discrete, local tissue-specific clusters of expression. This coordination is found across multiple gene genres: ECM synthesis (fibronectin and fibrillin), growth factors including those involved in TGF-β and Wnt β-catenin signaling, migration, lipid metabolism, and

developmental/differentiation genes. Forkhead box genes, as well as the hox family, correspond to topographic distribution of dermal interstitial fibroblasts [108]. This topographic tissue heterogeneity can be resolved into a minimum of three anatomic divisions (anterior-posterior, proximal-distal, and dermal-nondermal) based on gene expression patterns [118]. Further research into the differential expression elucidated the epigenetic mechanisms (in scalp and dura mater) which consist of persistent site and age-specific epigenetic 'memories' of individual fibroblasts [119]. This vertical slice of heterogeneity through pan-tissue markers, between tissues, and within tissues has been seen consistently through decades of fibroblasts research and remains generally unaddressed, frustrating attempts to paint fibroblasts with a single, broad brush.

In the context of wound healing there is yet another example of heterogeneity in the fetal fibroblast. It is noted that fetal wounds rarely scar [120]. The drivers of this regenerative phenotype, and its potential applications in the realms of inflammation and wound healing, are only just now being explored.

Somewhat paradoxically, fetal fibroblasts display a constant α-SMA^{+} phenotype that does not change in response to any TGF-β isoform [121,122], in contrast to adult fibroblasts which differentiate from quiescent α-SMA^{-} to myofibroblastic α-SMA^{+} cells upon treatment with TGF-β. Additionally, fetal and adult fibroblasts develop a diverging integrin composition when treated with TGF-β [122].

Fetal fibroblasts have been shown to be efficacious when used as a transplant in tendon repair, demonstrating a reduced capacity for unwanted ossification of the regenerating tendon [121]. Expression analyses show these fetal fibroblasts have an increase in myofibroblastic markers and a decrease in inflammatory and osteogenic expression relative to adult fibroblasts [121]. Fetal fibroblasts additionally secrete more collagen I and III than their adult counterparts and have a larger surface area [123].

Few steps have been undertaken to understand the nature of a fetal fibroblast. We do not know, for example, if these fibroblasts are positive for popular markers such as FSP1, or if they are derived from a common developmental lineage. It is possible these cells differentiate into less regenerative adult fibroblasts, or that they constitute a separate fibroblast family that dies out as development progresses. The efficacy of these fibroblasts in other healing contexts is unknown, but their seeming reluctance to participate in inflammation should make them attractive for biomaterials scientists. Therapeutic application and basic research of these fibroblasts will provide further insight into fibroblast heterogeneity and their potential utility in wound healing and biomaterial integration.

Acknowledging these heterogeneities in fibroblast populations can be uncomfortable; therefore, a popular approach within the biomaterial community has been to use immortalized cell lines of fibroblasts, including 3T3 and HFF cells. If we accept that the population of fibroblasts is heterogeneous within and between tissues, we are making a risky assumption about the applicability of conclusions generated from culture

experiments as they pertain to fibroblast biology writ large. Cells selected using the markers above may exclude a large portion of the phenotypically diverse fibroblast population, and these heterogeneities have stymied most attempts at settling on a robust molecular or genetic definition of the cell. Passable indicators have been found and are in widespread use, such as FSP1, but use of such markers requires understanding of their specific use cases.

Perhaps, then, the simple and easily-culturable definition for a fibroblast is not specific enough. Given the difficulty in isolating any truly unique molecular signature across tissues and disease contexts, do we need to revisit our definition of what constitutes a fibroblast? Asking this question is essential if we hope to engineer biomaterials that have the goal of accounting for and/or manipulating fibroblast behaviors. The prerogative of biomaterials scientists is to control the cues received by fibroblasts and limit damaging inflammatory and scarring responses. In the pursuit of this goal, the field has developed an armamentarium of materials and techniques to drive phenotype in the implanted context. An immense opportunity exists for these same techniques to be applied to help distinguish, delineate, and define fibroblast identity.

Alternative Definitions

Alternative approaches to defining the fibroblast use categorization **by remodeling potential** or by **cellular or developmental lineage**

Remodeling potential

Myofibroblasts are identified *in vitro* and *in vivo* by the presence of α-SMA stress fibers and a contractile, secretory, and TGF-β/PDGF sensitive phenotype [107,124–126]. These cells are derived from a bevy of progenitor lines, many outside the traditional interstitial fibroblast lineage. Perivascular cells (pericytes) [46,90,127], endothelial [128] and epithelial [129,130] cells, as well as the circulating bone marrow derived fibrocyte [130–134] all contribute towards fibroblast populations in inflammatory contexts, illustrated in Figure 2. These cells, while more difficult to isolate, respond to many of the same cues as the traditionally-defined fibroblast.

The prevailing hypothesis in the field is that a myofibroblast is a terminally differentiated cell which undergoes apoptosis upon resolution of inflammation, but isolated studies dispute this claim. It has been shown that nuclear factor erythroid 2-related factor 2 (Nrf2) is protective against pulmonary fibrosis [135–137]. Expression of Nrf2 is depressed in pulmonary myofibroblasts relative to quiescent fibroblasts in the contexts of bleomycin-induced IPF or TGF-β/PDGF-BB treatment. Exogenous knockdown of Nrf2 drives a myofibroblast transition from lung fibroblasts *in vitro*. Interestingly, knocking *in* Nrf2 translocation into the nucleus via knockdown of inhibitor Kelch-like erythroid cell-derived protein CNC homology-associated protein 1 (Keap1) causes myofibroblasts to de-differentiate as measured by reduced α-SMA and collagen production [138]. Further examination of the mechanisms by which a myofibroblast becomes phenotypically ‘unstuck’ is ongoing and includes factors such as MyoD and prostaglandin E_2 [71,72]. This emerging body of evidence challenges the long-held assumption that myofibroblasts die

and are cleared upon resolution of the wound healing response, and may simply be dedifferentiating into cells which are not myofibroblastic.

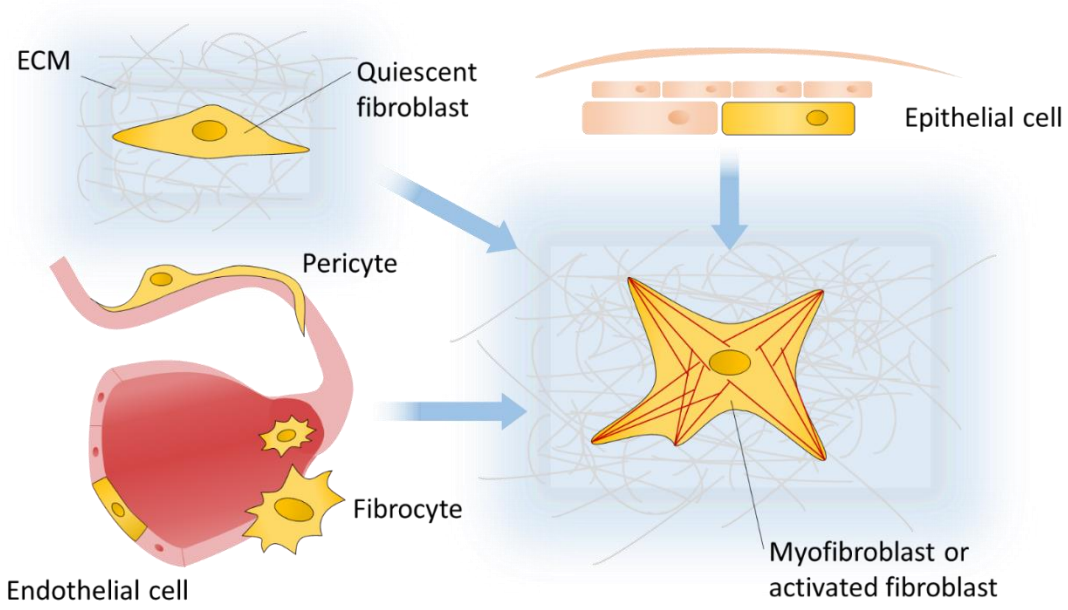

Figure 2.2: The range of cells which have been experimentally shown to become involved in fibrotic disease. Epithelial cells, tissue resident quiescent fibroblasts, microvasculature-associated pericytes, vascular endothelial cells, and circulating bone marrow derived fibrocytes can all differentiate into myofibroblasts and contribute towards fibrosis.

This consistency of remodeling potential is a strong contender for defining a fibroblast. It is not wholly unlike the current definition in that it relies upon a consistent phenotype, but is superior in that it does not exclude cells based on extrinsic factors such as the

difficulty of isolation and culturing. However, there are still problems with specificity in this definition. Components of the myofibroblast phenotype are not exclusive to those cells. For example, many cell types remodel the extracellular matrix; osteoblasts [139], astrocytes [140], vascular endothelium [141], macrophages [142] and pericytes [64,143] remodel ECM via MMP expression and/or matrix secretion. Perhaps these cells could also be classified as fibroblasts. Phenotypic behavior could be further clarified by a cell's ability to remodel various biomaterials.

Cellular or developmental lineage

The initial population of interstitial fibroblasts is generated during gestation and these fibroblasts maintain an epigenetic 'memory' of their origin even after multiple passages [81,102,119]. This memory has only been shown in the tissue resident fibroblast, but a similarly distinct epigenetic signature is entirely plausible for the more mobile fibroblasts/fibroblast progenitors discussed previously. This nascent field of fibroblast epigenomics could prove useful in identifying fibroblast subpopulations alone or in conjunction with more traditional systems of expression analysis.

Recent developments in lineage tracing have enabled the study of fibroblast and myofibroblast generation in specific tissues [46,127,132,144,145], but few comprehensive studies exist investigating the differences between fibroblast sources. Given the heterogeneity in

expression and phenotype described above, it follows that fibroblasts from two separate organ systems have a distinct lineage.

As it stands, the heterogeneous and tissue-specific definitions used across tissues and fields make comparisons between putative ‘fibroblasts’ difficult, and there seems no simple answer with which to satisfy all definitions of a fibroblast. For the purposes of this review, we have defined any cell which has been shown to potentiate ECM remodeling and mechanical loading as a fibroblast. This common, participatory phenotype provides a more consistent classification based on function. Later, we will discuss methods by which the scientific community may be able to better understand and define a fibroblast, particularly as this definition pertains to the context of biomaterials design.

Fibroblast Function

Chemo-mechanical signal integration

Cells are highly responsive to their sensed chemo-mechanical environment, with mechano-dependent phenotypes ranging across all classifications of cellular behavior. Migration [146], proliferation [147,148], secretion [149], and cellular differentiation [150–152] each have well-characterized relationships to their local environment. This recognition,

binding, and interaction is facilitated by integrin binding to the ECM through complexes called focal adhesions (FA).

The extracellular matrix is the load bearing and buffering structure which supports cells and tissues. Composed of fibrous proteins, proteoglycans, and other bioactive saccharides, the ECM facilitates cell adhesion and migration, and directs proliferation and development. The fibrous proteins are collagens and elastins which provide the primary structure. The polysaccharide hyaluronic acid forms a viscous gel with absorbed water, which provides space filling and compressive strength to the matrix, as well as a fluidity to matrix. Other components include fibronectin and laminin which facilitate cellular interactions with the matrix, and further modify the mechanical characteristics of the matrix [153]. Given the influence the extracellular matrix has on cell fate, and tissue integrity, biomaterials approaches must always consider its components as a core design objective. Fibronectin is the most highly studied extracellular matrix component given its ability to facilitate interactions between cells and their local matrix. Dysregulation of mechanosensing can drive pathologic ECM deposition and drives fibrotic disease [90,152].

Many soluble factors can activate a fibroblast towards pro-healing and pro-fibrotic behaviors, and many of those factors are also secreted by fibroblasts themselves. PDGF and TGF-β1 are the two most common factors used experimentally to activate fibroblasts. There are many more factors impacting fibroblasts that are outside the scope of this review, and a thorough review of these effectors can be found in the recent review from Kalluri [154]. We briefly diagram these factors in Figure 3.

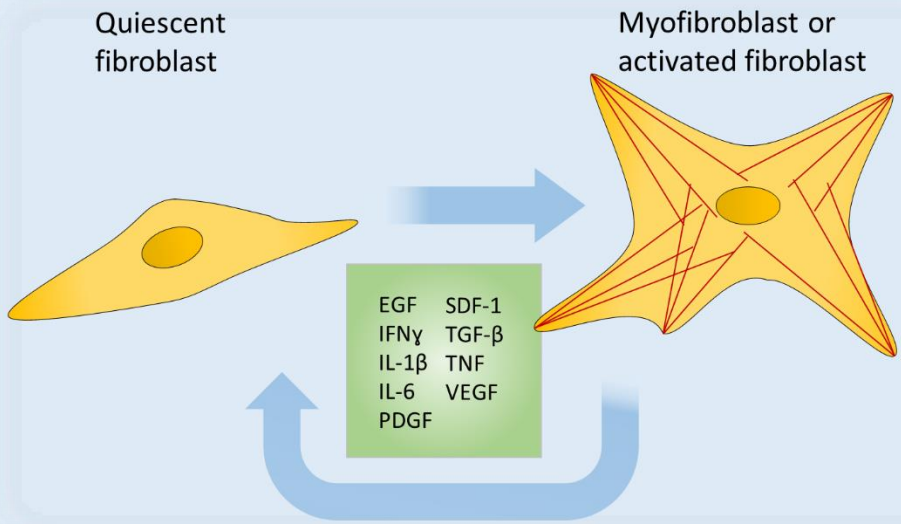

Figure 2.3: Soluble cues driving fibroblast activation into a proliferative, secretory, and remodeling phenotype. EGF, epidermal growth factor; IFNγ , interferon-γ; IL(s), interleukin; PDGF, platelet-derived growth factor; SDF-1, stromal cell-derived factor 1; TGF-β, transforming growth factor β; TNF, tumor necrosis factor; VEGF, vascular endothelial growth factor.

Focal adhesions and stiffness sensing

Focal adhesions (FA) can be divided into three regions along the 'z-axis' across the membrane: the outermost integrins, the adhesome proximal to the intracellular integrin tails, and the final actin/myosin network [151,155,156].

Integrins are heterodimeric transmembrane proteins with the ligand binding region composed of α and β subunits which allow for binding to various ECM proteins. The subunits combine for a total of 24 identified receptors [157]. These integrins bind to a variety of ECM ligands such as fibronectin, fibrinogen, and collagens. As such, the integrin composition of the FA determines the signals which are eventually integrated by the fibroblast. The multiple integrins for collagen and fibronectin have demonstrated distinct FA composition and signaling [158,159]. One prolific integrin ligand is the Arg-Gly-Asp sequence, or RGD. Found in fibronectin, fibrinogen, osteopontin [157,160], and several laminins and collagens [157], RGDs have long been a popular target for the study of mechanobiology and the development of biomaterials as the sequence allows for a functionalized material to better integrate into its local tissue environment.

The integrins are linked to the actin cytoskeleton via linker proteins talin, vinculin, integrin-linked protein kinase complex, α-actinin, tensin, and filamin [155,161]. These linker proteins, together with over two-hundred other associated components, are collectively referred to as the "integrin adhesome". The adhesome undergoes conformational changes in response to strain and affect a signaling change in the cell. Cumulatively, the

adhesome represents a systems level problem where wide genetic studies and large *in silica* analyses are being pursued. For a thorough review of the adhesome, see the 2014 review by Winograd-Katz *et al* [162].

Lastly, the force-generating actomyosin network – the 'stress fibers' referred to in myofibroblasts – sense and generate mechanical loading within the cell, which is transferred through the FA onto bound ECM [163]. This network is in a constant state of flux, striving towards dynamic equilibria of filament recruitment and degradation in response to sensed and generated tension. The precise mechanisms by which this network creates and transmits forces are still being elucidated, with research ongoing into transcription factors such as Myocardin-related transcription factor (MRTF). Upon polymerization of g-actin into f-actin (filaments), MRTF is unbound from g-actin and free to translocate to the nucleus where it forms a complex with Serum Response Factor (SRF) to drive many genes that are considered to be in the fibrotic program [164,165].

Understanding fibroblast function allows for targeting pro-healing and anti-fibrotic behavior. However, there is still a dearth of data regarding the function of these diverse cells and how they differ from one another.

Looking towards the future: trends in the field

We previously describe the difficulties in subjecting fibroblasts to rigorous pan-tissue definitions or molecular labels, elaborating on the controversies and unknowns facing the

field regarding fibroblast origin, identification, and fate. Individual groups studying fibroblasts often generate islands of fibroblast characterization, each separated from one another by gulfs in methodologies and vernacular. This compartmental regime of study comes about from a lack of adequate tooling - the throughput to analyze cellular heterogeneity in multiple dimensions (expression, lineage, microenvironment) has only recently come about. With these new and powerful methods exist a substantial opportunity within the field to thoroughly explore how we define a fibroblast; how fibroblasts from all tissues and lineages compare, and how those similarities and differences bring about cellular phenotype in the regenerative biomaterials context.

Fibroblast origins and tracing

Presumably any fibroblast or remodeling cell will contain some indicator of its fibrotic potential, and discovering markers, if any exist, will allow us to truly constrain the definition of a fibroblast. As we become capable of observing the origin and development of a cell in addition to its immediate phenotype, we will potentially be able to settle on a workable definition of a fibroblast as one of remodeling phenotype, specific lineage, or some combination of both criteria.

Lineage tracing techniques are increasing the diversity of fibroblasts which are available to study, and identifying previously unknown subsets of fibroblasts by their developmental markers. Inducible lineage tracing models include labeling developmental genes such as the forkhead box (FOX) group, which has been used to identify a subset of

perivascular fibroblasts in kidney [127,145] and lung [46]. Tcf21 [166] and Wt1 [144] in cardiac tissue are also being used to track fibroblast generation and phenotype. Fibrocyte lineages are more simple, with a collagen reporter bone marrow transplant into WT mice allowing for visualization of marrow-derived fibroblasts [132].

Another method to understand the lineage of a fibroblast, and its developmental environmental context, is to examine epigenetic markers of the cell. It has been shown that fibroblasts retain an epigenetic memory of a pathologically stiff environment for two weeks after removal [167,168]. What may not be detectable at the lineage or transcript level could in fact be epigenetic drivers of fibroblast phenotype. For example, the promoter region of Thy-1 has been shown to display hypermethylation resulting in a permanent Thy-1$^-$ phenotype [102], driving the progression of fibrotic disease and preventing the fibroblast from returning to quiescence or undergoing apoptosis.

Further techniques are being brought to bear on evaluating heterogeneous phenotype and identifying targets for study, such as cellular barcoding using multiplexed mass cytometry. Mass cytometry combines the high throughput of flow cytometry with the spectrographic ability to discern between dozens of unique mass markers, offering unprecedented throughput and efficiency in collecting data about individual cells [169]. Mass cytometry currently offers over forty [170] distinct mass tags, allowing for rapid and simultaneous quantitation of transcript and peptide levels within single cells.

Approaches from other fields which are embracing similar heterogeneities could be adapted to describing the heterogeneous fibroblast; similarly to how the macrophage M1 to M2 paradigm is being supplanted by the radial color wheel of fluid phenotype [171], an inclusive model of fibroblast lineage and functional markers might be applied to a multi-tissue analysis of fibroblasts. Dimensionality along the axes of lineage, mechanosensitivity, expression and epigenetic profiles would condense and contextualize the diverse data we collect on various fibroblasts.

Cues, metabolism, and networks

Computational models are a potential solution to the multidimensional quandary of inputs and outputs of fibroblast signaling. Simple, substantiated molecular events and interactions can be fed into a simulation of cellular behavior and reveal undiscovered relationships between phenotype and cellular, chemical, and mechanical environment. This process is used to explore hypotheses and inform further research [172–174]. Current fibroblast modeling is trending towards larger, multiscale modeling techniques which incorporate -omics and drug data into more complex and exhaustive systems. These systems allow for rapid assessment of cell-cell, cell-material, and cell-factor interactions and output genes, receptors, and signaling pathways which merit further study. *In silico* studies of fibroblast dynamics in pulmonary [175,176], liver [177], and kidney [178] demonstrate the increasing complexity and accuracy of these model systems. A comprehensive discussion of cardiac-centric fibroblast modeling by the Saucerman group [179] is recommended for further reading into fibroblast modeling.

To accurately parameterize these models requires massive amounts of phenotypic data. In addition to mass cytometry and traditional -omics approaches, powerful new methods such as stochastic profiling allow researchers to measure expression at the level of individual cells, providing insight into the high variability of cellular pathways within cells in a superficially homogeneous tissue or culture context [180]. These profiles allow models to much more accurately approximate the behaviors of heterogeneous cells within *in vitro* and *in vivo*.

Discussion

The disparity in phenotype between fibroblasts found across the body is a vital consideration for those seeking to control wound healing, inflammation, and the foreign body response/biomaterial-associated fibrosis. Heterogeneity can be seen across tissues and within tissues, and even found in the expression of 'pan-fibroblast' markers, such as FSP1. Cells not traditionally considered fibroblasts have demonstrated the ability to contribute to inflammation and fibrosis. Taken together, these difficulties may justify reevaluating what we choose to define as a fibroblast.

By whatever classification, these remodeling and mechanically active cells are vital to homeostasis. Their ability to sense and respond to cues both soluble and physical make them indispensable components of wound healing and regeneration. However, disruption

of these systems can result in disaster, with out-of-control deposition of ECM resulting in scarring and loss of biomaterial function.

A consequence of fibroblasts being so heterogeneous is the disclaimer in the introduction of many fibroblast papers, wherein the author claims his or her work should not be taken as representative of fibroblasts as a whole. We believe that these statements speak to an untapped opportunity for thorough, systems-level approaches to understand fibroblasts across tissues and bridge these disconnected islands of understanding through new technologies and approaches.

We think that biomaterials science is uniquely suited to approach these problems, for two reasons. First, out of necessity: term success of any implanted biomaterial requires mastering of the inflammation and scarring environment in order to ensure the implant functions appropriately. Second: biomaterials are invariably a simplified, constrained approximation of some physiologic feature. This constraint reduces variables and allows for the asking and answering of questions which may be intractable in a more complex experimental model. Collaborative efforts between biomaterials scientists and those studying fibrosis will yield dividends in both our basic understanding of fibroblast biology and the effectiveness of biomaterial-host integration.

Chapter 3 Extracellular Matrix Remodeling Associated with Bleomycin-Induced Lung Injury Supports Pericyte-To-Myofibroblast Transition

The text of this chapter has been adapted from Hannan RT, Miller AE, Hung RC, Sano C, Peirce SM, Barker TH. Extracellular Matrix Remodeling Associated with Bleomycin-Induced Lung Injury Supports Pericyte-To-Myofibroblast Transition. Matrix Biology Plus, *in press.*

Abstract

Of the many origins of pulmonary myofibroblasts, microvascular pericytes are a known source. Prior literature has established the ability of pericytes to transition into myofibroblasts, but provides limited insight into molecular cues that drive this process during lung injury repair and fibrosis. Fibronectin and RGD-binding integrins have long been considered pro-fibrotic factors in myofibroblast biology, and here we test the hypothesis that these known myofibroblast cues coordinate pericyte-to-myofibroblast transitions. Specifically, we hypothesized that αvβ3 integrin engagement on fibronectin induces pericyte transition into myofibroblastic phenotypes in the murine bleomycin lung injury model. Myosin Heavy Chain 11 (Myh11)-CreERT2 lineage tracing in transgenic mice allows identification of cells of pericyte origin and provides a robust tool for isolating pericytes from tissues for further evaluation. We used this murine model to track and characterize pericyte behaviors during tissue repair. The majority of Myh11 lineage-positive cells are positive for the pericyte surface markers, PDGFRβ (55%) and CD146 (69%), and display typical pericyte morphology with spatial apposition to microvascular networks. After intratracheal bleomycin treatment of mice, Myh11 lineage-positive cells showed significantly increased contractile and secretory markers, as well as αv integrin expression. According to RNASeq measurements, many disease and tissue-remodeling GeneSets were upregulated in Myh11 lineage-positive cells in response to bleomycin-induced lung injury. *In vitro*, blocking αvβ3 binding through cyclo-RGDfK prevented expression of the myofibroblastic marker αSMA relative to controls. In response to RGD-

containing provisional matrix proteins present in lung injury, pericytes may alter their integrin profile. This altered matrix-integrin axis contributes to pericyte-to-myofibroblastic transition and represents a possible therapeutic target for limiting the myofibroblastic burden in lung fibrosis.

Introduction

Acute lung injury most often leads to a transient activation of resident cells, tissue remodeling, and eventual injury resolution. However, under certain circumstances acute injury can progress into pulmonary fibrosis, a disease characterized by scar buildup and concomitant reduction in functional measures of respiration. These pathologies have largely unknown etiology and extremely limited palliative therapeutics [57]. Pulmonary fibrosis is specifically characterized by a reduction in vital respiratory metrics and a persistent wound repair environment consisting of inflammatory cytokines, early and late provisional extracellular matrix (ECM) proteins like fibrin, fibronectin and collagens, and ECM-remodeling enzymes in the lung [181–185]. Cellular infiltration, proliferation, and the expansion of interalveolar spaces in early fibrosis is referred to as fibroproliferation, which is the phase of disease wherein quiescent cells become activated and involved in the fibrotic process [186]. Through the exploration of these activated cells, there is the promise of understanding how transitions to a more chronic fibrotic remodeling program may occur.

The historical example of an activated, fibrotic effector cell is the myofibroblast. Myofibroblasts are defined by in situ observation of secretory, contractile, and tissue-remodeling phenotypes, typically through immunohistologic methods. There are no reliable lineage markers for myofibroblasts, as they derive from a variety of quiescent cell populations, the diversity of which can lead to vast differences in regeneration and tissue remodeling outcomes. Thus, recent research into tissue-resident stromal cell populations have focused on identifying and characterizing the various myofibroblast progenitor populations [187–191].

One known myofibroblast progenitor population is the perivascular mural cell, or pericyte, a cell physically associated with microvascular endothelial cells in capillary networks. Pericytes are phenotypically diverse and are typically identified by a variety of surface markers including CD146, PDGFRβ, NG2, and Desmin [40,63,192,193]. Pericyte investment in the microvasculature supports vessel integrity and is essential for vascular homeostasis and functional tissue regeneration after insult [44,192]. Pericytes have demonstrated phenotypic plasticity, acting as a source of myofibroblasts in fibrotic disease [194] and other pathologies [195–197]. The myofibroblastic pericyte can emerge in response to lung injury [65,194], responding to classic myofibroblast-promoting conditions, including TGF-β and ECM stiffness [65], two stimuli known to activate classically-defined myofibroblasts. Study of the molecular mechanisms involved in mechanotransduction and activation of latent TGF-β have identified the integrins as essential components in myofibroblastic activation [198].

Integrins are a class of heterodimeric transmembrane receptors that bind to a variety of ligands, the majority of which are found in the ECM. Specific integrin and ligand combinations can potentiate a range of cellular behaviors ranging from differentiation to apoptosis to extravasation. Fibroblast signaling through the αvβ3 integrin is thought to be at equilibrium with signaling through α5β1, and when this balance is disrupted in disease (known as an 'integrin switch'), greater αvβ3 integrin signaling drives disease phenotypes [199–201]. It is thought that this shift towards pro-myofibroblastic αvβ3 signaling is derived from the increase in Arginine, Glycine, and Aspartate (RGD) ligand found in the fibronectin-rich provisional matrix in early stages of tissue remodeling[200,202–206]

Integrins are no less important in mediating the responses of pericytes to their biochemical and biomechanical environments. The loss of pulmonary basement membrane, in which healthy pericytes are situated, is considered a hallmark of mature and non-resolving fibrosis [27]. Pericyte investment in the basement membrane and capillary network is facilitated by laminin binding to α6 heterodimers, α6β1 and α6β4 [25,207,208]. For pericytes, the transition from laminin- and collagen IV-rich basement membrane to a fibronectin-rich provisional matrix during early lung injury could invoke a stark change in integrin signaling, similar to the fibroblast integrin switch, leading to phenotypic switching [209]. Indeed, when αv integrin was selectively knocked out via use of a PDGFRβ-cre mouse, its loss was shown to be protective in a bleomycin lung injury model [210].

However, a direct linkage between ECM ligand, surface integrin expression, and pericyte-to-myofibroblast transition has yet to be explored, and whether fibronectin is sufficient to trigger the pericyte-to-myofibroblast transition is an open question. Additionally, characterization of the myofiboblastic pericyte *in vitro* and *in vivo* is typically limited to assessment of a single marker, such as alpha smooth muscle actin (αSMA), limiting our understanding of the broader phenotypic changes that the transitioning pericyte has undergone. Therefore, the goals of this study were to: 1) more comprehensively characterize the phenotypes of pulmonary pericytes and their local ECM environment following lung injury with bleomycin, and 2) test the hypothesis that RGD-mediated integrin signaling can precipitate the pericyte-to-myofibroblast transition.

Results

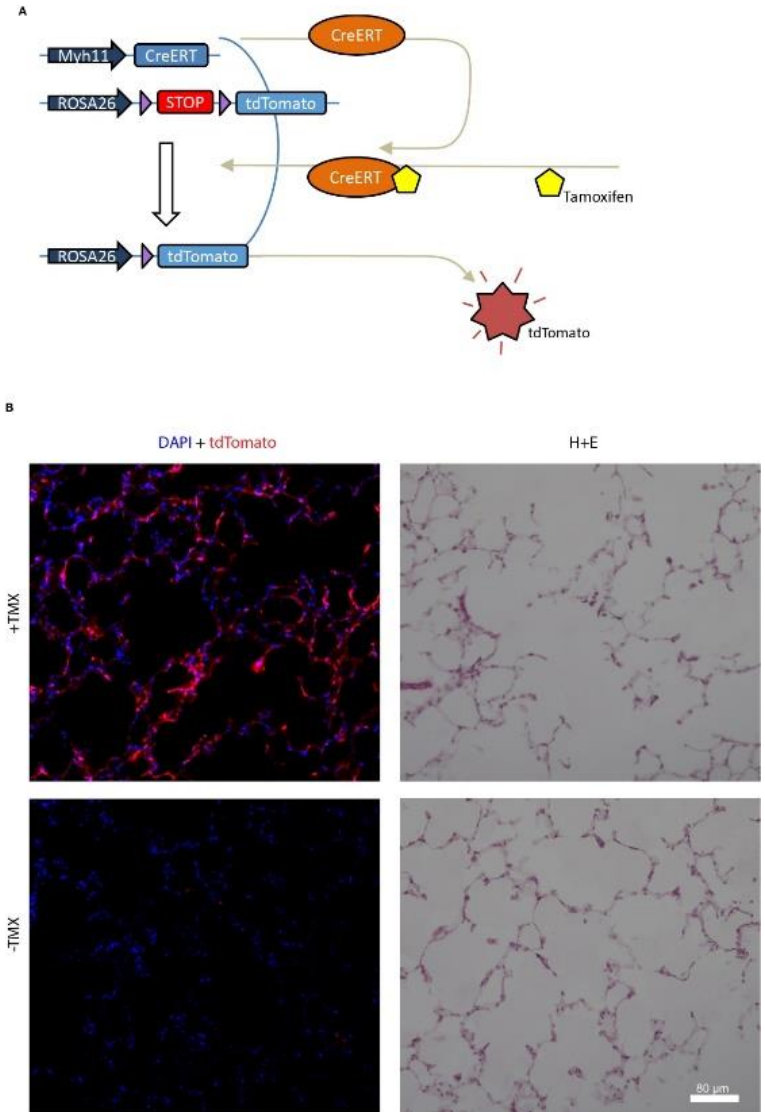

Figure 3.1 The Myh11-CreERT2 ROSA STOPfl/fl tdTomato reporter mouse requires tamoxifen for reporter induction and does not alter lung histology. (A) Schematic of the Myh11-CreERT2 ROSA STOPfl/fl tdTomato lineage reporter mouse (B) Representative immunofluorescence (IF) and hematoxylin and eosin (H&E) micrographs of lung. IF histology stained for tdTomato (red, endogenous fluorophore), and DAPI (blue).

Myh11 lineage reporter mouse labels pericytes in the lung microvasculature. The induction of *Myh11-CreERT2 ROSA STOPfl/fl tdTomato* mice (described in Figure 3.1A) with tamoxifen induces recombination and expression of tdTomato in pericytes, as well as vascular and bronchiolar smooth muscle cells (Figure 3.2A), consistent with prior work using Myh11 reporter mice [45,211–213]. The use of the tdTomato fluorescent reporter with the Myh11 Rosa26 construct allows for greater sensitivity in detecting Myh11 lineage-positive cells than the previously published eYFP fluorescent reporter lineage mouse. While observation of Myh11 lineage-positive cells in the pulmonary capillary bed has only been associated with injury in the eYFP reporter mouse [45], we can clearly identify the Myh11 lineage-positive pericytes as being tissue-resident cells before injury. These tdTomato-expressing, fluorescent pericytes become much brighter in disease models, as demonstrated by the differences in relative brightness between saline and bleomycin-treated lungs given the same confocal image acquisition settings in this text and prior literature [45]. Spontaneous recombination is not seen in uninduced mice prior to experimentation (Figure 3.1B). These Myh11 lineage-positive pericytes in the capillary bed extend abluminal processes along capillary endothelium (Figure 3.2A). The majority of Myh11 lineage-positive cells isolated from healthy, uninjured lung (gating described in Figure 1B) are positive for pericyte markers PDGFRβ (56%) and CD146 (69%) (Figure 3.2C). The observed location, morphology, surface markers, and body of prior work on this Myh11 lineage [45,212–214] provide robust evidence to support a classification of Myh11 lineage-positive cells as pericytes.

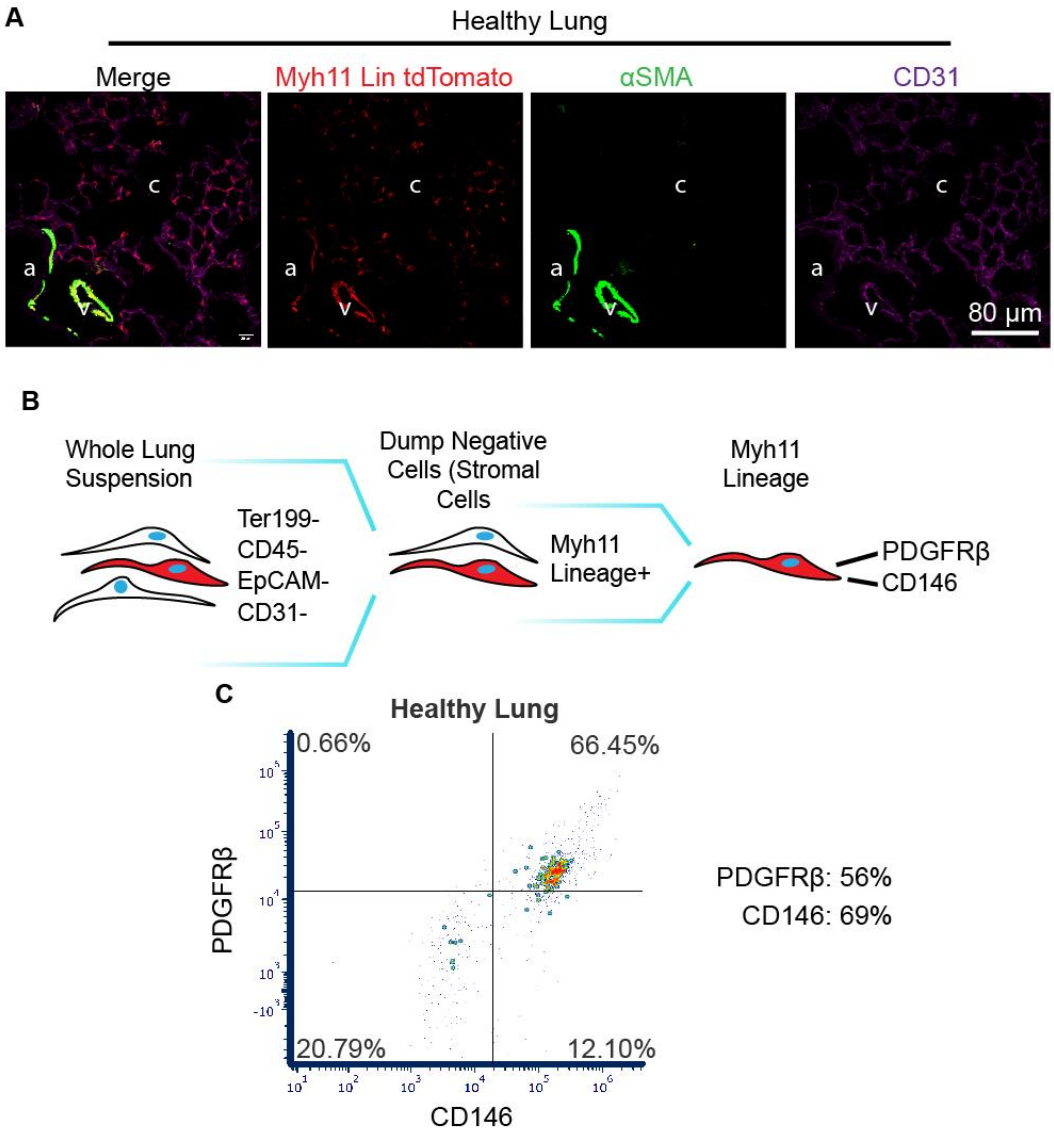

Figure 3.2 The Myh11-CreERT2 ROSA STOPfl/fl tdTomato reporter mouse labels pericytes in the lung capillary bed. A) Representative immunofluorescence (IF) micrographs of lung sections stained for tdTomato (red, endogenous fluorophore), αSMA (green), and CD31 (purple). Anatomical structures are denoted "a" for bronchiolar airway lumen, "v" for venule, and "c" for the alveolar capillary bed. (B) Gating

hierarchy to isolate Myh11 lineage-positive cells for phenotyping. (C) Representative scatter plot of PDGFRβ and CD146 surface markers on the Myh11 lineage. An average of 55.5% of Myh11 lineage-positive cells in healthy mice were positive for PDGFRβ, while an average of 69.3% were positive for CD146 (n=3).

Myh11 lineage-positive pericytes adopt myofibroblastic phenotypes within regions of fibroproliferative repair in the injured lung according to immunofluorescent histologic analyses. Using a single-dose intratracheal bleomycin lung injury model, immunofluorescent imaging and analyses were performed on lung specimens from saline-treated control mice and bleomycin-treated mice. Confocal micrographs of transverse sections taken from the midline left lung demonstrate the pronounced tissue remodeling characteristic of the bleomycin disease model (Figure 3.3A, B), where the interstitial tissue expands through fibroproliferation and ablates the alveolar airspaces [186,215]. This increase in tissue density and loss of alveolar spaces is known to be potentiated by myofibroblastic tissue remodeling. In saline-treated control lungs (Figure 3.3A), the vast majority of αSMA content can be found in the smooth muscle cells lining larger vessels (pulmonary venules and bronchioles), while more diffuse and non-luminal αSMA is abundant in the bleomycin treated lung (Figure 3.3B). The proportion of Myh11 lineage-positive pericytes in lung sections expressing αSMA more than doubles two weeks post-bleomycin treatment (Figure 3.3C). This analysis manually excludes Myh11 lineage-positive vascular smooth muscle cells in bronchioles or venules, as described in the Methods section. An analysis of fibronectin levels local to Myh11 lineage-positive

pericytes (within 12 microns of cell soma) revealed no significant difference in fluorescence intensity between saline-treated and bleomycin-treated lungs (Figure 3.3D). Active perivascular αvβ3 integrin (Figure 3.3E, Wow-1) increases in bleomycin-treated lung, with αSMA+/Wow-1+ pericytes significantly increasing in frequency in bleomycin-treated lung (Figure 3.3F).

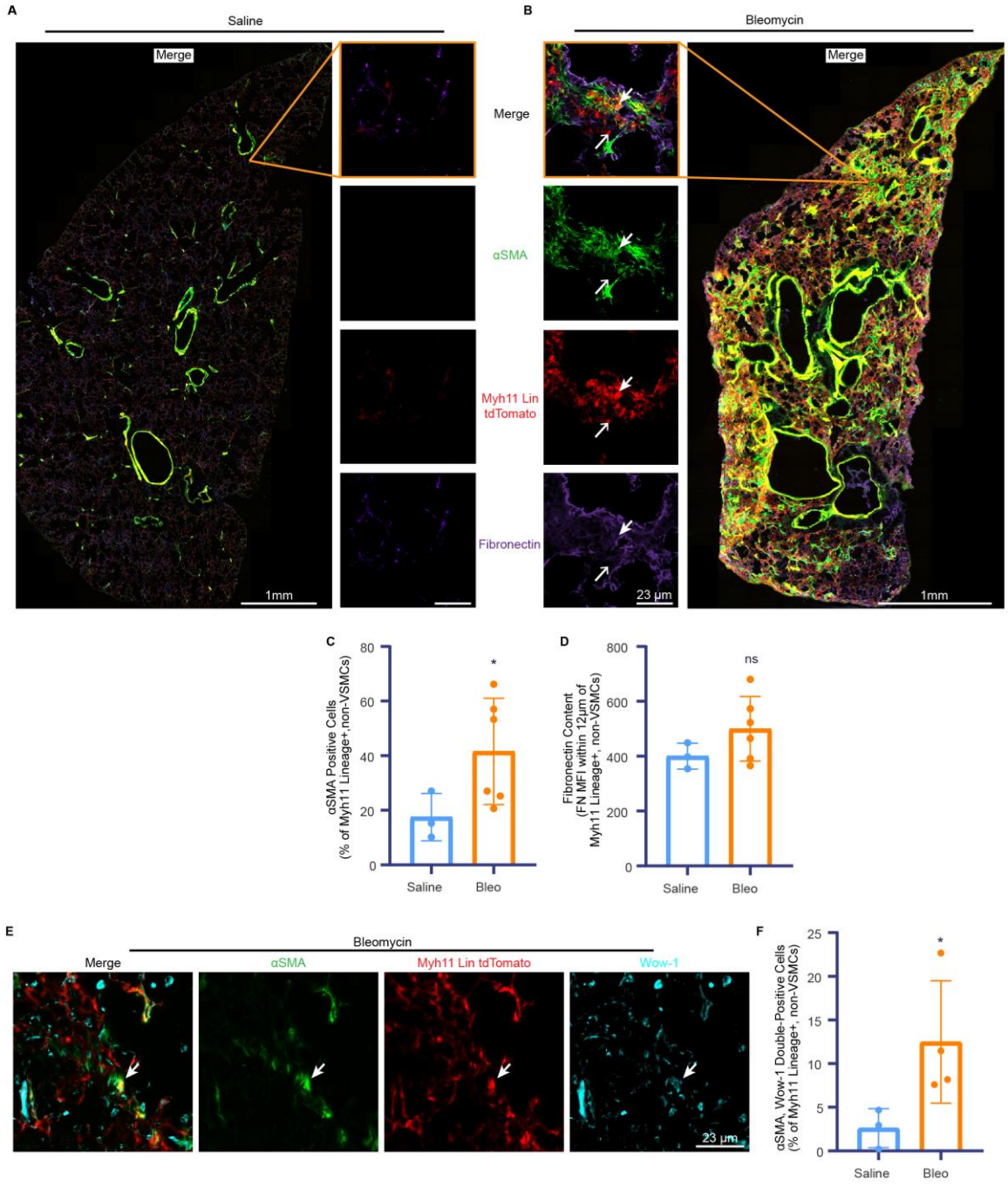
A
Saline
Merge
1mm
B
Bleomycin
Merge
αSMA
Myh11 Lin tdTomato
Fibronectin
23 μm
Merge
1mm
C
αSMA Positive Cells (% of Myh11 Lineage+, non-VSMCs)
80
60
40
20
0
*
Saline
Bleo
D
Fibronectin Content (FN MFI within 12μm of Myh11 Lineage+, non-VSMCs)
800
600
400
200
0
ns
Saline
Bleo
E
Bleomycin
Merge
αSMA
Myh11 Lin tdTomato
Wow-1
23 μm
F
αSMA, Wow-1 Double-Positive Cells (% of Myh11 Lineage+, non-VSMCs)
25
20
15
10
5
0
*
Saline
Bleo

*Figure 3.3 Immunofluorescence (IF) micrographs of lungs from saline and bleomycin treated mice lungs showed increases in perivascular αSMA and engaged αvβ3 integrin. (A,B) Representative confocal micrographs of transverse lung sections immunolabeled for αSMA (green), tdTomato (red, endogenous fluorophore), and fibronectin (purple) from saline (A, n=3) and bleomycin (B, n=6) treated mice. High-magnification inserts (middle) allow for identification and quantification of individual αSMA-positive pericytes (thick arrow) and αSMA-negative pericytes (thin arrow). (C) The number of Myh11 lineage-positive pericytes expressing αSMA is reported as a percentage of the number of total Myh11 lineage-positive pericytes counted across an entire lung section and the mean fluorescence intensity of fibronectin within 13 microns of each pericyte was measured (D). (E) Representative micrograph of Wow-1 staining in the bleomycin treated lung, with an αSMA, Wow-1 double positive pericyte shown (thick arrow) and quantitative comparison between saline (n=3) and bleomycin (n=5) lung sections (F). Data are expressed as means ± standard deviation. Statistical significance was determined via unpaired, one-tailed student's t-test. ns = not significant; $p < 0.05$ = *; $p < 0.01$ = **; $p < 0.001$ = ***.*

Myh11 lineage-positive pericytes isolated from fibrotic lungs show increases in tissue-remodeling markers by flow cytometry. Myh11 lineage-positive pericytes are defined here as live cells negative for the cell-surface markers of other cell lineages Ter119 (erythrocytes), CD45 (myeloid lineage), EpCAM (epithelial cells), CD31 (endothelial cells), which we refer to as "dump negative", and positive for Myh11 lineage and CD146 (pericyte marker). Cells were isolated from whole-lung digestions from bleomycin-treated and saline-treated lungs, as depicted in Figure 3.4A. Myh11 lineage-positive pericytes were evaluated for a panel of matrix-remodeling and matrix-binding markers, including: αSMA, Collagen type 1 alpha 1 (Col1a1) and integrin subunits α6 and αv. The prevalence of all these markers increased significantly in Myh11 lineage-positive pericytes (Figure 3.4 D, E, I, J). Representative plots of healthy and diseased lung for matrix-remodeling markers αSMA and Col1a1 (Figure 3.4B, C) demonstrate this shift. The amount of Myh11 lineage-positive pericytes positive for αSMA nearly doubles two weeks after bleomycin treatment (Figure 3.4D). Col1a1 is a collagen subunit that can be labeled intracellularly, provides a snapshot of cellular collagen synthesis, and is used as a measure of myofibroblastic tissue remodeling [33,216–218]. As with αSMA, the incidence of Col1a1+/Myh11 lineage-positive pericytes significantly increases by over two-fold in the bleomycin treatment group (Figure 3.4E). A tripling of the frequency of αSMA+/Col1a1+/Myh11 lineage-positive pericytes was observed (Figure 3.4F).

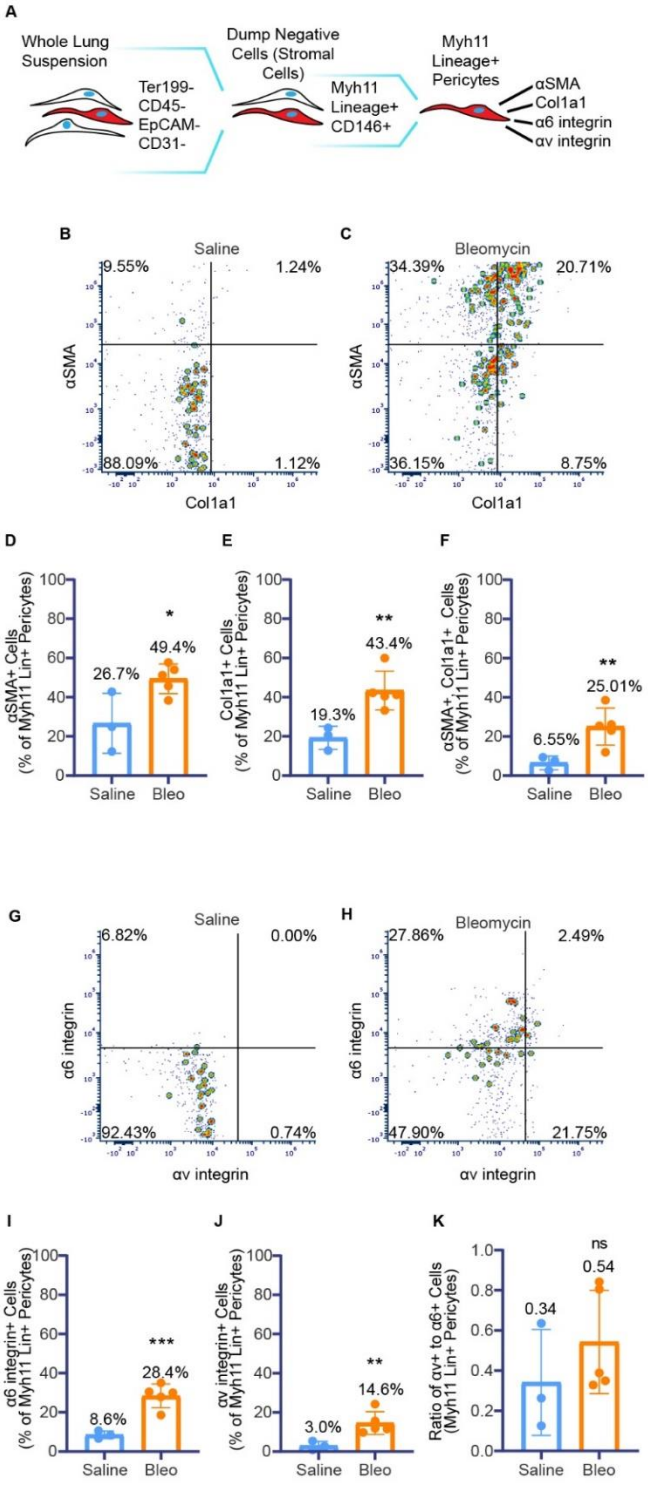
A
Whole Lung Suspension
Ter199- CD45- EpCAM- CD31-
Dump Negative Cells (Stromal Cells)
Myh11 Lineage+ CD146+
Myh11 Lineage+ Pericytes
αSMA
Col1a1
α6 integrin
αv integrin
B
Saline
9.55%
1.24%
88.09%
1.12%
αSMA
Col1a1
C
Bleomycin
34.39%
20.71%
36.15%
8.75%
αSMA
Col1a1
D
αSMA+ Cells (% of Myh11 Lin+ Pericytes)
26.7%
49.4%
*
Saline
Bleo
E
Col1a1+ Cells (% of Myh11 Lin+ Pericytes)
19.3%
43.4%
**
Saline
Bleo
F
αSMA+, Col1a1+ Cells (% of Myh11 Lin+ Pericytes)
6.55%
25.01%
**
Saline
Bleo
G
Saline
6.82%
0.00%
92.43%
0.74%
α6 integrin
αv integrin
H
Bleomycin
27.86%
2.49%
47.90%
21.75%
α6 integrin
αv integrin
I
α6 integrin+ Cells (% of Myh11 Lin+ Pericytes)
8.6%
28.4%
***
Saline
Bleo
J
αv integrin+ Cells (% of Myh11 Lin+ Pericytes)
3.0%
14.6%
**
Saline
Bleo
K
Ratio of αv+ to α6+ Cells (Myh11 Lin+ Pericytes)
0.34
0.54
ns
Saline
Bleo

*Figure 3.4 . Flow cytometry of Myh11 lineage-positive pericytes isolated from saline and bleomycin treated mouse lungs show increased matrix-remodeling and matrix-adhesion proteins. (A) Gating hierarchy to isolate Myh11 lineage-positive pericytes for phenotyping. (B-F) Analysis of the expression of tissue-remodeling markers, αSMA and Col1a1, in Myh11 lineage-positive pericytes. Representative plots of αSMA and Col1a1 from saline (n=3, B) and bleomycin (n=5, C) treatment groups. Quantitation of αSMA-positive (D), Col1a1-positive (E), and double-positive (F) cells. (G-K) Analysis of adhesion integrins, α6 and αv, in Myh11 lineage-positive pericytes. Representative plots of α6 and αv from saline (G) and bleomycin (H) treatment groups. Quantitation of α6 integrin (I), αv integrin (J) and the ratio of αv positive cells to α6 positive cells (K). Data are expressed as means ± standard deviation. Statistical significance determined via unpaired, one-tailed student's t-test. ns = not significant; $p < 0.05$ = *; $p < 0.01$ = **; $p < 0.001$ = ***.*

Integrin subunits α6 and αv confer affinities for the basement membrane protein laminin and the RGD motif, respectively. Representative plots from saline and bleomycin treatments (Figure 3.4G, H) demonstrate significant population shifts between saline control and bleomycin-treated mice. The frequency of α6+/Myh11 lineage-positive pericytes increases threefold in the bleomycin treatment group (Figure 3.4I), and αv+/Myh11 lineage-positive pericytes increase nearly fivefold (Figure 3.4J). No significant change in the ratio of αv to α6 integrin-expressing, Myh11 lineage-positive

pericytes between treatment groups can be seen (Figure 3.4K). This ratiometric quantification interrogates a shift in integrin expression across the population of Myh11 lineage-positive pericytes.

When Myh11 lineage-positive pericytes are compared to the broader population of stromal cells (defined as cells negative for lineages Ter119, CD45, CD31, EpCAM [216]), it can be observed that the relative ratio of αSMA+ pericytes to αSMA+ stromal cells decreases in bleomycin, even while the incidence of pericytes positive for αSMA increases (Figure 3.5D). Myh11 lineage-positive pericytes comprise the bulk of Col1a1+ cells in the stromal population of both healthy and diseased lung (Figure 3.5D).

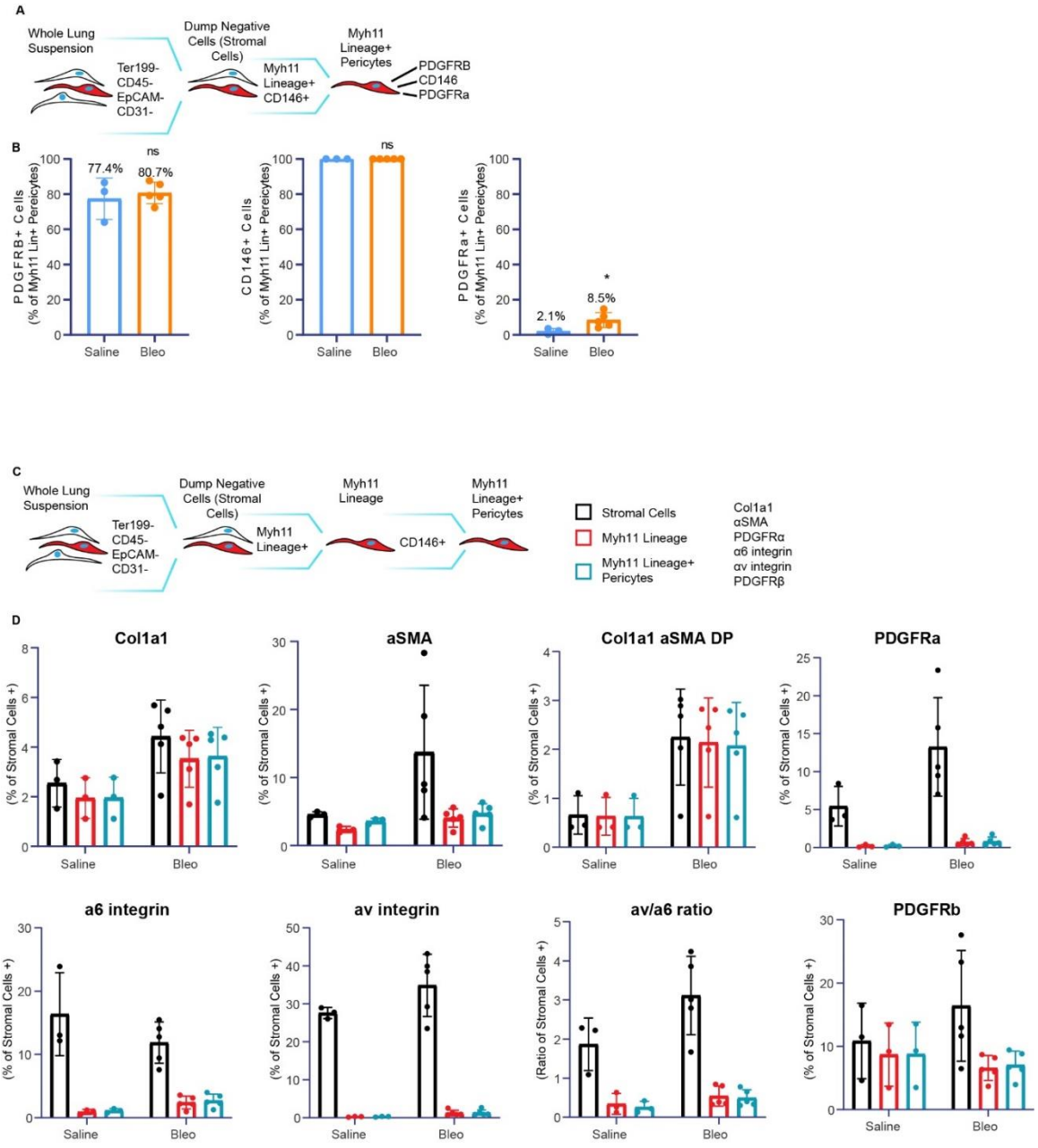

Figure 3.5 . Broader phenotyping of myh11 lineage pericytes and lineage pericytes in relation to the putative stromal cell population as identified by flow cytometry. Gating hierarchy to identify Myh11 lineage-positive pericytes for phenotyping. (B) Additional surface markers assayed (C) Gating hierarchy to isolate putative stromal cells via

negative marker selection. (D) Comparison of saline and bleomycin marker profiles on both stromal cells and the perivascular subset of that same population.

Myh11 lineage-positive pericytes isolated from fibrotic lungs are enriched for tissue-remodeling genes. Myh11 lineage-positive pericytes were isolated from whole-lung digestions that were obtained two weeks after bleomycin-treatment or saline-treatment, as described in Figure 4A. Cells were run through an Illumina sequencing platform, with details provided in the Methods section. A list of the top 30 ranked genes by fold change can be seen in Figure 4B, with an extended top 100 genes provided in Figure 3.6A. The top of the list consists of several ECM components, matrix metalloproteinases (MMPs), and genes associated with activation of immune complement. A GeneSet Enrichment Analysis (GSEA) allows for an unbiased perusal of 1378 mapped mouse GeneSets. Our analysis found no significant enrichment of GeneSets in the saline treated-group, and 49 GeneSets were found to be enriched in the bleomycin-treated group. A visual aide to understanding the multiple tests and scores of bulk GSEA can be found in Figure 3.6B. Genesets can be seen in Figure 4C and comprise Cellular Component (CC), Biological Processes (BP), Molecular Function (MF), and Matrisome (Matri) categories, of which the top five are shown. CC, MF, and BP are domains generated by the GeneOntology group [219,220], while Matri is a curated list of fibrosis and fibroproliferative-relevant GeneSets by Naba and Hynes [221].

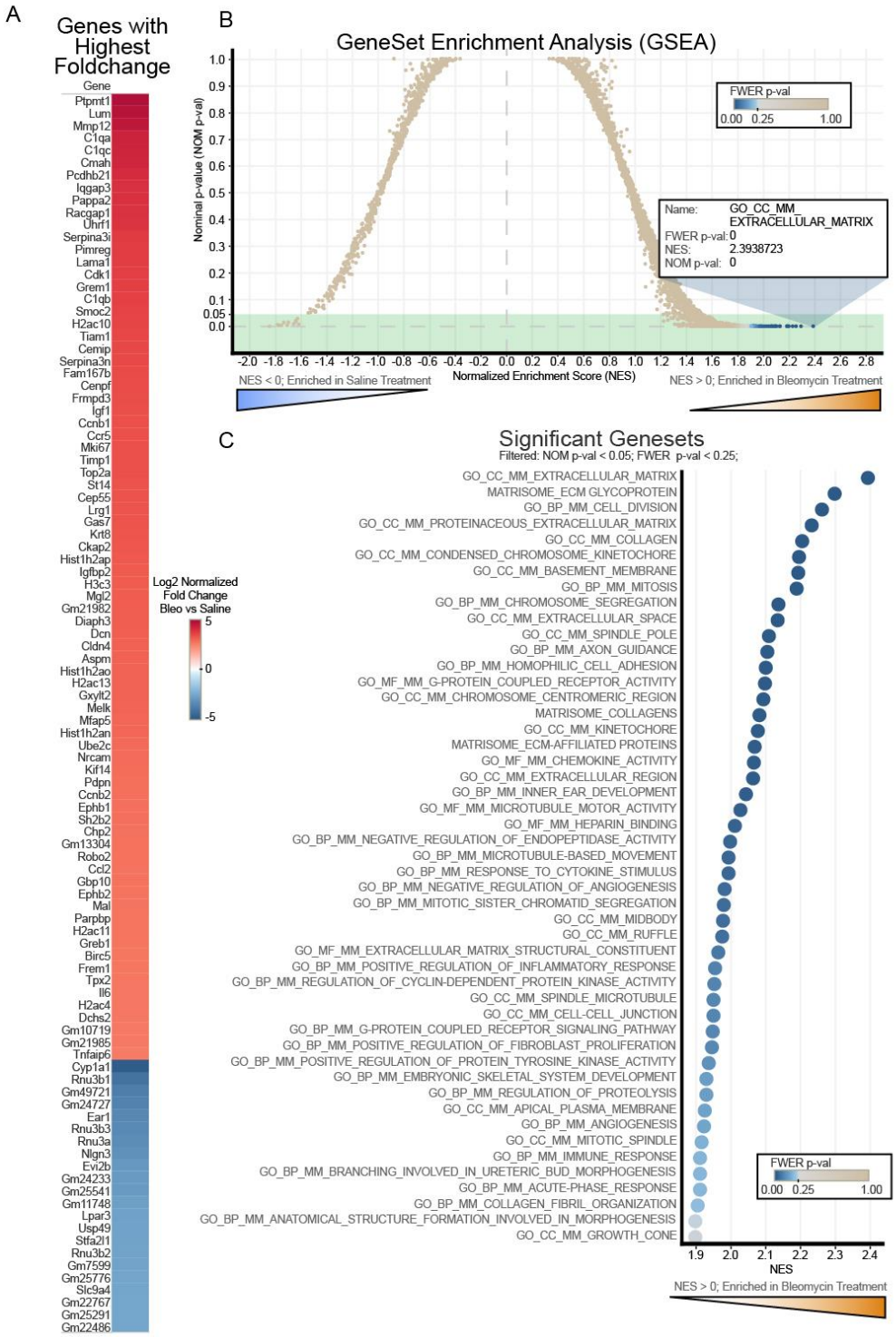
A
Genes with Highest Foldchange
Gene
Ptpmt1
Lum
Mmp12
C1qa
C1qc
Cmah
Pcdhb21
Iqgap3
Pappa2
Racgap1
Uhrf1
Serpina3i
Pimreg
Lama1
Cdk1
Grem1
C1qb
Smoc2
H2ac10
Tiam1
Cemip
Serpina3n
Fam167b
Cenpf
Frmpd3
Igf1
Ccnb1
Ccr5
Mki67
Timp1
Top2a
St14
Cep55
Lrg1
Gas7
Krt8
Ckap2
Hist1h2ap
Igfbp2
H3c3
Mgl2
Gm21982
Diaph3
Dcn
Cldn4
Aspm
Hist1h2ao
H2ac13
Gxylt2
Melk
Mfap5
Hist1h2an
Ube2c
Nrcam
Kif14
Pdpn
Ccnb2
Ephb1
Sh2b2
Chp2
Gm13304
Robo2
Ccl2
Gbp10
Ephb2
Mal
Parpbp
H2ac11
Greb1
Birc5
Frem1
Tpx2
Il6
H2ac4
Dchs2
Gm10719
Gm21985
Tnfaip6
Cyp1a1
Rnu3b1
Gm49721
Gm24727
Ear1
Rnu3b3
Rnu3a
Nlgn3
Evi2b
Gm24233
Gm25541
Gm11748
Lpar3
Usp49
Stfa2l1
Rnu3b2
Gm7599
Gm25776
Slc9a4
Gm22767
Gm25291
Gm22486
Log2 Normalized Fold Change Bleo vs Saline
5
0
-5
B
GeneSet Enrichment Analysis (GSEA)
Nominal p-value (NOM p-val)
1.0
0.9
0.8
0.7
0.6
0.5
0.4
0.3
0.2
0.1
0.05
0.0
FWER p-val
0.00 0.25 1.00
Name: GO_CC_MM_EXTRACELLULAR_MATRIX
FWER p-val: 0
NES: 2.3938723
NOM p-val: 0
-2.0 -1.8 -1.6 -1.4 -1.2 -1.0 -0.8 -0.6 -0.4 -0.2 0.0 0.2 0.4 0.6 0.8 1.0 1.2 1.4 1.6 1.8 2.0 2.2 2.4 2.6 2.8
NES < 0; Enriched in Saline Treatment
Normalized Enrichment Score (NES)
NES > 0; Enriched in Bleomycin Treatment
C
Significant Genesets
Filtered: NOM p-val < 0.05; FWER p-val < 0.25;
GO_CC_MM_EXTRACELLULAR_MATRIX
MATRISOME_ECM GLYCOPROTEIN
GO_BP_MM_CELL_DIVISION
GO_CC_MM_PROTEINACEOUS_EXTRACELLULAR_MATRIX
GO_CC_MM_COLLAGEN
GO_CC_MM_CONDENSED_CHROMOSOME_KINETOCHORE
GO_CC_MM_BASEMENT_MEMBRANE
GO_BP_MM_MITOSIS
GO_BP_MM_CHROMOSOME_SEGREGATION
GO_CC_MM_EXTRACELLULAR_SPACE
GO_CC_MM_SPINDLE_POLE
GO_BP_MM_AXON_GUIDANCE
GO_BP_MM_HOMOPHILIC_CELL_ADHESION
GO_MF_MM_G-PROTEIN_COUPLED_RECEPTOR_ACTIVITY
GO_CC_MM_CHROMOSOME_CENTROMERIC_REGION
MATRISOME_COLLAGENS
GO_CC_MM_KINETOCHORE
MATRISOME_ECM-AFFILIATED PROTEINS
GO_MF_MM_CHEMOKINE_ACTIVITY
GO_CC_MM_EXTRACELLULAR_REGION
GO_BP_MM_INNER_EAR_DEVELOPMENT
GO_MF_MM_MICROTUBULE_MOTOR_ACTIVITY
GO_MF_MM_HEPARIN_BINDING
GO_BP_MM_NEGATIVE_REGULATION_OF_ENDOPEPTIDASE_ACTIVITY
GO_BP_MM_MICROTUBULE-BASED_MOVEMENT
GO_BP_MM_RESPONSE_TO_CYTOKINE_STIMULUS
GO_BP_MM_NEGATIVE_REGULATION_OF_ANGIOGENESIS
GO_BP_MM_MITOTIC_SISTER_CHROMATID_SEGREGATION
GO_CC_MM_MIDBODY
GO_CC_MM_RUFFLE
GO_MF_MM_EXTRACELLULAR_MATRIX_STRUCTURAL_CONSTITUENT
GO_BP_MM_POSITIVE_REGULATION_OF_INFLAMMATORY_RESPONSE
GO_BP_MM_REGULATION_OF_CYCLIN-DEPENDENT_PROTEIN_KINASE_ACTIVITY
GO_CC_MM_SPINDLE_MICROTUBULE
GO_CC_MM_CELL-CELL_JUNCTION
GO_BP_MM_G-PROTEIN_COUPLED_RECEPTOR_SIGNALING_PATHWAY
GO_BP_MM_POSITIVE_REGULATION_OF_FIBROBLAST_PROLIFERATION
GO_BP_MM_POSITIVE_REGULATION_OF_PROTEIN_TYROSINE_KINASE_ACTIVITY
GO_BP_MM_EMBRYONIC_SKELETAL_SYSTEM_DEVELOPMENT
GO_BP_MM_REGULATION_OF_PROTEOLYSIS
GO_CC_MM_APICAL_PLASMA_MEMBRANE
GO_BP_MM_ANGIOGENESIS
GO_CC_MM_MITOTIC_SPINDLE
GO_BP_MM_IMMUNE_RESPONSE
GO_BP_MM_BRANCHING_INVOLVED_IN_URETERIC_BUD_MORPHOGENESIS
GO_BP_MM_ACUTE-PHASE_RESPONSE
GO_BP_MM_COLLAGEN_FIBRIL_ORGANIZATION
GO_BP_MM_ANATOMICAL_STRUCTURE_FORMATION_INVOLVED_IN_MORPHOGENESIS
GO_CC_MM_GROWTH_CONE
FWER p-val
0.00 0.25 1.00
1.9 2.0 2.1 2.2 2.3 2.4
NES
NES > 0; Enriched in Bleomycin Treatment

Figure 3.6 RNA sequencing (RNA-seq) of Myh11 lineage pericytes isolated from saline and bleomycin treated mouse lungs demonstrate increased expression of tissue-remodeling genes in the disease model. (A) Heat map of top 100 most differentially expressed genes out of 22,203 between pericytes from bleomycin (Bleo) and saline treatment groups. (B) GeneSet Enrichment Analysis (GSEA) plot of 1378 Gene Ontology (GO) sets, visualizing the test statistics: nominal p-value (NOM p-val); Normalized Enrichment Score (NES); Family-wise Error Rate (FWER). The threshold for significance is highlighted green (NOM p-val < 0.05) and white-to-blue color dots (FWER < 0.25). There is no signficance threshold for NES, as it is a measure of GO set expression on phenotype. (C) GO sets meeting the filter criteria (NOM p-val < 0.05; FWER < 0.25) are displayed. All sets have a NES score > 0, indicating all significant GO sets are enriched in bleomycin treatment. Cellular component (CC), molecular function (MF), biological process (BP), and matrisome denote separate categorical domains of gene ontologies.

Across all categories, significant enrichment of ECM and ECM-related processes is seen in cells procured from bleomycin-treated lungs. Also enriched are several cell cycle and proliferation GeneSets, implying a metabolically activated and mitotic cell population. The entire list of significant GeneSets can be found in Figure 3.6C.

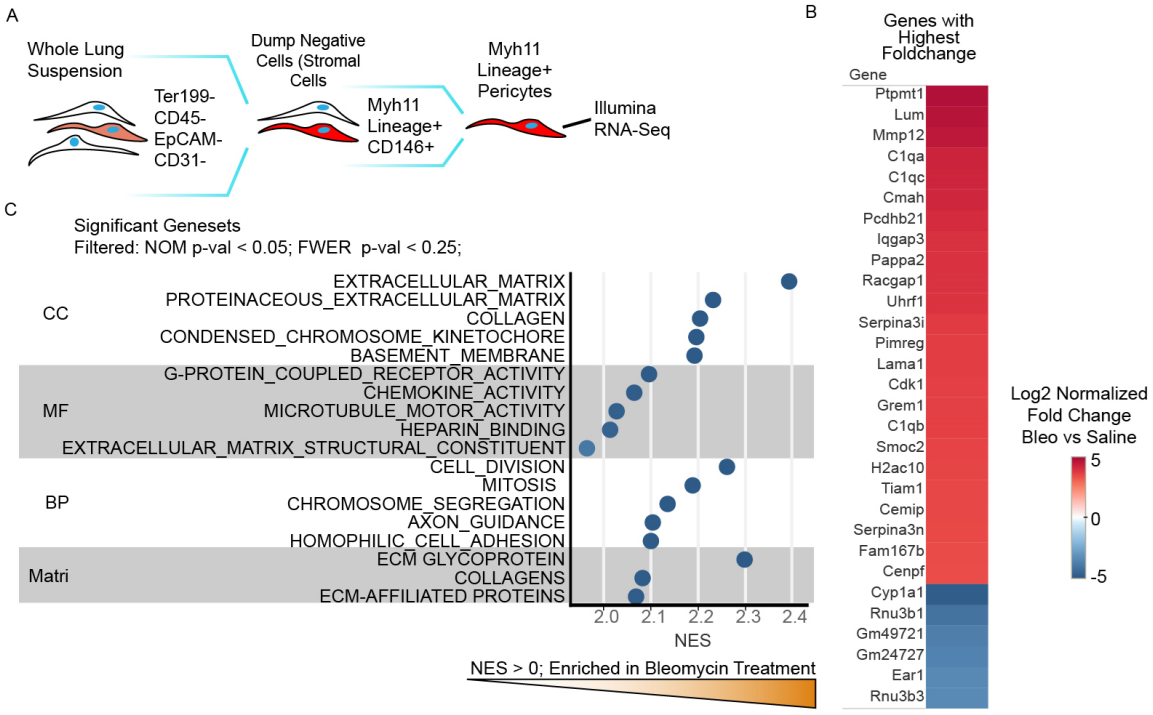

Figure 3.7 Subset of RNA sequencing (RNA-seq) of Myh11 lineage-positive pericytes isolated from saline and bleomycin treated mouse lungs demonstrate increased expression of tissue-remodeling genes in the disease model. (A) Gating hierarchy to isolate Myh11 lineage-positive pericytes for phenotyping. (B) Heat map of top 30 most differentially expressed genes out of 22,203 between pericytes from bleomycin (Bleo) and saline groups. (C) GeneSet Enrichment Analysis (GSEA) of RNA-seq data in Myh11 lineage-positive pericytes. The threshold for significance of tested genesets is nominal p-value (NOM p-val) < 0.05 and Family-wise Error Rate (FWER) < 0.25.

Primary Myh11 cell culture on fibronectin with RGD-inhibition reveals an RGD-dependent increase of cellular αSMA. Fibronectin coated, stiff substrates are thought to activate myofibroblasts through αv integrin focal adhesions [222]. A laminin coating with no readily available RGD integrin ligand was chosen for a negative control, as pericyte α6 investment in the laminin-rich basement membrane is a known requirement for cellular and tissue homeostasis and does not activate myofibroblastic phenotypes [207,223]. Cyclic RGD (cRGD) in an approximately 100-fold molar excess beyond reported IC_{50} values for αv heterodimer adhesion was used to prevent RGD engagement, with nonbinding cyclic RAD (cRAD) used as a control [224]. Mouse fibronectin or laminin-coated cover slips seeded with CD146+ MACS-enriched primary cells isolated from digested lung can be seen after 24 hours culture (Figure 5A). The prevention of cellular engagement with RGD results in less spread and less contractile cells, as observed by

αSMA. The mean fluorescence intensity (MFI) of cellular αSMA across cell preparations from several mice (n=3) can be seen in Figure 5B. The Myh11 lineage-positive cells plated on fibronectin with cRAD nonblocking control generated significantly increased αSMA compared to the cRGD blocked group (Figure 5B). The laminin surface controls show no αSMA increases relative to the fibronectin surface with either treatment and are shown together as “LAM + Peptide”.

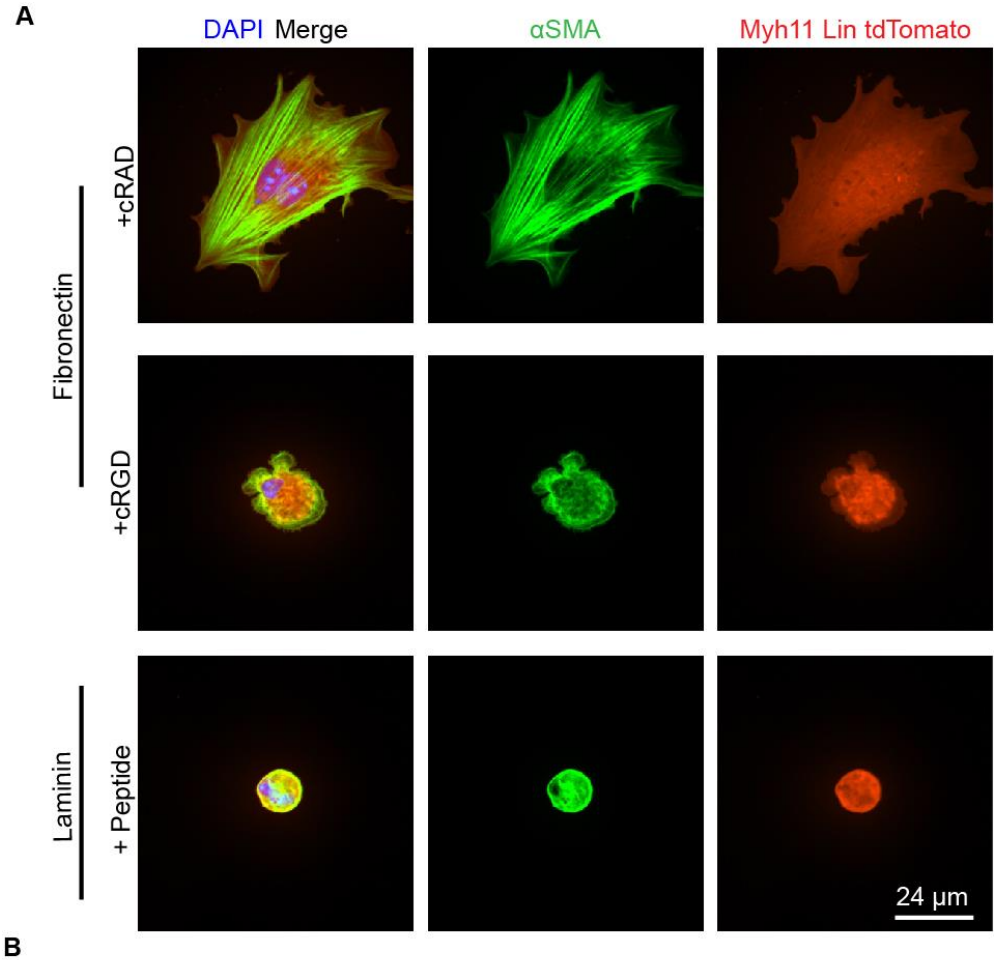
A
DAPI Merge
αSMA
Myh11 Lin tdTomato
Fibronectin
+cRAD
+cRGD
Laminin
+ Peptide
24 μm
B
Cellular αSMA
(MFI, per mouse mean)
5000
4000
3000
2000
1000
0
*
*
FN + RAD
FN + RGD
LAM + Peptide

*Figure 3.8 Cell culture of Myh11 lineage-positive cells with RGD inhibition reveals an RGD-dependent increase of αSMA on fibronectin-coated substrates but not on laminin-coated substrates. (A) Representative immunofluorescence (IF) micrographs of Myh11 lineage-positive cells (red, endogenous fluorophore) and αSMA (green). Cells were treated with the soluble RGD inhibitor, cyclo-RGDfK (cRGD), or the noninhibitory control cyclo-RADfK (cRAD). (B) Quantitation of mean fluorescence intensity (MFI) of αSMA within each cell. Data are expressed as means of cells from individual mice (n=3), with 16-60 cells averaged per mouse, ± standard deviation. No differences were seen between peptides in the laminin group, and they were thus merged. Dark green = LAM + RGD; light green = LAM + RAD. Statistical significance was determined via unpaired, one-tailed student's t-test. ns = not significant; $p < 0.05$ = *; $p < 0.01$ = **; $p < 0.001$ = ***.*

Discussion

We demonstrate the ability to identify pericyte-derived myofibroblasts using a pericyte lineage reporter mouse treated with bleomycin to induce lung injury. Using this model system, we have identified the pulmonary pericyte as a population of myofibroblast progenitors. We showed that pericytes adopt a tissue-remodeling phenotype in bleomycin-induced lung injury, and we identified the extracellular matrix ligand (RGD) in fibronectin as a potentiator of pericyte-to-myofibroblast transition *in vitro*.

The body of work describing pericyte contributions to fibrosis, and the pericyte-to-myofibroblast transition, is still nascent [65,194,196,225–228]. Foundational studies have shown pericytes can transition into myofibroblasts in disease [196,225,227], with additional research exploring possible molecular mechanisms driving the transition [65] and pericyte-specific knockdown studies, which confer protection in fibrotic disease models [45,210,228]. The detailed characterization of pericytes in this work through histological analysis, high-dimensional flow cytometry, and gene ontology RNASeq analyses provides an unprecedented level of insight into the response of pericytes in the early phases of repair following acute lung injury. Our characterization of pericytes using a variety of surface markers through extensive cytometric phenotyping contributes to the existing literature by comparing them to the broader stromal cell population. The ability to contextualize our population of interest among the broader stromal cell population allows for relative comparisons to be made between our pericyte lineage and the broader stromal cell population, something not possible without high-dimensional cytometric analyses. The abundance of pericyte collagen production (Col1a1+) within the larger stromal population agrees with prior pericyte research in kidney fibrosis [218]. Contrastingly, pericytes make up a much smaller proportion of the stromal contractile (αSMA+) population. This heterogeneity in relative contributions of myofibroblast markers to stromal cell population provides further evidence to support the growing understanding of fibroblast heterogeneity, which has mostly been obtained via single-cell RNA sequencing, showing that myofibroblasts originate from a variety of cell populations.

This new focus on myofibroblastic heterogeneity is revealing that phenotypes once considered pan-myofibroblastic (based on whole population analyses) can be attributed to distinct subpopulations of myofibroblasts [33,39,229]. Our data in Figure 3.5 suggest that pericytes are the primary collagen 1-producing stromal cells in both healthy and bleomycin-treated lung.

Our work examines integrin expression and activation for the first time in the murine Myh11 lineage model of pericytes. Integrins are known to be important in mediating fibroblast differentiation into myofibroblast phenotypes [199,210,222,230], so we posited that they might play a role in the pericyte-to-myofibroblast transition. Our findings show a pronounced increase in pericyte αv and α6 protein expression in response to bleomycin insult. This enhanced adhesion profile is not unexpected; ligand density for ECM-binding integrins increases in fibroproliferative injury [231,232]. While the ratio of αv to α6 surface expression is not significantly altered in the pulmonary pericyte population of murine lungs treated with bleomycin, the amount and activation/engagement of αv(β3) are both significantly increased in the injury model. The lack of significant increase in total fibronectin proximal to pericytes following bleomycin induced injury is curious, especially in light of significantly heightened levels of active αvβ3 integrin on the surface of pericytes. However, the bleomycin model of lung injury is a resolving model and these data may point to a more balanced fibroproliferative repair compared to pathological, chronic remodeling observed in human fibrotic diseases. These data further suggest additional regulatory mechanisms are at play that contribute to αvβ3 activation in

the pericyte population, including known inside-out mechanisms of integrin activation due to exogenous agonists that are known to be present in the provisional wound repair environment, such as thrombin and others [224,233]. We might also speculate, based on our previous work, that contractile (αSMA+) pericytes engage a known integrin switch driven through a mechanically sensitive conformational change within fibronectin's integrin binding domain that drives a strong preference for fibronectin-αvβ3 engagement [199,200,222]. In total, these data strongly suggest that there is a mechanically responsive/active, provisional matrix-engaged pericyte population during lung injury repair.

Studies of pericyte behaviors have been historically limited by the available approaches for identifying and tracking them in living tissues. Given the wide range of non-unique surface markers that pericytes express [192], morphologic criteria and physical orientation relative to capillary endothelium have been used to positively identify pericytes [214]. However, this morphologic description is limiting when the goal is to interrogate pericyte transitions into other cell types. The Myh11 lineage system is one of many published murine models [40] that has provided a means to identify this cell population and its lineage *in vivo*. However, we cannot assume that the pericytes labeled by this Myh11 lineage tracing system are identical to those labeled by other lineage tracing systems, nor can the Myh11 lineage be assumed to universally label all pericytes. Since the Myh11 lineage cell population also includes smooth muscle cells (SMCs) [197,234,235], and since SMCs have been shown to also express CD146 [236], it is possible that our RNAseq and cytometric

results include contributions from SMCs, in addition to pericytes. Given this caveat, we can still conclude that the mural cell population, which includes both pericytes and SMCs, are active participants in fibrotic remodeling following bleomycin-induced injury in the lung. And, considering our RNAseq and cytometric data in light of our histological data, which demonstrate based on cell morphologies and proximity to capillaries that pericytes are the predominant cells exhibiting myofibroblastic behaviors, we can conclude that if SMCs also undergo myofibroblast differentiation, their role in fibrotic tissue remodeling is relatively minor compared to that of pericytes.

We explored αv integrin, a fibronectin/provisional matrix binding protein known to potentiate myofibroblast phenotypes, in the context of pericyte-to-myofibroblast differentiation. However, αv does not only bind to RGD, but has many ligands, and studies of αv in the microcirculation tend to focus on αv-platelet endothelial cell adhesion molecule (PECAM) interactions. We do not evaluate the contributions of endothelial cell remodeling or behaviors to pericyte-to-myofibroblast transitions, but we acknowledge the remodeling of microvessel networks as essential components of lung fibrosis [237].

We acknowledge there are limitations in our model systems and techniques which must be considered in the interpretation of our results. The bleomycin injury model for resolving lung fibrosis has been extensively used and cited in literature, but does not accurately recapitulate many aspects of human lung fibrosis [68,215,238]. It should be thought of as a platform to study cell and tissue-scale phenomena in fibroproliferative injury, which has enabled our extensive research on myofibroblasts in fibrotic lung injury

[201,202,222]. The cell dissociation process necessary for preparing cells for cytometry sorting and analyses, including RNASeq, subjects the isolated cells to a brief period of enzymatic and mechanical perturbation, which may skew data in unforeseen ways, though care was taken to limit known artifactual stimulants of cells, such as titration of digestion and lysis steps, and addition of DNAse and EDTA to sorting and digestion steps. Additionally, published research verifies the stability of many of our surface markers in our digestion model [239]. The spectral flow cytometry we employed provides an unprecedented, highly dimensional cytometric dataset, but potential fluorescence overlap limits the number of cell populations that can be accurately compared within a given gating hierarchy.

Translating known downstream signaling of integrins in fibroblasts to other stromal cell populations, including pericytes, has provided some insight into biologic processes required for the generation of myofibroblastic cell phenotypes from non-fibroblast precursor populations. Myocardin-related transcription factor (MRTF) is an essential component of integrin-mediated myofibroblast activation, and recent studies have shown its requirement for various stromal cell to myofibroblast transitions [59,65]. Likewise, YAP/TAZ/Hippo signaling is known to regulate myofibroblast phenotype and is dysregulated in disease [240], while studies of YAP/TAZ deficient pericytes have demonstrated the loss of YAP/TAZ in Gli1 perivascular stromal cells is protective in fibrotic injury of kidneys [241,242]. The increase in active pericyte αvβ3 measured in this study is known to potentiate those signaling cascades, but direct measurement of these pathways was outside the scope of this manuscript.

Many other opportunities to investigate myofibroblast biology as it pertains to pericytes are enabled by the Myh11 pericyte lineage, and this will allow for a more complete understanding of the process by which pericytes and other stromal cells can be driven towards pathologic myofibroblastic behavior. While myofibroblast responses to various collagenous and fibronectin-rich substrates are well understood [200,232,243], pericyte responses to the changes in ECM composition during injury are less understood. The study of basement membrane remodeling in fibrotic injury as it coincides with generation of provisional matrix has begun here with our evaluation of fibronectin in locations that are proximal to pericytes. Indeed, our findings link ECM-based integrin ligand RGD with cell surface αv integrin activation in the pericyte-to-myofibroblast transition. Further study into the mechanisms underpinning phenotypic changes in pericytes during lung fibrosis may reveal new potential diagnostic and therapeutic targets for lung fibrosis.

Materials and Methods

Mice

All procedures were performed in accordance with the Institutional Animal Care and Use Committee of the University of Virginia. Myh11-CreERT2 ROSA STOPfl/fl tdTomato mice 6-12 weeks of age were injected intraperitoneally with 1mg tamoxifen (10mg/mL of tamoxifen (Sigma-Aldritch, St.Louis, MO, USA) in 100 uL peanut oil (Sigma-Aldritch) each day for 10 days over two weeks.) Mice were rested for four weeks to allow clearance of tamoxifen, oil, and transient circulating cells before subsequent procedures.

Tracheal Bleomycin Administration

Animals were anesthetized with a ketamine/xylazine cocktail (60-80/5-10 mg/kg). Animals were placed on a commercial board from Hallowell EMC and hung by their incisors at 45 degrees. Bleomycin sulfate (1-3 U/kg) (Meitheal Pharmaceuticals, Chicago, IL, USA) in saline or saline vehicle control (2uL/gm) was instilled into the lungs through the trachea through angiocatheter tubing placed down the animal's throat and connected to a 1mL syringe. Mice were monitored during and post- procedure to ensure recovery from anesthesia and not returned to housing until they were fully ambulatory and breathing normally.

Harvest of Lung Tissue

Animals were euthanized two weeks post-bleomycin via CO2 asphyxiation with secondary cervical dislocation. Mice were sprayed with 70% ethanol to sterilize and mat fur, and an incision was made through the skin extending from 5mm below the sternum to the mandible. A bilateral incision was made perpendicular from the abdominal end of the previous incision, exposing the caudal edge of the ribcage and the abdominal cavity and peritoneum. The peritoneum along the caudal ribcage edge was cut along the entire length of the ribcage. The diaphragm was dissected away and the ribcage cut or moved away to expose the cardiopulmonary unit. The inferior vena cava was cut and the heart perfused with 5-10ml of sterile saline or PBS, until blanching of the lungs was complete.

In the submandibular area, salivary glands were dissected away and the trachea cannulated with a blunt tipped needle or trachea tube and secured with suture. Lungs were then washed 3x with sterile saline or PBS, and then inflated with 2% UltraPure LMP Agarose (ThermoFisher, Waltham, MA, USA) for histology or sterile saline/PBS for lung dissociation. The entire cardiopulmonary unit was dissected out of the thorax and placed into saline/PBS on ice for subsequent protocols.

Histologic Staining

Lungs for histologic analyses were submerged in 4% paraformaldehyde (PFA) for 30 minutes or were fresh frozen. Lungs were placed in 30% sucrose solution until they sink,

at which point they were embedded in OCT and frozen. Lungs were cryosectioned at 8 or 30 micron thickness for histochemical and immunofluorescent staining.

Slides for histochemical analyses were and stained with hematoxylin and eosin (Ricca, Arlington TX, USA) and Picrosirius Red (Abcam, Cambridge MA, USA) following manufacturer protocols.

All steps performed in a hydration chamber. All antibodies and dilutions are listed in Table 3.1. OCT was washed away with PBS and section was fixed (if necessary) with 4% PFA or methanol. Section was then permeabilized for 1 hour with 0.5% TritonX-100 in PBS. Section was then blocked with the mouse serum (if not available, FBS) at 5% and the secondary antibody host serum at 5% in PBS for 1 hour at RT or overnight at 4C. Primary antibodies added for 3 hours RT or overnight at 4C. Section was washed with PBS for 5m 5x. Secondaries and conjugated primaries were added for 3 hours RT or overnight at 4C. Section was washed with PBS for 10m 5x. Tissue was washed and mounted with Prolong Diamond (ThermoFisher). DAPI Counterstain from mounting with Prolong Diamond with DAPI (ThermoFisher)

Immunofluorescence Imaging

Images captured on an UltraView Vox Spinning Disk Confocal Microscope (PerkinElmer, Waltham MA, USA) using Volocity 6.3.1 software (PerkinElmer) and Nikon PlanFluor 20x and Nikon Apo TIRF 60x objectives, or a BZ-X810 widefield fluorescence microscope (Keyence, Osaka, Japan) Tiled images taken at 10% overlap and

stitched using in-house software (https://bitbucket.org/pythoncardiacmodel/publicpythoncardiacmodel/src/master/) and Volocity. Analyses and particle counts performed in Volocity or Fiji/Imagej [244].

Lung Dissociation/Single Cell Isolation

All steps performed on ice unless otherwise indicated. Heart, fat, connective tissue and primary bronchi were dissected away from the lung lobes, minimizing non-lobe tissue. Lung lobes/large chunks from a single mouse were placed into into a 2ml microfuge tube and chopped into small (< 2mm) chunks with sterile scissors. 1ml of digestion solution (TM Liberase at 4 units/mL (Roche, Basel, Switzerland) and DNAse Type I at 800 units/mL (ThermoFisher) made in sterile PBS) was added to each tube. Tubes were placed on a rotisserie at 37C for 20 minutes. Digest was then mechanically ground through 100um nylon filters (ThermoFisher) and placed in ACK RBC Lysis buffer (ThermoFisher) for 3 minutes at RT or as needed. Cells were pelleted and, if further cleanup was needed, a densisty gradient was used (debris removal soluton, Miltenyi, Bergisch Gladbach, GER) according to manufacturer direction.

Cell Culture

Primary cell culture performed in DMEM (ThermoFisher, Waltham MA, USA) with fibronectin-depleted (depleted via column purification using gelatin sepharose) FBS at 10% on glass coverslips coated with 10ug/mL murine fibronectin (natural mouse fibronectin, Abcam) or laminin (laminin mouse protein, natural, ThermoFisher).

Inhibition studies included 100 μM of Cyclo(-RGDfK) or Cyclo(-RADfK-) (Anaspec, Fremont CA, USA) in PBS to single cell suspensions immediately prior to plating. Cells allowed to adhere overnight, and media was replaced. Cells fixed at 24 hours, permeablized, and stained.

Flow Cytometric Analyses

All antibodies and dilutions are listed in Table 3.1.

Live cell sorting performed on AutoMACS (Miltenyi) and BD Influx (BD Biosciences, San Jose, CA, USA) sorters. Cells suspended in FACS buffer (PBS+5% FBS+1mM EDTA) for staining and sorting. CD146 (LSEC) MACS Beads (Miltenyi) added to cells according to manufacturer directions and sorted in a poseld2-protocol on the AutoMACS.

Phenotyping panels performed on Cytek Aurora spectral flow cytometers with fixing and permeablizing by Fix&Perm kit (ThermoFisher). Cells suspended in FACS buffer (PBS+5% FBS+1mM EDTA) for staining and sorting. FMO gating for positivity visible in Figure 3.9

RNA Sequencing

Cells isolated from murine lung were used to generate mRNA libraries for RNA sequencing. Extraction and library prep were performed commercially with rRNA depletion (GeneWiz, South Plainfield, NJ, USA). All libraries were sequenced using single lane of the Illumina HiSeq sequencer to generate 150bp paired-end reads at a total

read depth of 350 million reads (GeneWiz). Following sequencing, the resulting fastq files were processed to remove low-quality reads (Phred quality score < 20) and the presence of any adapter sequences using TrimGalore[245]The resulting quality of each sample was independently evaluated using FastQC[246]. Files that passed QC were further processed to obtain gene expression counts following a previously defined protocol by Pertea et al.[247]. Briefly, reads were aligned to the mouse genome (UCSC mm10) using the HISAT2 aligner[248] and transcripts assembled with StringTie[249]. The resulting StringTie output was used to produce read coverage tables for input into DESeq2[250].

RNA Data Analysis

DESeq2's median of ratios method was used to normalize for differences in sequencing depth and RNA composition between samples. Normalized counts were subsequently used to quantify differential expression in the diseased state (bleomycin vs. saline control). All gene ontologies were curated from The Gene Ontology (GO) Consortium or the MSigDB NABA_MATRISOME gene set[221], with murine GO homologes sourced from Xijin Ge et.al. [251]. Gene set enrichment analysis (GSEA) was used to identify significantly enriched gene sets performed using the GSEA-MSigDB desktop application and default parameters[252].

Statistical analyses

A two-way ANOVA or a Student's t-test was performed using Prism (GraphPad, San Diego CA, USA), as indicated in each figure caption. Statistical significance was asserted at p-values < 0.05. All data are presented as average + standard deviation.

Table 3-1: Antibodies and Dilutions

ANTIBODY	CLONE	DILUTION	PRODUCT INFO
FLOW			
ASMA	1A4	1/200	NBP2-34522
A6 INTEGRN/CD49F	GoH3	1/100	Bio legend 313612
AV INTEGRIN/CD51	RMV7	1/100	BD 551380
PDGFRB/CD140B	APB5	1/100	Bio Legend 136008
PDGFRA/CD140A	APA5	1/100	ThermoFisher 25-1401-82
CD31	MEC 13.3	1/50	BD 612802
EPCAM/CD326	EBA-1	1/100*	BD 743544
CD146	ME-9F1	1/100	BD 562232
CD45	30-F11	1/100*	Bio Legend 103147
TER119/RBC	TER-119	1/100*	BD 740686
COL1A1	poly	1/100	ABNova PAB17204
L/D NIR	n/a	as directed	ThermoFisher L34975
COMBINED DILUTION OF ALL 'DUMP' ABS IS 1/100, EACH INDIVIDUAL AB IS <1/100			

HISTOLOGY			
CD31	MEC 13.3	1:100	BioLegend 102504
ASMA	1a4	1:200	NBP2-34522
FIBRONECTIN	poly	1:200	Abcam ab2413
ACTIVE AVB3 INTEGRIN/WOW1	n/a	1:200	gift of Sanford Shattil, University of California, San Diego
SECONDARIES		1:1000	AF conjugates

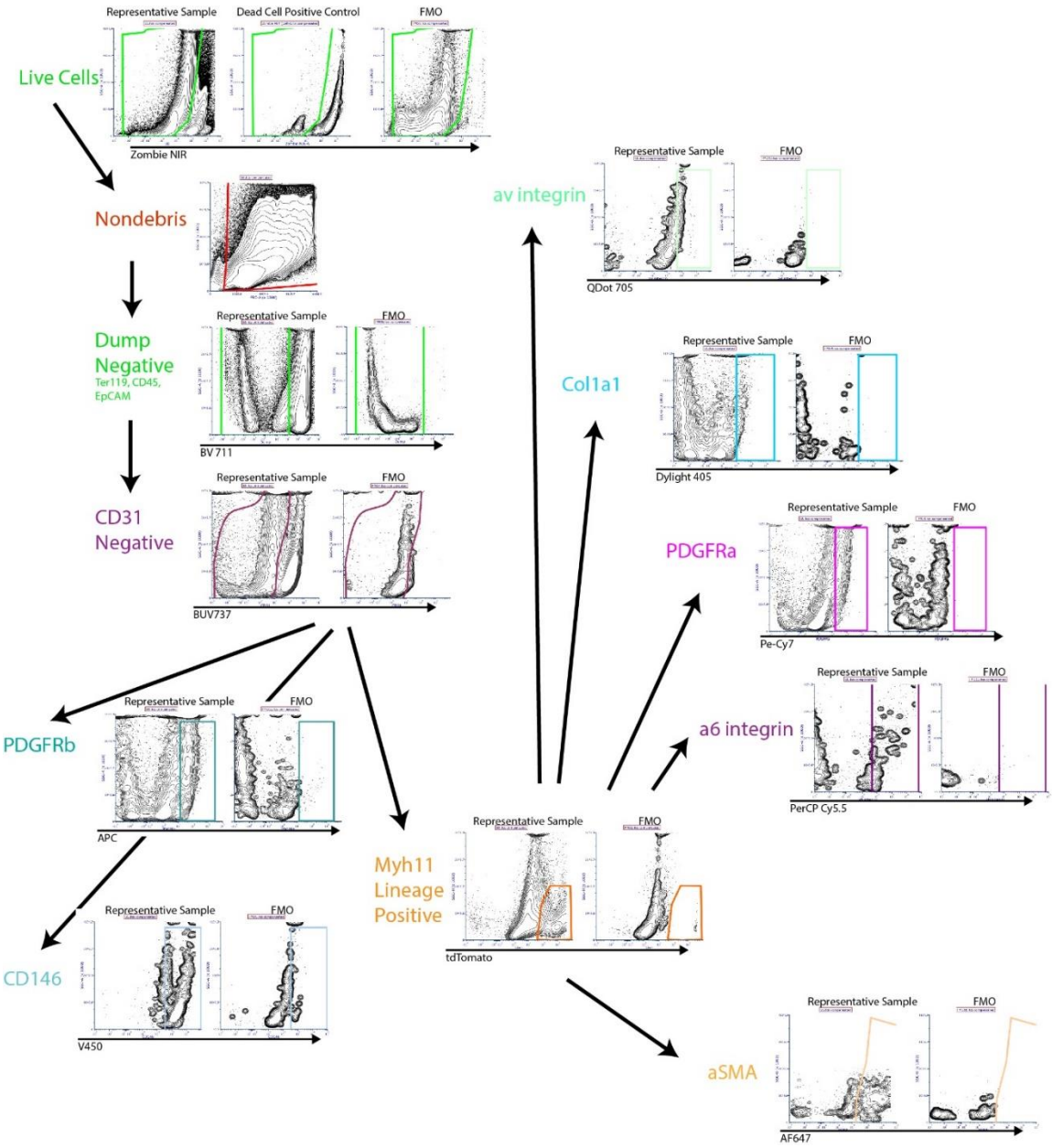

Figure 3.9 Methods - Fluorescence Minus Ones (FMOs) and positive gating for flow cytometric probes. Representative plots of the gating strategy for cellular phenotyping. Some positive gates were simplified to rectangles for readability.

Chapter 4 Role of KLF4 in Murine Lung Pericyte Phenotypic Plasticity

Abstract

The ability of perivascular cells to differentiate, transdifferentiate, or be classified as pluri- or multi-potent stem cells been the subject of much research and debate. Herein we describe experimental observations to support the concept of pericyte plasticity, beyond the myofibroblastic pericyte described previously. Using a murine pericyte reporter mouse with pericyte-specific knockdown of stem cell transcription factor KLF4, we report KLF4-dependent changes in pericyte surface marker expression and mRNA in a lung injury model. We describe how our observations fit in to a body of observations on the potential role of KLF4 in pericyte phenotypic plasticity.

Introduction

Depending on the specific definitions used to identify and study the pericyte, compelling evidence exists to classify pericytes as both a phenotypically plastic stem cell [253–256] and a terminally-differentiated cell that does not have the ability to differentiate into other cell types [257]. Recently, the process of defining various stromal cell types has shifted away from rigid, surface-antigen derived definitions and has focused on narrow, antigen-agnostic definitions enabled by genetic lineages or -omics approaches with single-cell resolution [38,191,228,258,259]. Whereas in the past, a PDGFRβ^{+}, NG2^{+} cell as defined by surface antibody staining would likely be called a pericyte, today, single cell RNA sequencing of tissues or cell lines might identify a cluster of PDGFRβ^{-high} expressing cells, upon which a strict cell type is not assigned [33] but would be have been defined as pericytes in the old scheme.

Due to the ubiquity of pericytes across tissue beds and rapid phenotypic changes in culture systems, pericytes likely comprise a non-insignificant proportion of primary stem cell lineages which have previously been described in literature, including mesenchymal stem cells (MSCs)[260] and adipose-derived stem cells (ASCs)[261]. This pericyte contribution towards these populations is often described not by mention of pericytes as a contributing cell type, but by the characterization and isolation of stem cells using pericyte markers, such as CD146 [63,262–265] and PDGFRβ [266–269], with a recent exception confirming pericytes specifically as a source of ASCs [270].

These changing definitions complicate efforts to draw a contiguous line through developments in our understanding of pericyte biology, and place a large burden upon the individual to maintain a consistent mental model of 'pericytes' as they relate to stem cell research. On a positive note, with the increasing complexity and granularity of cellular definitions comes a litany of new descriptive data supporting the theory of 'stemmy' perivascular cells, and the factors required for pericytes to differentiate into a variety of other cells.

The Yamanaka Factors (OCT4, SOX2, cMyc, KLF4) identified as essential factors to induce pluripotent stem cells from fibroblast lines in culture[271] have subsequently been studied as factors enabling the plasticity of a variety of tissue-resident mesenchymal and stromal cell populations in regeneration, injury, and cancer. These cells have been given several names (Mesenchymal stem/stromal cells, adipose-derived stem cells, etc), and their plasticity described as cellular de-differentiation, transdifferentiation,

deprogramming, stemness, and phenotype switching [45,197,212,235,272–283]. The commonality between these definitions and characterizations is the ability of the described cells to change from a presumed quiescent, terminally-differentiated phenotype into a disease-interacting, phenotypically plastic cell in a Yamanaka Factor-dependent manner.

Recent discoveries of pericyte plasticity have been enabled by the discovery of mural cell-specific expression of smooth myosin heavy chain 11 (Myh11) and the subsequent generation of Myh11 lineage reporter mice with lineage-specific Yamanaka Factor knockouts [235,284]. These model systems have revealed multiple Yamanaka Factor-dependent pericyte phenotypes[45,212,213] in contexts of cancer metastatic microenvironments, atherosclerosis, and angiogenic wound healing. Specifically, KLF4 was found to modulate perivascular cell investment in the microvasculature[212], with Myh11 lineage KLF4 required for the de-differentiation of pericytes and an increase pro-remodeling, pro-cancer metastatic extracellular matrix environment[45].

The contents of this chapter are the description and characterization two KLF4-dependent pericyte phenotypes that were observed over the course of research performed for Chapter 3 of this dissertation. As these data were acquired in pursuit of other research, this chapter will be highly descriptive, with analyses of mRNA and FACS data with limited statistical rigor. The first observed KLF4-dependent phenotype is one of a pericyte-vascular endothelial ‘double positive cell’, which will hereafter be referred to as “DP” pericytes. The second KLF4-dependent phenotype explored is the myofibroblastic differentiation of pericytes.

Results

Pericyte-endothelial double-positive cells exist in the lung.

Figure 4.1 shows representative FACS plots of four samples of pericytes sorted from whole lung digest obtained from induced Myh11-CreERT2 ROSA STOPfl/fl eYFP+/+ Klf4fl/fl ($KLF4^{\Delta/\Delta}$) and Myh11-CreERT2 ROSA STOPfl/fl eYFP+/+ Klf4wt/wt ($KLF4^{wt/wt}$) mice treated with either bleomycin to induce injury or saline (vehicle control). Cells are live, singlets, negative for 'dump' makers Ter119 (erythrocytes), CD45 (myeloid lineage), EpCAM (epithelial cells, and positive for the Myh11 reporter eYFP (Myh11 lineage positive). All FACS plots shown have endothelial marker CD31 on the y axis, with pericyte marker CD146 on the x axis. Cells that are double positive for the Myh11 reporter eYFP and CD31 are considered "DP" pericytes. $KLF4^{wt/wt}$ DP pericytes (upper right quadrant, UR) are measured at a frequency of 67.97% two weeks after saline treatment and a frequency of 93.93% two weeks after bleomycin treatment. There is a commensurate reduction in the frequency of CD31-negative pericytes (lower right quadrant, LR) between saline-treated and bleo-treated lungs, with a frequency of 24.98% in saline treatment compared to 5.16% in the bleomycin treated group. $KLF4^{\Delta/\Delta}$ pericytes express CD31 at a much lower level than $KLF4^{wt/wt}$ pericytes in the saline treated group, with DP pericyte frequencies of 5.98% and 67.97%, respectively. This DP pericyte phenotype also exists in lungs treated with bleomycin**,** with $KLF4^{\Delta/\Delta}$ pericytes again expressing CD31 at a much lower level than $KLF4^{wt/wt}$ pericytes in the saline treated group, with DP pericyte frequencies of 16.98% and 93.93%, respectively. The

change in frequency of DP seen in bleomycin treated KLF4$^{\Delta/\Delta}$ pericytes (5.98% to 16.98%, or 2.83 fold increase) is greater than that measured in bleomycin treated KLF4$^{wt/wt}$ pericytes (67.97% to 93.93%, or 1.38 fold increase), while the total proportion of DP pericytes remains much higher in KLF4$^{wt/wt}$ pericytes than in KLF4$^{\Delta/\Delta}$ pericytes for both saline and bleomycin treatment groups.

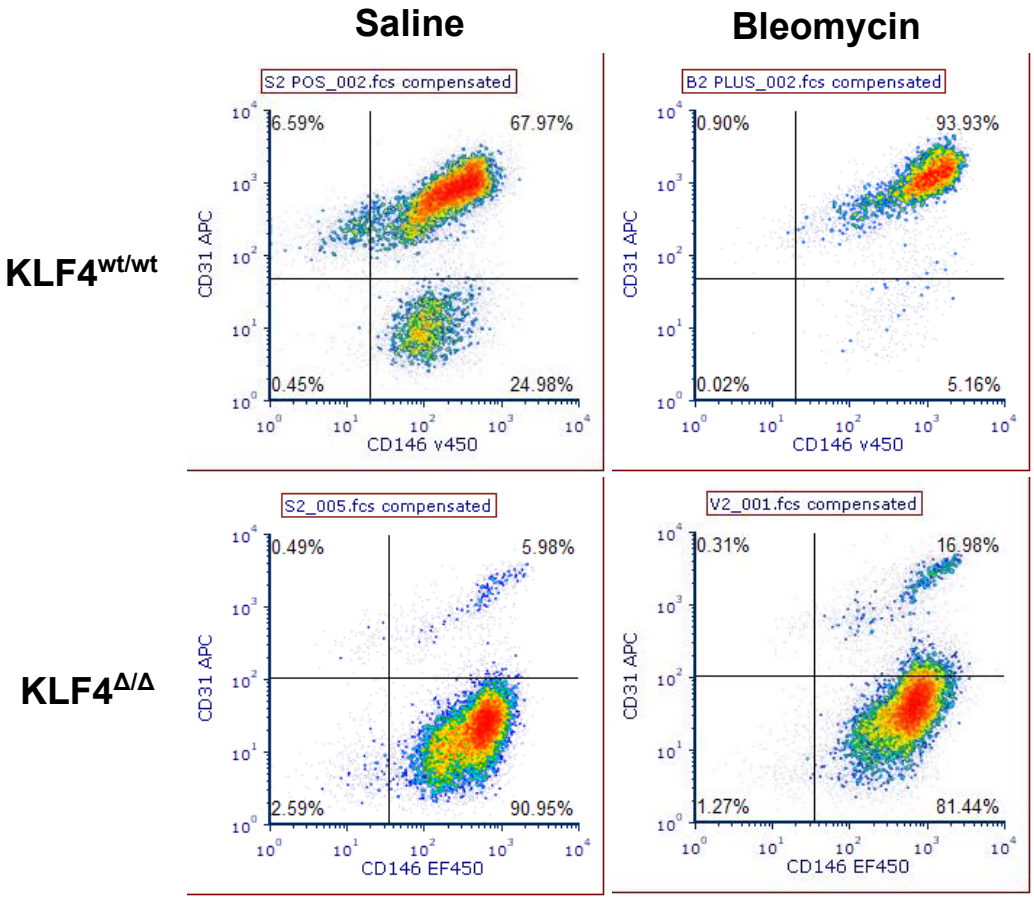

Figure 4.1 KLF4-dependent Pericyte Surface Expression of CD31 in Bleomycin Lung Injury. Myh11 lineage cells isolated from saline or bleomycin-treated lungs (columns) and two Myh11 lineage genotypes (rows). Representative FACS density plots of perivascular marker CD146 (x-axis) and vascular endothelial marker CD31 (y-axis).

The cell populations described in Figure 4.2, top were generated by FACS. After gating for live, singlet, and 'dump' negative cells, cells were sorted into one of four groups: Myh11 lineage positive, CD146 positive, CD31 positive DP pericytes; Myh11 lineage positive, CD146 positive, CD31 negative pericytes; Myh11 lineage negative, CD146 negative, CD31 positive endothelial cells; Myh11 lineage negative, CD146 negative,

CD31 negative stromal cells. These four populations were collected and processed for library preparation. However, for $KLF4^{\Delta/\Delta}$ lungs, only the pericyte population was able to generate sufficient material for a usable library for the Illumina sequencing. Additionally, neither the $KLF4^{\Delta/\Delta}$ or $KLF4^{wt/wt}$ lungs provided sufficient stromal cells for Illumina sequencing, and thus no stromal cell RNA was sequenced.

The samples which were able to be sequenced are clustered based on similarity derived from a Pearson's correlation test in Figure 4.2, bottom. The plot is mirrored along the x:y diagonal, with self:self comparisons necessarily meeting 1.0 (identical) correlation coefficient values. The dendrogram adjacent to each axis provides information to the relative similarities of each sample to its neighbors. The bifurcations along branches moving from the tip towards individual samples indicate increasing similarities as the bifurcation nest depth increases. Thus, the final bifurcation is the most granular separation of samples by correlation and the preceding bifurcations become broader in their criterion for splitting. The three sorted types of cells are organized by similarity, with pericytes along the left, endothelial cells on the right, and DP pericytes found within the endothelial population. This nesting of DP pericytes within the endothelial cluster indicates a similarity high enough to consider those two sorted cell populations as subsets of a single larger population.

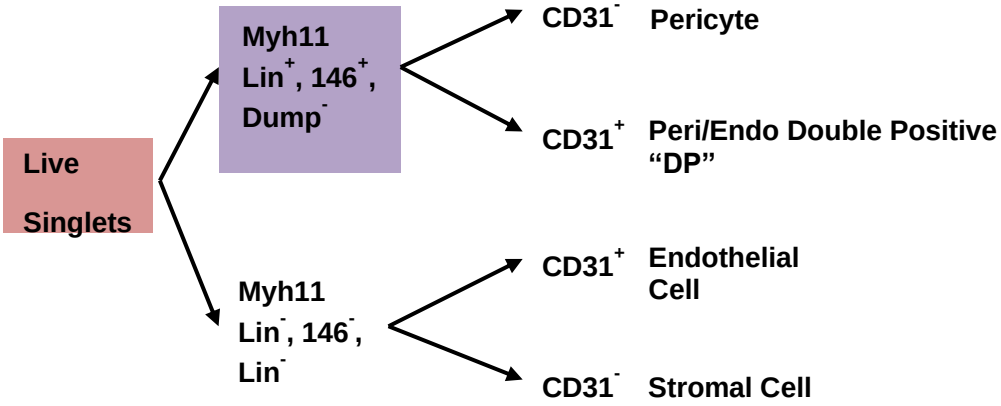
Live
Singlets
Myh11
Lin+, 146+,
Dump-
CD31- Pericyte
CD31+ Peri/Endo Double Positive
"DP"
Myh11
Lin-, 146-,
Lin-
CD31+ Endothelial
Cell
CD31- Stromal Cell

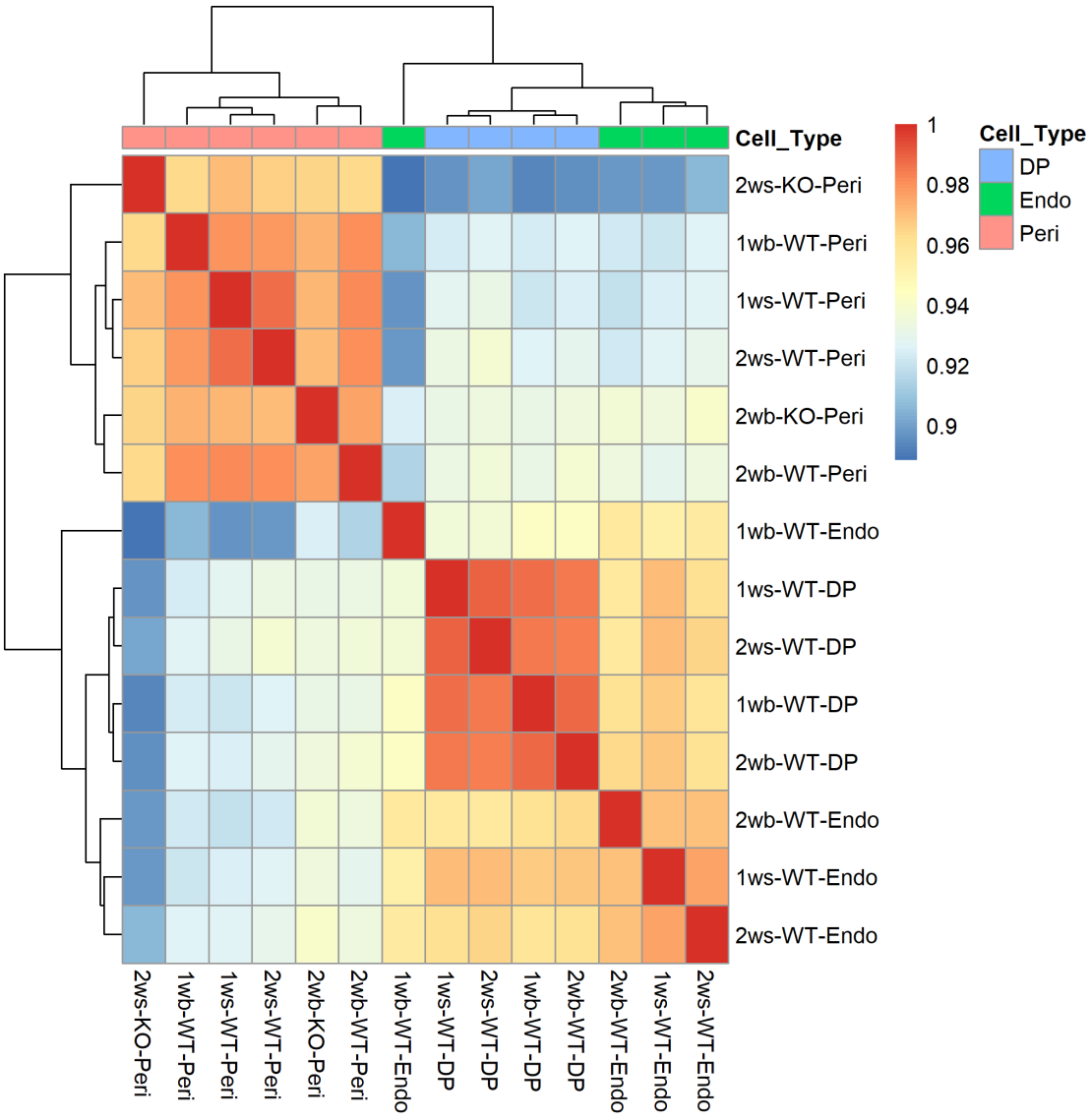
Cell_Type
2ws-KO-Peri
1wb-WT-Peri
1ws-WT-Peri
2ws-WT-Peri
2wb-KO-Peri
2wb-WT-Peri
1wb-WT-Endo
1ws-WT-DP
2ws-WT-DP
1wb-WT-DP
2wb-WT-DP
2wb-WT-Endo
1ws-WT-Endo
2ws-WT-Endo
1
0.98
0.96
0.94
0.92
0.9
Cell_Type
DP
Endo
Peri

Figure 4.2 Clustering of Pericytes, Endothelial Cells, and Double-Positive Pericytes Using RNASeq Expression Data. Top: Schematic for gating hierarchy and cellular classifications for FACS into RNA Sequencing. Bottom: Hierarchical clustering of Pearson correlations along rows and columns of fourteen RNASeq samples sorted from bleomycin or saline-treated mouse lung at one or two weeks post treatment. Color scale of correlation coefficient runs from 0.9 (blue) to 1.0/identical (red). Sample names are formatted as time and treatment-KLF4 genotype-cell type. 2ws indicates two weeks post saline administration; 1wb indicates one week post bleomycin treatment. WT indicates $KLF4^{wt/wt}$ *pericytes, while KO indicates* $KLF4^{\Delta/\Delta}$ *pericytes. DP indicates a Myh11 lineage positive, CD146 positive, CD31 positive cell; Endo indicates a Myh11 lineage negative, CD146 negative, CD31 positive cells; Peri indicates a Myh11 lineage positive, CD146 positive, CD31 negative cell.*

KLF4 as a requirement for pericyte differentiation into myofibroblasts

As there was enough material gathered from $KLF4^{\Delta/\Delta}$ or $KLF4^{wt/wt}$ pericytes for RNASeq in both bleomycin and saline treatment, we are able to measure the impact of KLF4 on pericyte phenotype in the bleomycin lung injury model. Figure 4.3 visualizes fold changes in expression in bleomycin-treated lungs with an array of gene categories which are pathologically relevant in tissue remodeling and fibrosis. Fold changes are reported as a log2 transformation of the expression ratio of bleomycin to saline. Increases in gene expression in bleomycin relative to saline are positive numbers and reported as shades of red, while decreases in bleomycin relative to saline are negative numbers and reported as shades of blue. Changes in directionality of pericyte response to bleomycin are indicated by inversions of colors across a row of both pericyte genotypes for a given gene. For example, mRNA for interleukin 1-α (Il1a) is shown to be downregulated in response to bleomycin in the $KLF4^{wt/wt}$ pericyte but is upregulated in the $KLF4^{\Delta/\Delta}$ pericyte population.

Manually curated gene lists are informative when exploring specific hypotheses, but an unbiased, manual accounting of the tens of thousands of transcripts measured by the Illumina platform is impossible. Thus, we turn to gene ontologies: a peer reviewed, functionally annotated and categorized gene clustering which pools genes by cellular component (CC), molecular function (MF), or biologic process (BP) developed by the Gene Ontology (GO) group [219]. Included in these three domains is an additional category,

Matrisome, which is a peer-reviewed subset of GeneSets with more granular specificity to tissue remodeling processes than those provided from the GO group.

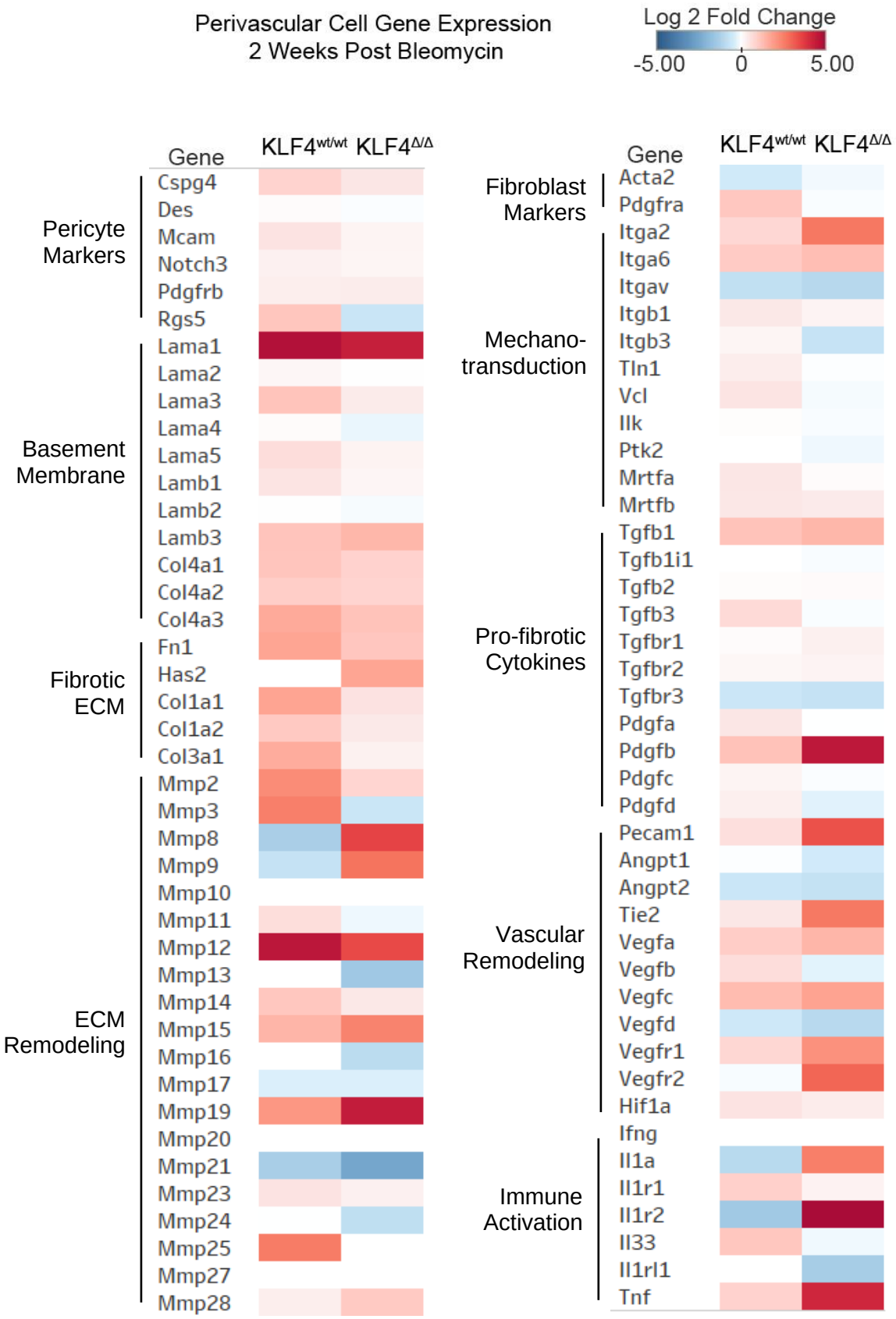
Perivascular Cell Gene Expression
2 Weeks Post Bleomycin
Log 2 Fold Change
-5.00
0
5.00
Gene
KLF4wt/wt
KLF4Δ/Δ
Pericyte Markers
Cspg4
Des
Mcam
Notch3
Pdgfrb
Rgs5
Basement Membrane
Lama1
Lama2
Lama3
Lama4
Lama5
Lamb1
Lamb2
Lamb3
Col4a1
Col4a2
Col4a3
Fibrotic ECM
Fn1
Has2
Col1a1
Col1a2
Col3a1
ECM Remodeling
Mmp2
Mmp3
Mmp8
Mmp9
Mmp10
Mmp11
Mmp12
Mmp13
Mmp14
Mmp15
Mmp16
Mmp17
Mmp19
Mmp20
Mmp21
Mmp23
Mmp24
Mmp25
Mmp27
Mmp28
Gene
KLF4wt/wt
KLF4Δ/Δ
Fibroblast Markers
Acta2
Pdgfra
Mechano-transduction
Itga2
Itga6
Itgav
Itgb1
Itgb3
Tln1
Vcl
Ilk
Ptk2
Mrtfa
Mrtfb
Pro-fibrotic Cytokines
Tgfb1
Tgfb1i1
Tgfb2
Tgfb3
Tgfbr1
Tgfbr2
Tgfbr3
Pdgfa
Pdgfb
Pdgfc
Pdgfd
Vascular Remodeling
Pecam1
Angpt1
Angpt2
Tie2
Vegfa
Vegfb
Vegfc
Vegfd
Vegfr1
Vegfr2
Hif1a
Immune Activation
Ifng
Il1a
Il1r1
Il1r2
Il33
Il1rl1
Tnf

Figure 4.3 KLF4-Dependent Expression of Pro-Fibrotic and Tissue-Remodeling Genes in Myh11 Lineage Pericytes in Lung Injury. Log2-normalized fold change (bleomycin-treated lung vs saline-treated control lung) compared between KLF4$^{wt/wt}$ and KLF4$^{\Delta/\Delta}$ Myh11-lineage pericytes. Genes shown manually selected as representative of their descriptive category.

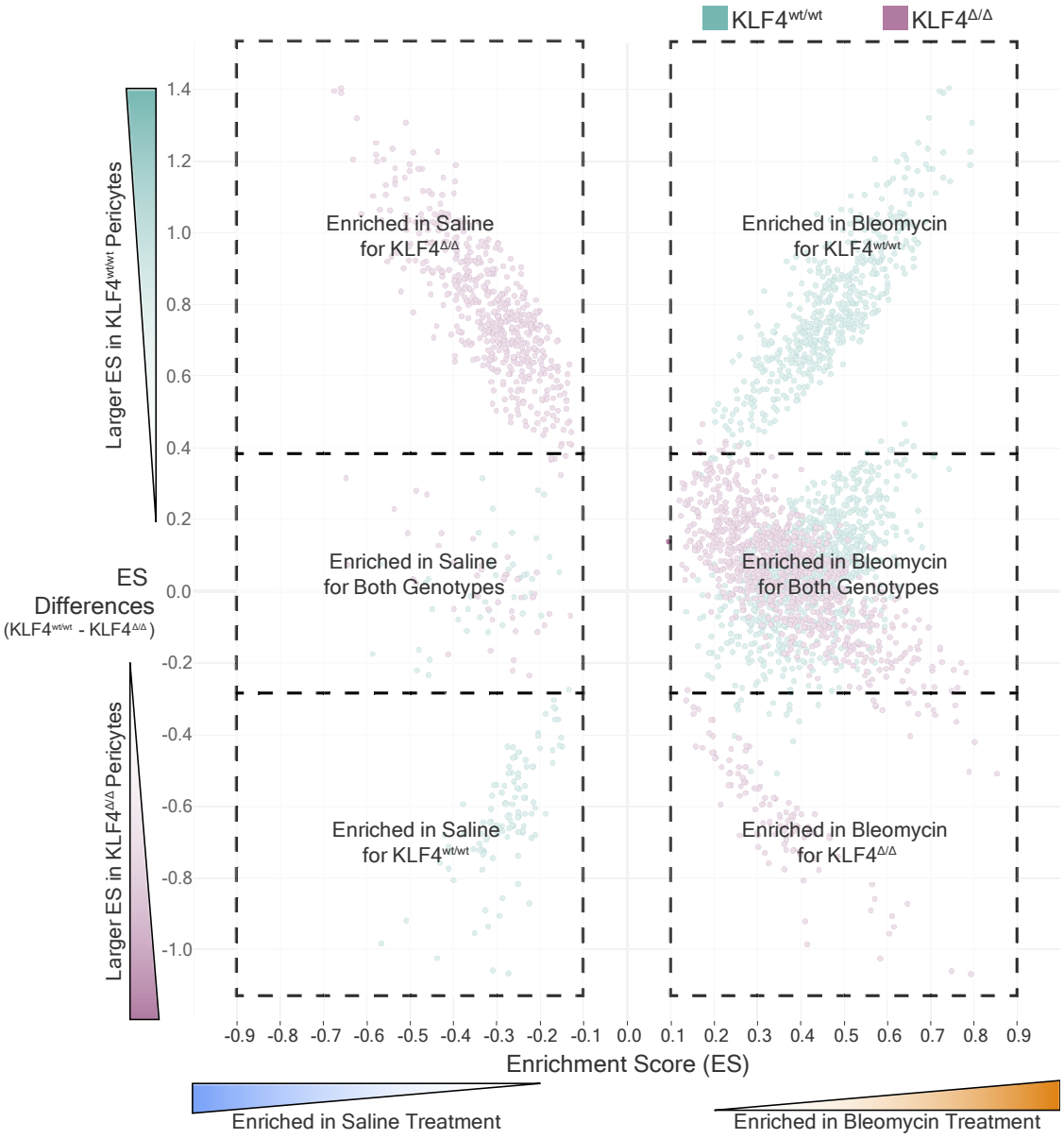

Figure 4.4 KLF4-Dependent Pericyte Responses to Bleomycin. Plot of GeneSet enrichment scores (ES) between bleomycin treated and saline treated pairs of KLF4$^{wt/wt}$ (Aqua) or KLF4$^{wt/wt}$ (Magenta) GeneSets from Myh11-lineage pericytes. X-axis: strength of relationship between treatment and GeneSet (negative scores are enriched in saline,

positive scores in bleomycin). Y-axis: Differential in enrichment scores between KLF4$^{wt/wt}$ and KLF4$^{\Delta/\Delta}$ (larger absolute values indicate greater differences in enrichment scores between KLF4$^{wt/wt}$ and KLF4$^{\Delta/\Delta}$, positive values indicate GeneSets more differentially enriched in KLF4$^{wt/wt}$ pericytes, and negative values indicate GeneSets more differentially enriched in KLF4$^{\Delta/\Delta}$ pericytes. Bounded regions are heuristically derived and annotated to characterize the GeneSets contained within.

Figure 4.4, we introduce a plot of pairs of GeneSets from both KLF4$^{wt/wt}$ and KLF4$^{\Delta/\Delta}$ pericytes. Enrichment scores in GeneSet enrichment analysis (GSEA) are a measure of the strength of association between the expression of a GeneSet and the experimental variable; in this case, bleomycin or saline treatment. We use enrichment scores (ES) here instead of the normalized enrichment score (NES), as normalization is done per individual GSEA analysis according to a randomly generated null distribution, and we are here comparing enrichment values across two GSEA analyses. GSEA does not support multiple simultaneous comparisons with normalization.

At low y-values lie GeneSets which have minimal differences in enrichment score between KLF4$^{wt/wt}$ and KLF4$^{\Delta/\Delta}$ pericytes. These two genotypes can be seen overlapping in both bleomycin-enriched (positive) and saline-enriched (negative) regions along the x-axis, with the majority of GeneSets in the positive segment of the plot, indicating a general upregulation of these genes in both KLF4$^{wt/wt}$ and KLF4$^{\Delta/\Delta}$ pericytes.

Distinct groups of genes which are divergently enriched between $KLF4^{wt/wt}$ and $KLF4^{\Delta/\Delta}$ pericytes are found in each of the four corners of the plot, and appear diagonal relative to the axes. Inversions of the relationship between GeneSet and bleomycin or saline can be seen when gene pairs cross the y-axis, as can be seen in the upper and lower regions of the plot. These inversions indicate an inverse response to bleomycin between $KLF4^{wt/wt}$ and $KLF4^{\Delta/\Delta}$ pericytes for a given GeneSet.

The region from -0.1 to 0.1 along the x-axis is sparsely populated as GeneSets with low enrichment scores are frequently discarded as the threshold for GSEA to determine enrichment does not generate lower enrichment scores ($ES < \pm 0.2$). The chart is similarly sparse along diagonals as the Y-axis values are generated from the enrichment scores of the two pericyte populations, and thus will have similar gaps as described above no values due to a lack of low enrichment scores.

Figure 4.5 visualizes the GeneSets found significantly upregulated in the results reported in Chapter 3, with the addition of the dimension of KLF4. $KLF4^{wt/wt}$ and $KLF4^{\Delta/\Delta}$ 17 of the 18 GeneSets able to be mapped across both $KLF4^{wt/wt}$ and $KLF4^{\Delta/\Delta}$ datasets. The plot is sorted by largest differential in enrichment score, which corresponds to the largest differences in the strength of relationship between GeneSet and experimental treatment. All $KLF4^{wt/wt}$ GeneSets are enriched for in bleomycin, as found in Chapter 3, while the corresponding $KLF4^{\Delta/\Delta}$ GeneSets range from being enriched for in saline to enriched for in bleomyin, but to a lesser extent than the $KLF4^{wt/wt}$ GeneSets. There are four GeneSets demonstrating a KLF4-dependent enrichment inversion, where enrichment scores switch

from positive to negative. There are no instances of a KLF4$^{\Delta/\Delta}$ GeneSet having a higher enrichment in bleomycin treatment than its equivalent KLF4$^{wt/wt}$.

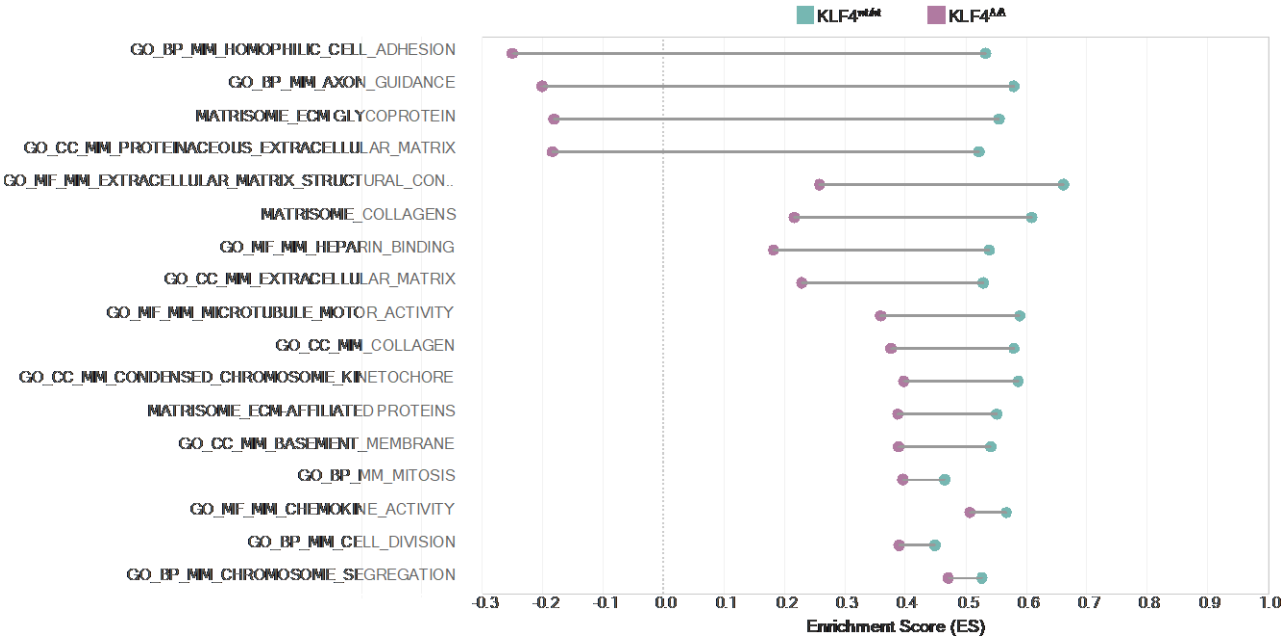

Figure 4.5 Differential Analysis of Bleomycin-Upregulated Pericyte GeneSets. GeneSets identified as significantly upregulated in pericytes from bleomycin-treated lung in Chapter 3 are highlighted, and the inset chart shows those GeneSets ordered by the magnitude of difference between the enrichment scores of KLF4$^{wt/wt}$ and KLF4$^{\Delta/\Delta}$ pericytes in bleomycin lung injury.

Discussion

Pericyte-Endothelial Double-Positive (DP) Cells

Vascular endothelium and microvascular pericytes are spatially apposed in the capillary network, with pericytes typically located abluminal to microvessels. Distinguishing between vascular endothelial cells (VECs) and pericytes in non-reporter mice is typically

done using antibodies against CD31/Platelet endothelial cell adhesion molecule-1 (PECAM-1) and VE-cadherin, as no literature has reported pericyte expression of these proteins. This endothelial exclusivity is not the case for several other common endothelial markers such as CD105/Endoglin, vascular endothelial growth factor receptor 1 (VEGFR1), which are also expressed by pericytes, VSMCs, MSCs, and glial and some hematopoietic cells[285–289].

The directionality of study in phenotypic plasticity along the VEC-pericyte axis has historically been one exploring the contributions of "stemmy" endothelial cells to pericyte populations [290,291]. This endoMT phenomena has been most thoroughly characterized in atherosclerosis [292,293] and cancer [294–296]. As has been discussed in this text, it can be exceedingly difficult to observationally prove the transdifferentiation of one cell type into a separate cell type, especially when the transdifferentiation process involves an intermediate, undifferentiated, "stemmy" phenotype. This mesenchymal stem cell identification problem is only really solvable with lineage reporter models or epigenetic signature profiling (e.g. with ATACSeq) to compare against an atlas of cell population chromatin states.

The observations reported encourage consideration the inverse of the endothelial-to-pericyte transition: the pericyte-to-endothelial transition. If these mesenchymal cell sources can adopt endothelial cell properties, it would require a reframing of existing research into pathologic processes. Take, for example, the body of work describing the loss of pericytes in the microvasculature (pericyte dropout) and the subsequent

microvascular dysfunction which results. Many diabetic pathologies can result in excessive blood vessel formation and leakiness [192,214,297]. It is worth investigating whether pericytes themselves become phenotypically shifted towards the DP pericyte in these models, and thus begin to directly contribute to pathologic angiogenesis as tip cells or other pro-angiogenic endothelial cells.

We were unable to collect enough RNA from the DP pericytes in the $KLF4^{\Delta/\Delta}$ mouse to perform RNASeq, which precludes a naïve fold-change analysis or GSEA-based comparison of enrichment scores between $KLF4^{wt/wt}$ and $KLF4^{\Delta/\Delta}$ DP pericytes. This analysis of KLF4-dependent DP phenotype is a clear next step in the study of the DP pericyte.

The KLF4-dependent CD31 expression in Myh11 lineage pericytes has been observed by two semi-independent methods; surface marker expression via immunofluorescent flow cytometry and mRNA from bulk RNASeq. It is worth noting that the sorting of cells into categories (pericyte, DP pericyte, endothelial cell, stromal cell) for RNASeq relied on surface marker staining. Others using this murine lineage model have observed these DP pericytes but none of these observations have been published at this writing, and remain anecdotal. A recent prepublication by He et al. does show CD31 expression in pericytes as determined by scRNASeq [298]. However, CD31 does not have any explicit link by promoter or enhancer to KLF4 expression in current literature.

The most discussed control is the difficulty in confirming a true, positive identification of a DP pericyte. The first-order assumption is one of contamination: that our measurements are a Myh11 lineage pericyte and endothelial cell bound together and recorded both cytometrically and by gene expression as a single cell. Cells were gated on singlets and it is unlikely that the singlet gating would include sufficient doublets in the numbers to constitute an entirely distinct DP pericyte population. The second-order assumption is that one host pericyte is carrying surface marker (CD31) of a donor endothelial cell. This would require cell-cell contacts between the donor and host cell to persist after mechanical and enzymatic separation and allow for the host cell to be measured as a mixture of both cells by antibody immunofluorescence on CD31. Were this the case, we would expect the expression data of DP pericytes to be clustered with the pure pericyte population, which is not the case (as seen in Figure 4.2). The inverse scenario, where a host endothelial cell contains surface markers of a donor pericyte, is even less likely; as pericytes are gated on Myh11 lineage-dependent fluorescent reporters which reside in the cytosol (either eYFP or tdTomato), loss of membrane integrity of a pericyte would result in the loss of fluorescent reporter protein as the cells undergo the washing steps for FACS processing. We have thusly determined it is most likely that these hybrid cells are truly lineage-positive pericytes which are expressing surface CD31 and adopting expression profiles of vascular endothelial cells, but more controlled study is warranted to assuage these and other concerns.

KLF4 as a possible regulator for pericyte differentiation into myofibroblasts

Our analysis of mRNA across $KLF4^{wt/wt}$ and $KLF4^{\Delta/\Delta}$ pericytes in the bleomycin injury model have revealed several patterns of expression with interesting implications for the role of KLF4 in pericyte response to insult. Based on these expression changes, we hypothesize $KLF4^{\Delta/\Delta}$ pericytes to be less involved in tissue remodeling and myofibroblastic behaviors but more involved in vascular homeostasis/angiogenesis and immune activity. $KLF4^{wt/wt}$ pericytes are enriched in myofibroblastic/tissue remodeling GeneSets, as reported in Chapter 3. $KLF4^{\Delta/\Delta}$ pericytes are less enriched for those same genes, with four out of the seventeen GeneSets having enrichment inversion.

$KLF4^{\Delta/\Delta}$ pericytes are less active or phenotypically polarized in lung injury as measured by mRNA. The enrichment scores in 4.4 and 4.5 demonstrate clear differences in the amount and magnitude of GeneSets enriched in bleomycin in $KLF4^{\Delta/\Delta}$ pericytes (lower right GeneSets). The implication of the large differences in bleomycin-enriched GeneSets is that KLF4 is required for pericytes to undergo the larger changes in expression seen in myofibroblastic differentiation. Instead, $KLF4^{\Delta/\Delta}$ pericytes mostly remain unchanged or upregulate the same GeneSets which are upregulated by $KLF4^{wt/wt}$ pericytes. In essence, KLF4 allows for a larger transcriptional response for pericytes in the bleomycin injury model.

Exploration of required stem cell factors for myofibroblastic differentiation of pericytes is in its infancy, and our reporting here marks the first time KLF4 has been tied to a reduction in myofibroblastic phenotype.

Results reported here are limited to various analyses enabled by bulk RNASeq. Future work will evaluate these phenotypes in several more contexts: immunofluorescent histology to compare $KLF4^{wt/wt}$ to $KLF4^{\Delta/\Delta}$ pericytes in the bleomycin model of pulmonary fibrosis. Direct comparisons of the number and magnitude of pericyte-derived myofibroblasts will elucidate the necessity of KLF4 to the myofibroblastic transdifferentiation of pericytes. We will also investigate overall disease phenotype, both in severity and duration. We expect the loss of KLF4 to have a rescue effect in bleomycin lung injury by reducing the disease burden of pericyte-derived myofibroblasts.

We did not evaluate individual genes in this GSEA as we are not looking to directly isolate genes of interest with this comparison between $KLF4^{\Delta/\Delta}$ and $KLF4^{wt/wt}$ pericytes. By focusing on bulk changes in enrichment score, we are able to include GeneSets which would not have met the more stringent statistical criterion for individual evaluation. In the future we would produce more sample for RNASeq and isolate GeneSet samples with enough statistical power to isolate specific gene families.

Methods

FACS

Live cell sorting performed on AutoMACS (Miltenyi) and BD Influx (BD Biosciences, San Jose, CA, USA) sorters. Cells suspended in FACS buffer (PBS+5% FBS+1mM EDTA) for staining and sorting. CD146 (LSEC) MACS Beads (Miltenyi) added to cells according to manufacturer directions and sorted in a poseld2-protocol on the AutoMACS. Cells gated as described in the text, and antibodies can be found in Table 3.1

RNA Sequencing

Cells isolated from murine lung were used to generate mRNA libraries for RNA sequencing. Extraction and library prep were performed commercially with rRNA depletion (GeneWiz, South Plainfield, NJ, USA). All libraries were sequenced using single lane of the Illumina HiSeq sequencer to generate 150bp paired-end reads at a total read depth of 350 million reads (GeneWiz). Following sequencing, the resulting fastq files were processed to remove low-quality reads (Phred quality score < 20) and the presence of any adapter sequences using TrimGalore[245]The resulting quality of each sample was independently evaluated using FastQC[246]. Files that passed QC were further processed to obtain gene expression counts following a previously defined protocol by Pertea et al.[247]. Briefly, reads were aligned to the mouse genome (UCSC mm10) using

the HISAT2 aligner[248] and transcripts assembled with StringTie[249]. The resulting StringTie output was used to produce read coverage tables for input into DESeq2[250].

RNA Data Analysis

DESeq2's median of ratios method was used to normalize for differences in sequencing depth and RNA composition between samples. Normalized counts were subsequently used to quantify differential expression in the diseased state (bleomycin vs. saline control). Pearson's Correlations were generated using normalized expression using R's Pheatmap[299] as described by Fogg et.al.[300] All gene ontologies were curated from The Gene Ontology (GO) Consortium or the MSigDB NABA_MATRISOME gene set[221], with murine GO homologes sourced from Xijin Ge et.al. [251]. Gene set enrichment analysis (GSEA) was used to identify significantly enriched gene sets performed using the GSEA-MSigDB desktop application and default parameters[252].

Chapter 5 Conclusions, and Future Directions

Fibroblasts and Fibrosis

The end goal of biomedical research into myofibroblasts is one of control over the tissue remodeling process: by redirecting aberrant, fibrotic behaviors towards functional tissue regeneration and homeostasis, it is thought that fibrotic pathologies can be prevented, their severity reduced, or their phenotypes reversed. While a "final common fibrotic pathway" has been the mantra of fibrosis researchers over the last several decades [301–304], enabling dismissal of the vast heterogeneity of myofibroblast progenitor populations, recent data suggest that pathologic myofibroblasts themselves are remarkably diverse: discrete ECM secreting, highly contractile, or immune-responding populations exist within the larger myofibroblast population [33,39].

It is not unreasonable to assert that over the course of this thesis work, fibroblast heterogeneity has become the topic *du jour* in most fields studying tissue- and organ-level diseases [33,189,189,229,258]. At the beginning of this thesis work we struggled to synthesize a definition for fibroblasts, and we came to understand substantial and fundamental limitations of the standard, cell culture-derived description of a fibroblast. Namely, the phenotype of a tissue-resident adhesive cell expanded and passaged in a plastic flask has little resemblance to the diverse cells which potentiate tissue remodeling *in vivo.* This confusion and struggle motivated our writing and publication of the review "*Fibroblasts: Diverse Cells Critical to Biomaterials Integration"* in early 2017. At the time of this writing in late 2020, fibroblasts are increasingly thought of not as a terminally differentiated cell, but instead as an observed *in situ* cellular phenotype, and

current discussions at fibrosis and stromal cell conferences frequently center on *what* a fibroblast is and *how* to define a fibroblast. As another example of this trend toward a more holistic questioning, the number of fibroblast single-cell RNA-sequencing papers indexed on PubMed has increased from six in 2016 to over ninety at the time of this writing. These single cell approaches, together with functional or developmental lineage reporter models, are opening up a much more granular environment for fibroblasts and myofibroblasts to be discussed.

This body of work explores the variety and diversity of sources and phenotypes of fibroblasts, with a specific focus on perivascular cells, or pericytes. Pericytes are similar to fibroblasts in that they do not have agreed-upon molecular methods of identification, and instead are identified based on morphologic and anatomic features relative to microvascular endothelium[42]. Pericytes also do not easily culture and will rapidly differentiate into fibroblast-like cells without specific surfaces and supplemented media[193,270,305]. Pericytes have been shown to differentiate into myofibroblasts, but the mechanisms by which they are driven to undergo this differentiation and their contributions towards the progression of fibroproliferative disease are still poorly understood, motivating this body of work.

Pericyte Differentiation into Myofibroblasts

This research reports and investigates the endogenous transition of pericytes to myofibroblasts in the Myh11-driven murine pericyte reporter mouse for the first time. In

the bleomycin lung injury model, pericyte-derived myofibroblasts were characterized as adopting a contractile and matrix-secreting phenotype via immunofluorescence and RNASeq. We additionally report the increase in surface adhesion molecules integrins αv and α6, specifically active αv in tissue, and we identified the αv extracellular matrix ligand (RGD) in fibronectin as a potentiator of pericyte-to-myofibroblast transition *in vitro*.

The enhanced integrin adhesion profile is not unexpected; ligand density for ECM-binding integrins increases in disease[231,232]. The activation of αv(β3) as measured by Wow-1 has never been reported in pericytes, and it is shown to be significantly increased in the injury model.

The pericyte GeneSets significantly upregulated in bleomycin treatment as determined by GSEA lie almost entirely tissue-remodeling realm. This result provides affirmation that pericytes are responding to bleomycin insult by activating myofibroblastic transcription programs, to the exclusion of inflammatory or angiogenic pathways which were not represented in the results.

Our findings link ECM-based integrin ligand RGD with cell surface αv integrin activation in the pericyte-derived myofibroblasts transition. We expect the results reported and methods developed and reported here to facilitate further exploration of perivascular cell differentiation mechanisms.

Pericyte Plasticity

The ability of perivascular cells to adopt endothelial cell phenotypes is unreported in the literature and while the pericyte-endothelial hybrid cell observations reported in this text are not currently peer-reviewed, we expect further investigation to positively identify and characterize this new, exciting endothelial progenitor population. Additionally, the ability for pericytes to be shown differentiating into yet another cell type, especially *in vivo*, would further bolster the emerging narrative.

The exploration of necessary and sufficient transcription factors for perivascular cell differentiation is still in its infancy, and the work here evaluates the differential gene expression of pericytes as dependent on Yamanaka Factor KLF4 in the bleomycin lung injury model. Our analysis shows distinct KLF4-dependent and KLF4-independent expression changes in the lung injury model. Notably, all the genes identified as significantly enriched in our study of the myofibroblastic pericyte are less enriched in $KLF4^{\Delta/\Delta}$ pericytes. Additionally, angiogenic and immunogenic genes show enrichment in $KLF4^{\Delta/\Delta}$ as compared to $KLF4^{wt/wt}$, which indicate the vascular support and immune sentinel roles of pericytes are being protected by a loss of KLF4 in disease.

Future Directions

Single source bulk RNASeq and phenotypic data can, in theory, be mapped to existing datasets of whole tissues or organs within literature by similarity profiling. There are several scRNAseq atlases for human and murine lung in development which are not yet

fully built out or public[306,307]. We look forward to the ability to map our RNAseq to the larger cell atlases and corroborate our findings with established and robust datasets.

Many transgenic mice exist which would enable further *in vivo* mechanistic analyses of pericyte differentiation if crossed with the Myh11-CreERT2 ROSA STOPfl/fl tdTomato mouse used in this work. Generation of a pericyte-specific col1a1 or αv(β3) knockout behind via crossing floxed mice with our Myh11 CreERT2 mouse would enable the study of pericyte contributions to myofibroblastic remodeling. Crossing with floxed-stop diphtheria toxin receptor (DTR) behind Myh11 CreERT2 would allow for selective ablation of pericytes from healthy adult tissue.

Multiple KLF4-dependent differential responses reported in this work could indicate a population level change or the emergence or suppression of distinct pericyte subpopulations. This is an open question which merits further study, and we are extremely excited to see what follow-up studies with single cell resolution will reveal. Beyond cellular heterogeneity, we have not yet characterized the impact of a pericyte-specific KLF4 knockdown on the progression of the murine disease model.

Should it be the case that pericyte KLF4 knockdown is protective in the murine model, we should seek to understand what behaviors of $KLF4^{\Delta/\Delta}$ pericytes are protective in fibroproliferative injury. Our expression data suggest $KLF4^{\Delta/\Delta}$ pericytes are more participatory in angiogenic and immune recruitment responses than $KLF4^{wt/wt}$ pericytes, both of which may be mechanisms by which pericytes stabilize tissue and reduce fibrosis.

Additional pericyte-specific models for other Yamanaka Factors exist, and recent data show OCT4 regulates migration and angiogenic response in various injury models[213]. Even without these mice currently available, we can use newly available data regarding the targets of KLF4 to make compelling experimental designs as the project continues.

KLF4 Chromatin Immunoprecipitation (ChIP)Seq datasets lack specificity to perivascular cells, but if we assume no pericyte-specific modifications to KLF4's activity as a transcription factor, we can use recently published data sets that are not cell specific. The relative strength of KLF4's association with individual genes was determined using Cistrome-GO, an online utility for interpretation of ChIPSeq datasets[308]. We integrated ChIPSeq data from two sources: in vivo mesenteric arcades[212,309] and in vitro commercially available R1 embryonic stem cells (ESCs)[310,311]. The product of RP scores from two KLF4 ChIPSeq datasets provide a measure of consensus; the sources differ in antibody used for immunoprecipitation and the isolation of genetic material. Thus, a high score indicates strong agreement between the sources. Because this score is a product,

any one score of zero will cause the final integrated score to also be zero – this is an extremely conservative methodology but ensures a minimum of false positives.

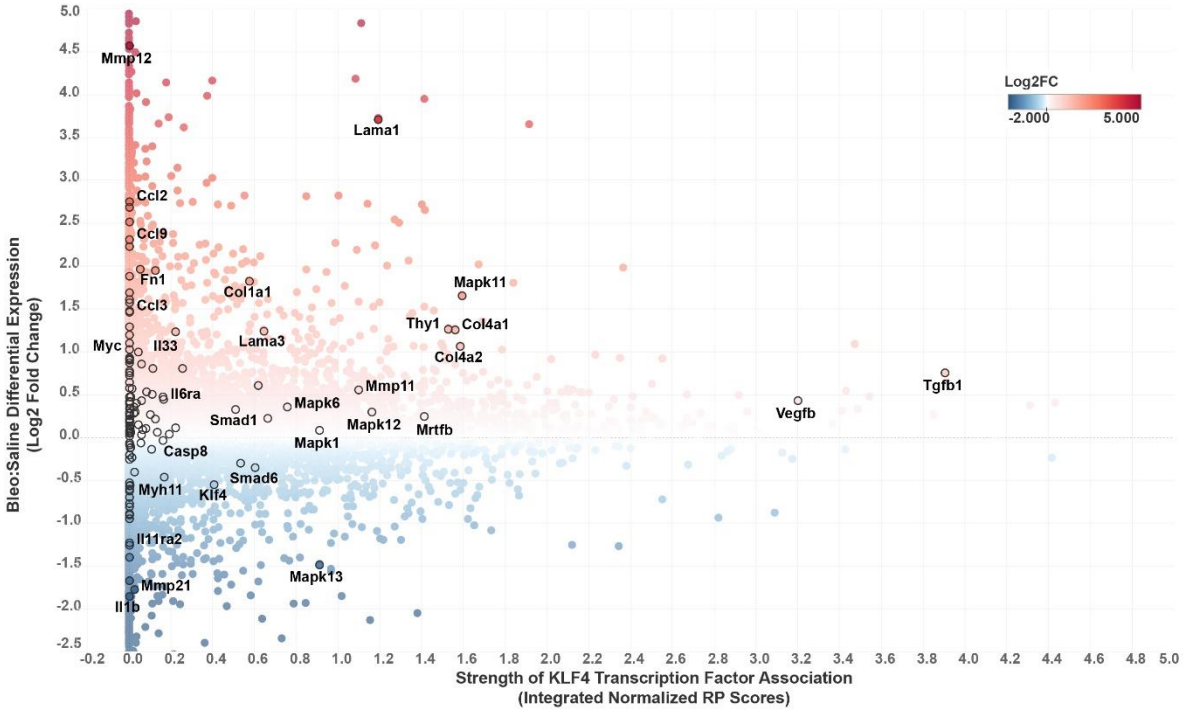

Figure 5.1 RNASeq Paired to ChIPSeq Reveals KLF4 Regulation of Disease Phenotype-Associated Genes. The degree to which KLF4 is associated with known regulators of a gene is shown along the x axis, while the gene response to bleomycin insult in isolated pulmonary pericytes is shown as a fold change over saline treatment about the y axis.

The strength of KLF4 association was paired with KLF4$^{wt/wt}$ RNASeq data described in previous chapters to visualize the potential role KLF4 has in potentiating myofibroblastic or other tissue-remodeling phenotypes. This visualization can be seen in Figure 5-1. Compellingly, TGF-β and VEGF-B expression are found to be highly associated with

KLF4. Both of these molecules belong to a cohort of receptor signaling against which the only FDA-approved treatments for IPF are directed: Nintedanib and Pirfenidone. Nintedanib is a receptor tyrosine kinase (RTK) inhibitor and as such prevents transduction of signal from a variety of receptors, with the most attention given to signaling through PDGF, FGF, and VEGF RTKs[312,313]. Pirfenidone inhibits TGF signaling through a currently unknown mechanism[314]. Little focus has been given to the effect of these drugs on pericyte function *in vitro* or *in vivo*. Work by Sava et al. has demonstrated the ability of Nintedanib to rescue TGF-β-mediated myofibroblastic activation of pericytes *in vitro*[65] , and Ackermann et al. showed stabilization of the pulmonary microvasculature as the largest effect of Nintedanib, outperforming metrics of inflammation and vital capacity[315]. There are no studies directly evaluating the effect of Pirfenidone on pericytes or the pulmonary microcirculation as of this writing.

With this ChIPSeq data and our current understanding of pericytes as arbiters of both fibrotic tissue remodeling and angiogenesis, we are poised for very impactful and novel research into the mechanistic underpinnings of pericyte behavior in disease. To this end, we propose below a series of experiments to be undertaken to more fully evaluate

pericyte responses to fibrotic insult along the clinically-relevant axes of TGF-β and VEGF-B.

TGF-β Investigations

The relationship of TGF-β and pericytes is relatively well-characterized. TGF-β drives pericytes to adopt myofibroblastic phenotypes, much as it does epithelial, endothelial, and other myofibroblast progenitors[149,316,317]. This understanding allows us to leverage the robust tools used across cancer, fibrosis, and developmental biology for use with our pericyte questions.

We would cross the commercially available floxed TGF-β mouse with our Myh11-CreERT2 ROSA STOPfl/fl tdTomato mouse, generating an inducible, pericyte specific TGF-β knockout mouse. Upon generation of this mouse, the standard bleomycin model would be administered as described in previous chapters, with the addition of a treatment variable: Pirfenidone. Bleomycin and saline-treated groups would be subdivided further into Pirfenidone treated (300mg/kg/day)[314] and vehicle treated groups. If we posit that pericytes are the primary drivers of early fibroproliferation and contributions from other cells are negligible, than we would expect to see no difference in disease measures between TGF-$\beta^{wt/wt}$ + Pirfenidone and TGF-$\beta^{\Delta/\Delta}$ + vehicle. Alternatively, as Pirfenidone is known to influence TGF-β signaling through SMAD-dependent and -independent

means[314], a more granular signaling hypothesis using SMAD2 could likewise be generated and assayed as described above.

Understanding the contributions of perivascular TGF-β in human lung fibrosis will necessarily be less direct. We would use proximity ligation assay (PLA) to identify the complexes of SMADs which have translocated to the nucleus[318,319]. Nuclear translocation of SMAD complexes is the final step in the TGF-β signaling process[316]. We will use pericyte marker NG2 to positively identify pericytes with a nuclear counterstain to identify individual cells. We will be able to compare the ratio of SMAD complex-positive pericytes to the total number of SMAD complex-positive cells in the lung. We will quantify this ratio in healthy, low-severity, and high-severity fibrotic human lung, as scored on the Ashcroft scale[320]. This analysis will provide us a measure of perivascular cell *and* total tissue TGF-β signaling in healthy, low severity, and high-severity disease states. This is a novel analysis which will provide important information regarding the populations of TGF-β-responsive cells in fibrotic disease, and will provide a springboard into more targeted application of anti- TGF-β therapeutics.

VEGF-B Investigations

The outcome of VEGF-B signaling is not as well understood or clear-cut as the distinctly pro-fibrotic TGF-β pathway. VEGF-B is one of several VEGFs, and is the least understood. VEGF-A is the classic angiogenic molecule and is often simply referred to as VEGF in literature. VEGFs C and D are associated with lymphangiogenesis[321]. VEGF-B

binds with VEGF-A to form dimers. It is thought these dimerization kinetics can modulate the strength of signaling by modulating VEGF-A availability to VEGF receptors. Additionally, VEGF-B, while not induced by hypoxia, competes with hypoxia-induced VEGF-A in binding to VEGFR-1 in apparent antagonism of hypoxia-mediated angiogenesis[322,323]. VEGF-B is additionally implicated in pericyte maintenance and vessel homeostasis, as well as enhanced cancer metastatic burden through promotion of both endothelial and perivascular cell survival[324,325].

Given the strength of KLF4's association with VEGF-B, we would seek to understand VEGF-B's impact on pericyte phenotype in our bleomycin injury model. As there are currently no available VEGF-B knockout mice, we would generate a floxed VEGF-B mouse using CRISPR/Cas9. It is reported that a SNP at the 167th amino acid (putative receptor binding region) reduces but does not eliminate VEGF-B binding to VEGFR-1[322]. We would seek to fully excise this exon via flanking insertion with flox sites, after validating that full exonal deletion prevents VEGF-B binding to receptor as described in literature[322]. We would then cross this mouse to our Myh11-CreERT2 ROSA STOPfl/fl tdTomato mouse as described above.

Our first experiment would not include RTK inhibitor Nintedanib, as we do not fully understand the impact that the loss of VEGF-B will have on pericyte phenotype – and Nintedanib has much more broad effect than simply abrogating a single VEGF. We would seek to identify any pericyte VEGF-B-dependent disease phenotype in the bleomycin injury model. If we expect VEGF-B to stabilize pericytes in the

microvasculature, we should expect the loss of VEGF-B to increase the rate at which pericytes move off-vessel and differentiate into myofibroblasts. This myofibroblastic pericyte phenotype would be quantitated as described in Chapter 3. From this we could identify VEGF-B as a possible anti-fibrotic therapeutic target, and extend our investigation of therapeutic VEGF-B treatment into other fibrotic and angiogenic pathologies.

Other Investigations

Our understanding of angiogenesis in fibrotic pathologies is inconclusive; there are data to support both inhibition and overexpression of angiogenic factors as viable therapeutic vectors for combating fibrotic disease[237,326]. We believe that stabilization of pericytes in the microvasculature is key to tissue homeostasis, and angiogenic factors are pro-healing to the point which a critical mass of pericytes migrate off-vessel. Comparing pericyte coverage of pulmonary microvessels [327] and Ang-Tie2 levels along the pericyte-endothelial junction would provide a snapshot of perivascular stability and function[328]. Knockouts of pericyte Tie2 behind the Myh11 lineage would destabilize pericyte coverage and allow for direct probing of perivascular Tie2's relationship with bleomycin induced fibrosis[328].

There is much we have yet to learn about the pulmonary pericyte in fibrosis and other pathologies, and the Myh11 lineage model system has acquitted itself well in recent work. However, we must couch these results with the caveat that we are using a gene-

specific reporter mouse which does not necessarily label all perivascular cells in all tissues, and additionally labels vascular smooth muscle cells found along larger vessels. Unless a universal pericyte indicator is found, pericyte research will always be limited by these constraints of specificity and selectivity in the model systems and methods used to study them. The work proposed above seeks to maximally exploit the available tools in this research space to better understand pericyte biology in the diverse milieu of signaling and cells which constitute fibrotic disease.

Chapter 6 <u>References</u>

(1) Kinne, F. L. Mass Transfer in the Human Respiratory System. **1972**.

(2) H, L.; W, M. A Species Comparison of Alveolar Size and Surface Forces. *J. Appl. Physiol. Bethesda Md 1985* **1987**, *62* (5), 1865–1871. https://doi.org/10.1152/jappl.1987.62.5.1865.

(3) McDonald, M. A.; Hildebrand, J. A.; Mesnick, S. Worldwide Decline in Tonal Frequencies of Blue Whale Songs. *Endanger. Species Res.* **2009**, *9* (1), 13–21.

(4) Gehr, P.; Sehovic, S.; Burri, P. H.; Claassen, H.; Weibel, E. R. The Lung of Shrews: Morphometric Estimation of Diffusion Capacity. *Respir. Physiol.* **1980**, *40* (1), 33–47. https://doi.org/10.1016/0034-5687(80)90003-1.

(5) Seadler, B. D.; Toro, F.; Sharma, S. Physiology, Alveolar Tension. In *StatPearls*; StatPearls Publishing: Treasure Island (FL), 2020.

(6) Gal, A. A.; Staton, G. W. Current Concepts in the Classification of Interstitial Lung Disease. *Am J Clin Pathol* **2005**, *123*.

(7) Kasper, M.; Barth, K. Potential Contribution of Alveolar Epithelial Type I Cells to Pulmonary Fibrosis. *Biosci. Rep.* **2017**, *37* (6). https://doi.org/10.1042/BSR20171301.

(8) Barkauskas, C. E.; Cronce, M. J.; Rackley, C. R.; Bowie, E. J.; Keene, D. R.; Stripp, B. R.; Randell, S. H.; Noble, P. W.; Hogan, B. L. M. Type 2 Alveolar Cells Are Stem Cells in Adult Lung. *J. Clin. Invest.* **2013**, *123* (7), 3025–3036. https://doi.org/10.1172/JCI68782.

(9) Hlastala, M. P.; Berger, A. J. *Physiology of Respiration*; Oxford University Press, 2001.

(10) Tawhai, M. H.; Burrowes, K. S. Modelling Pulmonary Blood Flow. *Respir. Physiol. Neurobiol.* **2008**, *163* (1–3), 150–157. https://doi.org/10.1016/j.resp.2008.02.016.

(11) Townsley, M. I. Structure and Composition of Pulmonary Arteries, Capillaries and Veins. *Compr. Physiol.* **2012**, *2*, 675–709. https://doi.org/10.1002/cphy.c100081.

(12) Horsfield, K. Morphometry of the Small Pulmonary Arteries in Man. *Circ. Res.* **1978**, *42* (5), 593–597. https://doi.org/10.1161/01.res.42.5.593.

(13) Jones, R. Ultrastructural Analysis of Contractile Cell Development in Lung Microvessels in Hyperoxic Pulmonary Hypertension. Fibroblasts and Intermediate Cells Selectively Reorganize Nonmuscular Segments. *Am. J. Pathol.* **1992**, *141* (6), 1491–1505.

(14) Hyde, D. M.; Tyler, N. K.; Putney, L. F.; Singh, P.; Gundersen, H. J. G. Total Number and Mean Size of Alveoli in Mammalian Lung Estimated Using Fractionator Sampling and Unbiased Estimates of the Euler Characteristic of Alveolar Openings. *Anat. Rec. A. Discov. Mol. Cell. Evol. Biol.* **2004**, *277* (1), 216–226. https://doi.org/10.1002/ar.a.20012.

(15) Jiang, Z. L.; Kassab, G. S.; Fung, Y. C. Diameter-Defined Strahler System and Connectivity Matrix of the Pulmonary Arterial Tree. *J. Appl. Physiol. Bethesda Md 1985* **1994**, *76* (2), 882–892. https://doi.org/10.1152/jappl.1994.76.2.882.
(16) Zhuang, F. Y.; Yen, M. R.; Fung, Y. C.; Sobin, S. S. How Many Pulmonary Alveoli Are Supplied by a Single Arteriole and Drained by a Single Venule? *Microvasc. Res.* **1985**, *29* (1), 18–31. https://doi.org/10.1016/0026-2862(85)90003-2.
(17) Gan, R. Z.; Yen, R. T. Vascular Impedance Analysis in Dog Lung with Detailed Morphometric and Elasticity Data. *J. Appl. Physiol. Bethesda Md 1985* **1994**, *77* (2), 706–717. https://doi.org/10.1152/jappl.1994.77.2.706.
(18) Huang, W.; Yen, R. T.; McLaurine, M.; Bledsoe, G. Morphometry of the Human Pulmonary Vasculature. *J. Appl. Physiol. Bethesda Md 1985* **1996**, *81* (5), 2123–2133. https://doi.org/10.1152/jappl.1996.81.5.2123.
(19) Yen, R. T.; Zhuang, F. Y.; Fung, Y. C.; Ho, H. H.; Tremer, H.; Sobin, S. S. Morphometry of Cat's Pulmonary Arterial Tree. *J. Biomech. Eng.* **1984**, *106* (2), 131–136. https://doi.org/10.1115/1.3138469.
(20) Fung, Y.; Sobin, S. Theory of Sheet Flow in Lung Alveoli. *J. Appl. Physiol.* **1969**, *26* (4), 472–488.
(21) Guntheroth, W. G.; Luchtel, D. L.; Kawabori, I. Pulmonary Microcirculation: Tubules Rather than Sheet and Post. *J. Appl. Physiol.* **1982**, *53* (2), 510–515. https://doi.org/10.1152/jappl.1982.53.2.510.
(22) Sobin, S. S.; Fung, Y. Response to Challenge to the Sobin-Fung Approach to the Study of Pulmonary Microcirculation. *Chest* **1992**, *101* (4), 1135–1143.
(23) Jo, D. H.; Kim, J. H.; Heo, J.-I.; Kim, J. H.; Cho, C.-H. Interaction between Pericytes and Endothelial Cells Leads to Formation of Tight Junction in Hyaloid Vessels. *Mol. Cells* **2013**, *36* (5), 465–471. https://doi.org/10.1007/s10059-013-0228-1.
(24) Wallez, Y.; Huber, P. Endothelial Adherens and Tight Junctions in Vascular Homeostasis, Inflammation and Angiogenesis. *Apical Junctional Complexes Part I* **2008**, *1778* (3), 794–809. https://doi.org/10.1016/j.bbamem.2007.09.003.
(25) Pozzi, A.; Yurchenco, P. D.; Iozzo, R. V. The Nature and Biology of Basement Membranes. *Matrix Biol.* **2017**, *57–58*, 1–11. https://doi.org/10.1016/j.matbio.2016.12.009.
(26) Welling, L.; Zupka, M.; Welling, D. Mechanical Properties of Basement Membrane. *Physiology* **1995**, *10* (1), 30–35. https://doi.org/10.1152/physiologyonline.1995.10.1.30.
(27) Strieter, R. M. What Differentiates Normal Lung Repair and Fibrosis? *Proc. Am. Thorac. Soc.* **2008**, *5* (3), 305–310. https://doi.org/10.1513/pats.200710-160DR.
(28) Lambrechts, D.; Wauters, E.; Boeckx, B.; Aibar, S.; Nittner, D.; Burton, O.; Bassez, A.; Decaluwé, H.; Pircher, A.; Eynde, K. V. den; Weynand, B.; Verbeken, E.; Leyn, P. D.; Liston, A.; Vansteenkiste, J.; Carmeliet, P.; Aerts, S.; Thienpont, B. Phenotype Molding of Stromal Cells in the Lung Tumor

Microenvironment. *Nat. Med.* **2018**, *24* (8), 1277–1289. https://doi.org/10.1038/s41591-018-0096-5.

(29) Curtis, J. L. Cell-Mediated Adaptive Immune Defense of the Lungs. *Proc. Am. Thorac. Soc.* **2005**, *2* (5), 412–416.

(30) Martin, T. R.; Frevert, C. W. Innate Immunity in the Lungs. *Proc. Am. Thorac. Soc.* **2005**, *2* (5), 403–411.

(31) Rehan, V. K.; Sugano, S.; Wang, Y.; Santos, J.; Romero, S.; Dasgupta, C.; Keane, M. P.; Stahlman, M. T.; Torday, J. S. Evidence for the Presence of Lipofibroblasts in Human Lung. *Exp. Lung Res.* **2006**, *32* (8), 379–393. https://doi.org/10.1080/01902140600880257.

(32) El Agha, E.; Moiseenko, A.; Kheirollahi, V.; De Langhe, S.; Crnkovic, S.; Kwapiszewska, G.; Szibor, M.; Kosanovic, D.; Schwind, F.; Schermuly, R. T. Two-Way Conversion between Lipogenic and Myogenic Fibroblastic Phenotypes Marks the Progression and Resolution of Lung Fibrosis. *Cell Stem Cell* **2017**, *20* (2), 261–273.

(33) Xie, T.; Wang, Y.; Deng, N.; Huang, G.; Taghavifar, F.; Geng, Y.; Liu, N.; Kulur, V.; Yao, C.; Chen, P.; Liu, Z.; Stripp, B.; Tang, J.; Liang, J.; Noble, P. W.; Jiang, D. Single-Cell Deconvolution of Fibroblast Heterogeneity in Mouse Pulmonary Fibrosis. *Cell Rep.* **2018**, *22* (13), 3625–3640. https://doi.org/10.1016/j.celrep.2018.03.010.

(34) Reyfman, P. A.; Walter, J. M.; Joshi, N.; Anekalla, K. R.; McQuattie-Pimentel, A. C.; Chiu, S.; Fernandez, R.; Akbarpour, M.; Chen, C.-I.; Ren, Z.; Verma, R.; Abdala-Valencia, H.; Nam, K.; Chi, M.; Han, S.; Gonzalez-Gonzalez, F. J.; Soberanes, S.; Watanabe, S.; Williams, K. J. N.; Flozak, A. S.; Nicholson, T. T.; Morgan, V. K.; Winter, D. R.; Hinchcliff, M.; Hrusch, C. L.; Guzy, R. D.; Bonham, C. A.; Sperling, A. I.; Bag, R.; Hamanaka, R. B.; Mutlu, G. M.; Yeldandi, A. V.; Marshall, S. A.; Shilatifard, A.; Amaral, L. A. N.; Perlman, H.; Sznajder, J. I.; Argento, A. C.; Gillespie, C. T.; Dematte, J.; Jain, M.; Singer, B. D.; Ridge, K. M.; Lam, A. P.; Bharat, A.; Bhorade, S. M.; Gottardi, C. J.; Budinger, G. R. S.; Misharin, A. V. Single-Cell Transcriptomic Analysis of Human Lung Provides Insights into the Pathobiology of Pulmonary Fibrosis. *Am. J. Respir. Crit. Care Med.* **2018**, *199* (12), 1517–1536. https://doi.org/10.1164/rccm.201712-2410OC.

(35) Braga, F. A. V.; Kar, G.; Berg, M.; Carpaij, O. A.; Polanski, K.; Simon, L. M.; Brouwer, S.; Gomes, T.; Hesse, L.; Jiang, J.; Fasouli, E. S.; Efremova, M.; Vento-Tormo, R.; Affleck, K.; Palit, S.; Strzelecka, P.; Firth, H. V.; Mahbubani, K. T. A.; Cvejic, A.; Meyer, K. B.; Saeb-Parsy, K.; Luinge, M.; Brandsma, C.-A.; Timens, W.; Angelidis, I.; Strunz, M.; Koppelman, G. H.; Oosterhout, A. J. van; Schiller, H. B.; Theis, F. J.; Berge, M. van den; Nawijn, M. C.; Teichmann, S. A. A Cellular Census of Healthy Lung and Asthmatic Airway Wall Identifies Novel Cell States in Health and Disease. *bioRxiv* **2019**, 527408. https://doi.org/10.1101/527408.

(36) Ordovas-Montanes, J.; Dwyer, D. F.; Nyquist, S. K.; Buchheit, K. M.; Vukovic, M.; Deb, C.; Wadsworth, M. H.; Hughes, T. K.; Kazer, S. W.; Yoshimoto, E.; Cahill, K. N.; Bhattacharyya, N.; Katz, H. R.; Berger, B.; Laidlaw, T. M.; Boyce, J. A.; Barrett, N. A.; Shalek, A. K. Allergic Inflammatory Memory in Human Respiratory Epithelial Progenitor Cells. *Nature* **2018**, *560* (7720), 649–654. https://doi.org/10.1038/s41586-018-0449-8.

(37) Jones, D. L.; Meridew, J. A.; Ducharme, M. T.; Lydon, K. L.; Choi, K. M.; Caporarello, N.; Tan, Q.; Link, P. A.; Espinosa, A. M. D.; Xiong, Y.; Lee, J.-H.; Ye, Z.; Yan, H.; Ordog, T.; Ligresti, G.; Varelas, X.; Tschumperlin, D. J. ZNF416 Is a Pivotal Transcriptional Regulator of Fibroblast Mechano-Activation. *bioRxiv* **2020**, 2020.07.23.218842. https://doi.org/10.1101/2020.07.23.218842.

(38) Rondini, E. A.; Granneman, J. G. Single Cell Approaches to Address Adipose Tissue Stromal Cell Heterogeneity. *Biochem. J.* **2020**, *477* (3), 583–600.

(39) Habiel, D. M.; Hogaboam, C. Heterogeneity in Fibroblast Proliferation and Survival in Idiopathic Pulmonary Fibrosis. *Front. Pharmacol.* **2014**, *5*, 2. https://doi.org/10.3389/fphar.2014.00002.

(40) Hung, C. F.; Wilson, C. L.; Schnapp, L. M. Pericytes in the Lung. In *Pericyte Biology in Different Organs*; Birbrair, A., Ed.; Advances in Experimental Medicine and Biology; Springer International Publishing: Cham, 2019; pp 41–58. https://doi.org/10.1007/978-3-030-11093-2_3.

(41) Ferland-McCollough, D.; Slater, S.; Richard, J.; Reni, C.; Mangialardi, G. Pericytes, an Overlooked Player in Vascular Pathobiology. *Pharmacol. Ther.* **2017**, *171*, 30–42. https://doi.org/10.1016/j.pharmthera.2016.11.008.

(42) Armulik Annika; Abramsson Alexandra; Betsholtz Christer. Endothelial/Pericyte Interactions. *Circ. Res.* **2005**, *97* (6), 512–523. https://doi.org/10.1161/01.RES.0000182903.16652.d7.

(43) Rowley, J. E.; Johnson, J. R. Pericytes in Chronic Lung Disease. *Int. Arch. Allergy Immunol.* **2014**, *164* (3), 178–188.

(44) Armulik, A.; Genové, G.; Betsholtz, C. Pericytes: Developmental, Physiological, and Pathological Perspectives, Problems, and Promises. *Dev. Cell* **2011**, *21* (2), 193–215. https://doi.org/10.1016/j.devcel.2011.07.001.

(45) Murgai, M.; Ju, W.; Eason, M.; Kline, J.; Beury, D.; Kaczanowska, S.; Miettinen, M. M.; Kruhlak, M.; Lei, H.; Shern, J. F.; Cherepanova, O. A.; Owens, G. K.; Kaplan, R. N. KLF4-Dependent Perivascular Cell Plasticity Mediates Pre-Metastatic Niche Formation and Metastasis. *Nat. Med.* **2017**, *23* (10), 1176–1190. https://doi.org/10.1038/nm.4400.

(46) Hung, C.; Linn, G.; Chow, Y.-H.; Kobayashi, A.; Mittelsteadt, K.; Altemeier, W. A.; Gharib, S. A.; Schnapp, L. M.; Duffield, J. S. Role of Lung Pericytes and Resident Fibroblasts in the Pathogenesis of Pulmonary Fibrosis. *Am. J. Respir. Crit. Care Med.* **2013**, *188* (7), 820–830.

(47) Campbell, D. J.; Kim, C. H.; Butcher, E. C. Chemokines in the Systemic Organization of Immunity. *Immunol. Rev.* **2003**, *195*, 58–71. https://doi.org/10.1034/j.1600-065x.2003.00067.x.

(48) Moore, T. A.; Moore, B. B.; Newstead, M. W.; Standiford, T. J. Gamma Delta-T Cells Are Critical for Survival and Early Proinflammatory Cytokine Gene Expression during Murine Klebsiella Pneumonia. *J. Immunol. Baltim. Md 1950* **2000**, *165* (5), 2643–2650. https://doi.org/10.4049/jimmunol.165.5.2643.

(49) D'Souza, C. D.; Cooper, A. M.; Frank, A. A.; Mazzaccaro, R. J.; Bloom, B. R.; Orme, I. M. An Anti-Inflammatory Role for Gamma Delta T Lymphocytes in Acquired Immunity to Mycobacterium Tuberculosis. *J. Immunol. Baltim. Md 1950* **1997**, *158* (3), 1217–1221.

(50) King, D. P.; Hyde, D. M.; Jackson, K. A.; Novosad, D. M.; Ellis, T. N.; Putney, L.; Stovall, M. Y.; Van Winkle, L. S.; Beaman, B. L.; Ferrick, D. A. Cutting Edge: Protective Response to Pulmonary Injury Requires Gamma Delta T Lymphocytes. *J. Immunol. Baltim. Md 1950* **1999**, *162* (9), 5033–5036.

(51) Kaiko, G. E.; Horvat, J. C.; Beagley, K. W.; Hansbro, P. M. Immunological Decision-Making: How Does the Immune System Decide to Mount a Helper T-Cell Response? *Immunology* **2008**, *123* (3), 326–338. https://doi.org/10.1111/j.1365-2567.2007.02719.x.

(52) Gieseck, R. L.; Wilson, M. S.; Wynn, T. A. Type 2 Immunity in Tissue Repair and Fibrosis. *Nat. Rev. Immunol.* **2018**, *18* (1), 62–76. https://doi.org/10.1038/nri.2017.90.

(53) Morris, M. A.; Ley, K. Trafficking of Natural Killer Cells. *Curr. Mol. Med.* **2004**, *4* (4), 431–438. https://doi.org/10.2174/1566524043360609.

(54) Ardavín, C. Origin, Precursors and Differentiation of Mouse Dendritic Cells. *Nat. Rev. Immunol.* **2003**, *3* (7), 582–590. https://doi.org/10.1038/nri1127.

(55) Curato, C.; Bernshtein, B.; Zupancič, E.; Dufner, A.; Jaitin, D.; Giladi, A.; David, E.; Chappell-Maor, L.; Leshkowitz, D.; Knobeloch, K.-P.; Amit, I.; Florindo, H. F.; Jung, S. DC Respond to Cognate T Cell Interaction in the Antigen-Challenged Lymph Node. *Front. Immunol.* **2019**, *10*. https://doi.org/10.3389/fimmu.2019.00863.

(56) Friedman, S. L.; Sheppard, D.; Duffield, J. S.; Violette, S. Therapy for Fibrotic Diseases: Nearing the Starting Line. *Sci. Transl. Med.* **2013**, *5* (167), 167sr1-167sr1. https://doi.org/10.1126/scitranslmed.3004700.

(57) Somogyi, V.; Chaudhuri, N.; Torrisi, S. E.; Kahn, N.; Müller, V.; Kreuter, M. The Therapy of Idiopathic Pulmonary Fibrosis: What Is Next? *Eur. Respir. Rev.* **2019**, *28* (153). https://doi.org/10.1183/16000617.0021-2019.

(58) Wijsenbeek, M.; Cottin, V. Spectrum of Fibrotic Lung Diseases. *N. Engl. J. Med.* **2020**, *383* (10), 958–968. https://doi.org/10.1056/NEJMra2005230.

(59) Werner, S.; Lützkendorf, J.; Müller, T.; Müller, L. P.; Posern, G. MRTF-A Controls Myofibroblastic Differentiation of Human Multipotent Stromal Cells

and Their Tumour-Supporting Function in Xenograft Models. *Sci. Rep.* **2019**, *9* (1), 11725. https://doi.org/10.1038/s41598-019-48142-z.

(60) Bae, S.; Park, C. W.; Son, H. K.; Ju, H. K.; Paik, D.; Jeon, C. J.; Koh, G. Y.; Kim, J.; Kim, H. Fibroblast Activation Protein Alpha Identifies Mesenchymal Stromal Cells from Human Bone Marrow. *Br J Haematol* **2008**, *142*. https://doi.org/10.1111/j.1365-2141.2008.07241.x.

(61) Lemos, D. R.; Duffield, J. S. Tissue-Resident Mesenchymal Stromal Cells: Implications for Tissue-Specific Antifibrotic Therapies. *Sci. Transl. Med.* **2018**, *10* (426).

(62) Kramann, R.; Goettsch, C.; Wongboonsin, J.; Iwata, H.; Schneider, R. K.; Kuppe, C.; Kaesler, N.; Chang-Panesso, M.; Machado, F. G.; Gratwohl, S.; Madhurima, K.; Hutcheson, J. D.; Jain, S.; Aikawa, E.; Humphreys, B. D. Adventitial MSC-like Cells Are Progenitors of Vascular Smooth Muscle Cells and Drive Vascular Calcification in Chronic Kidney Disease. *Cell Stem Cell* **2017**, *19* (5), 628–642. https://doi.org/10.1016/j.stem.2016.08.001.

(63) Espagnolle, N.; Guilloton, F.; Deschaseaux, F.; Gadelorge, M.; Sensébé, L.; Bourin, P. CD146 Expression on Mesenchymal Stem Cells Is Associated with Their Vascular Smooth Muscle Commitment. *J. Cell. Mol. Med.* **2014**, *18* (1), 104–114. https://doi.org/10.1111/jcmm.12168.

(64) Birbrair, A.; Zhang, T.; Files, D. C.; Mannava, S.; Smith, T.; Wang, Z.-M.; Messi, M. L.; Mintz, A.; Delbono, O. Type-1 Pericytes Accumulate after Tissue Injury and Produce Collagen in an Organ-Dependent Manner. *Stem Cell Res. Ther.* **2014**, *5* (6), 122. https://doi.org/10.1186/scrt512.

(65) Sava, P.; Ramanathan, A.; Dobronyi, A.; Peng, X.; Sun, H.; Ledesma-Mendoza, A.; Herzog, E. L.; Gonzalez, A. L. Human Pericytes Adopt Myofibroblast Properties in the Microenvironment of the IPF Lung. *JCI Insight 2* (24). https://doi.org/10.1172/jci.insight.96352.

(66) Tashiro, J.; Rubio, G. A.; Limper, A. H.; Williams, K.; Elliot, S. J.; Ninou, I.; Aidinis, V.; Tzouvelekis, A.; Glassberg, M. K. Exploring Animal Models That Resemble Idiopathic Pulmonary Fibrosis. *Front. Med.* **2017**, *4*. https://doi.org/10.3389/fmed.2017.00118.

(67) Gendron, D. R.; Lemay, A.-M.; Lecours, P. B.; Perreault-Vallières, V.; Huppé, C.-A.; Bossé, Y.; Blanchet, M.-R.; Dion, G.; Marsolais, D. FTY720 Promotes Pulmonary Fibrosis When Administered during the Remodelling Phase Following a Bleomycin-Induced Lung Injury. *Pulm. Pharmacol. Ther.* **2017**, *44*, 50–56. https://doi.org/10.1016/j.pupt.2017.03.010.

(68) Moore, B. B.; Hogaboam, C. M. Murine Models of Pulmonary Fibrosis. *Am. J. Physiol. - Lung Cell. Mol. Physiol.* **2008**, *294* (2), L152. https://doi.org/10.1152/ajplung.00313.2007.

(69) Jenkins, R. G.; Moore, B. B.; Chambers, R. C.; Eickelberg, O.; Königshoff, M.; Kolb, M.; Laurent, G. J.; Nanthakumar, C. B.; Olman, M. A.; Pardo, A.; Selman, M.; Sheppard, D.; Sime, P. J.; Tager, A. M.; Tatler, A. L.; Thannickal, V. J.;

White, E. S. An Official American Thoracic Society Workshop Report: Use of Animal Models for the Preclinical Assessment of Potential Therapies for Pulmonary Fibrosis. *Am. J. Respir. Cell Mol. Biol.* **2017**, *56* (5), 667–679. https://doi.org/10.1165/rcmb.2017-0096ST.

(70) Schiller, H. B.; Fernandez, I. E.; Burgstaller, G.; Schaab, C.; Scheltema, R. A.; Schwarzmayr, T.; Strom, T. M.; Eickelberg, O.; Mann, M. Time-and Compartment-resolved Proteome Profiling of the Extracellular Niche in Lung Injury and Repair. *Mol. Syst. Biol.* **2015**, *11* (7), 819.

(71) Hecker, L.; Jagirdar, R.; Jin, T.; Thannickal, V. J. Reversible Differentiation of Myofibroblasts by MyoD. *Exp. Cell Res.* **2011**, *317* (13), 1914–1921. https://doi.org/10.1016/j.yexcr.2011.03.016.

(72) Garrison, G.; Huang, S. K.; Okunishi, K.; Scott, J. P.; Kumar Penke, L. R.; Scruggs, A. M.; Peters-Golden, M. Reversal of Myofibroblast Differentiation by Prostaglandin E(2). *Am. J. Respir. Cell Mol. Biol.* **2013**, *48* (5), 550–558. https://doi.org/10.1165/rcmb.2012-0262OC.

(73) Wietecha, M. S.; DiPietro, L. A. Therapeutic Approaches to the Regulation of Wound Angiogenesis. *Adv. Wound Care* **2013**, *2* (3), 81–86. https://doi.org/10.1089/wound.2011.0348.

(74) Atluri, P. The Surgical Review: An Integrated Basic and Clinical Science Study Guide; Lippincott Williams & Wilkins, 2005; p 300.

(75) Sinno, H.; Prakash, S. Complements and the Wound Healing Cascade: An Updated Review. *Plast. Surg. Int.* **2013**, *2013*.

(76) Robbins, S.; Cotran, R. S. Acute and Chronic Inflammation. In *Pathologic Basis of Disease*; Saunders: Philadelphia, 1989; pp 47–86.

(77) Simpson, D. M.; Ross, R. The Neutrophilic Leukocyte in Wound Repair: A Study with Antineutrophil Serum. *J. Clin. Invest.* **1972**, *51* (8), 2009–2023. https://doi.org/10.1172/JCI107007.

(78) Major, M. R.; Wong, V. W.; Nelson, E. R.; Longaker, M. T.; Gurtner, G. C. The Foreign Body Response: At the Interface of Surgery and Bioengineering. *Plast. Reconstr. Surg.* **2015**, *135* (5), 1489–1498.

(79) Anderson, J. M.; Rodriguez, A.; Chang, D. T. FOREIGN BODY REACTION TO BIOMATERIALS. *Semin. Immunol.* **2008**, *20* (2), 86–100. https://doi.org/10.1016/j.smim.2007.11.004.

(80) Tang, L.; Eaton, J. W. Inflammatory Responses to Biomaterials. *Am. J. Clin. Pathol.* **1995**, *103* (4), 466–471.

(81) Hagood, J. S.; Prabhakaran, P.; Kumbla, P.; Salazar, L.; MacEwen, M. W.; Barker, T. H.; Ortiz, L. A.; Schoeb, T.; Siegal, G. P.; Alexander, C. B.; Pardo, A.; Selman, M. Loss of Fibroblast Thy-1 Expression Correlates with Lung Fibrogenesis. *Am. J. Pathol.* **2005**, *167* (2), 365–379.

(82) Clark, R. A.; Lanigan, J. M.; DellaPelle, P.; Manseau, E.; Dvorak, H. F.; Colvin, R. B. Fibronectin and Fibrin Provide a Provisional Matrix for Epidermal Cell

Migration during Wound Reepithelialization. *J. Invest. Dermatol.* **1982**, *79* (5), 264–269.

(83) Sottile, J.; Hocking, D. C. Fibronectin Polymerization Regulates the Composition and Stability of Extracellular Matrix Fibrils and Cell-Matrix Adhesions. *Mol. Biol. Cell* **2002**, *13* (10), 3546–3559. https://doi.org/10.1091/mbc.E02-01-0048.

(84) Booth, B. A.; Polak, K. L.; Uitto, J. Collagen Biosynthesis by Human Skin Fibroblasts. I. Optimization of the Culture Conditions for Synthesis of Type I and Type III Procollagens. *Biochim. Biophys. Acta BBA - Nucleic Acids Protein Synth.* **1980**, *607* (1), 145–160. https://doi.org/10.1016/0005-2787(80)90228-2.

(85) Visse, R.; Nagase, H. Matrix Metalloproteinases and Tissue Inhibitors of Metalloproteinases Structure, Function, and Biochemistry. *Circ. Res.* **2003**, *92* (8), 827–839.

(86) Abercrombie, M.; Flint, M.; James, D. Wound Contraction in Relation to Collagen Formation in Scorbutic Guinea-Pigs. *Development* **1956**, *4* (2), 167–175.

(87) Desmoulière, A.; Redard, M.; Darby, I.; Gabbiani, G. Apoptosis Mediates the Decrease in Cellularity during the Transition between Granulation Tissue and Scar. *Am. J. Pathol.* **1995**, *146* (1), 56–66.

(88) Akilbekova, D.; Bratlie, K. M. Quantitative Characterization of Collagen in the Fibrotic Capsule Surrounding Implanted Polymeric Microparticles through Second Harmonic Generation Imaging. *PLOS ONE* **2015**, *10* (6), e0130386. https://doi.org/10.1371/journal.pone.0130386.

(89) Leask, A.; Abraham, D. J. TGF-Beta Signaling and the Fibrotic Response. *FASEB J* **2004**, *18*.

(90) Liu, F.; Mih, J. D.; Shea, B. S.; Kho, A. T.; Sharif, A. S.; Tager, A. M.; Tschumperlin, D. J. Feedback Amplification of Fibrosis through Matrix Stiffening and COX-2 Suppression. *J. Cell Biol.* **2010**, *190* (4), 693–706.

(91) Aarabi, S.; Bhatt, K. A.; Shi, Y.; Paterno, J.; Chang, E. I.; Loh, S. A.; Holmes, J. W.; Longaker, M. T.; Yee, H.; Gurtner, G. C. Mechanical Load Initiates Hypertrophic Scar Formation through Decreased Cellular Apoptosis. *FASEB J.* **2007**, *21* (12), 3250–3261. https://doi.org/10.1096/fj.07-8218com.

(92) Wilgus, T. A.; Ferreira, A. M.; Oberyszyn, T. M.; Bergdall, V. K.; DiPietro, L. A. Regulation of Scar Formation by Vascular Endothelial Growth Factor. *Lab. Investig. J. Tech. Methods Pathol.* **2008**, *88* (6), 579–590. https://doi.org/10.1038/labinvest.2008.36.

(93) Travers, J. G.; Kamal, F. A.; Robbins, J.; Yutzey, K. E.; Blaxall, B. C. Cardiac Fibrosis. *Circ. Res.* **2016**, *118* (6), 1021. https://doi.org/10.1161/CIRCRESAHA.115.306565.

(94) Datta, A.; Scotton, C. J.; Chambers, R. C. Novel Therapeutic Approaches for Pulmonary Fibrosis. *Br. J. Pharmacol.* **2011**, *163* (1), 141–172. https://doi.org/10.1111/j.1476-5381.2011.01247.x.

(95) Prasad, B. R.; Brook, M. A.; Smith, T.; Zhao, S.; Chen, Y.; Sheardown, H.; D'souza, R.; Rochev, Y. Controlling Cellular Activity by Manipulating Silicone Surface Roughness. *Colloids Surf. B Biointerfaces* **2010**, *78* (2), 237–242. https://doi.org/10.1016/j.colsurfb.2010.03.006.

(96) Janmey, P. A.; Winer, J. P.; Weisel, J. W. Fibrin Gels and Their Clinical and Bioengineering Applications. *J. R. Soc. Interface* **2009**, *6* (30), 1–10. https://doi.org/10.1098/rsif.2008.0327.

(97) Beale, E. W.; Hoxworth, R. E.; Livingston, E. H.; Trussler, A. P. The Role of Biologic Mesh in Abdominal Wall Reconstruction: A Systematic Review of the Current Literature. *Am. J. Surg. 204* (4), 510–517. https://doi.org/10.1016/j.amjsurg.2012.03.009.

(98) Cheng, A.; Lakhiani, C.; Saint-Cyr, M. Treatment of Capsular Contracture Using Complete Implant Coverage by Acellular Dermal Matrix: A Novel Technique. *Plast. Reconstr. Surg.* **2013**, *132* (3), 519–529.

(99) Hagood, J. S.; Miller, P. J.; Lasky, J. A.; Tousson, A.; Guo, B.; Fuller, G. M.; McIntosh, J. C. Differential Expression of Platelet-Derived Growth Factor-α Receptor by Thy-1$^-$ and Thy-1$^+$ Lung Fibroblasts. *Am. J. Physiol. - Lung Cell. Mol. Physiol.* **1999**, *277* (1), L218.

(100) Slany, A.; Meshcheryakova, A.; Beer, A.; Ankersmit, H. J.; Paulitschke, V.; Gerner, C. Plasticity of Fibroblasts Demonstrated by Tissue-Specific and Function-Related Proteome Profiling. *Clin. Proteomics* **2014**, *11* (1), 41. https://doi.org/10.1186/1559-0275-11-41.

(101) Fiore, V. F.; Strane, P. W.; Bryksin, A. V.; White, E. S.; Hagood, J. S.; Barker, T. H. Conformational Coupling of Integrin and Thy-1 Regulates Fyn Priming and Fibroblast Mechanotransduction. *J Cell Biol* **2015**, *211* (1), 173–190.

(102) Sanders, Y. Y.; Pardo, A.; Selman, M.; Nuovo, G. J.; Tollefsbol, T. O.; Siegal, G. P.; Hagood, J. S. Thy-1 Promoter Hypermethylation: A Novel Epigenetic Pathogenic Mechanism in Pulmonary Fibrosis. *Am. J. Respir. Cell Mol. Biol.* **2008**, *39* (5), 610–618. https://doi.org/10.1165/rcmb.2007-0322OC.

(103) Koumas, L.; Smith, T. J.; Feldon, S.; Blumberg, N.; Phipps, R. P. Thy-1 Expression in Human Fibroblast Subsets Defines Myofibroblastic or Lipofibroblastic Phenotypes. *Am. J. Pathol.* **2003**, *163* (4), 1291–1300.

(104) Sanders, Y. Y.; Tollefsbol, T. O.; Varisco, B. M.; Hagood, J. S. Epigenetic Regulation of Thy-1 by Histone Deacetylase Inhibitor in Rat Lung Fibroblasts. *Am. J. Respir. Cell Mol. Biol.* **2011**, *45* (1), 16–23. https://doi.org/10.1165/rcmb.2010-0154OC.

(105) Tarin, D.; Croft, C. Ultrastructural Studies of Wound Healing in Mouse Skin. II. Dermo-Epidermal Interrelationships. *J. Anat.* **1970**, *106* (Pt 1), 79.

(106) Fries, K. M.; Blieden, T.; Looney, R. J.; Sempowski, G. D.; Silvera, M. R.; Willis, R. A.; Phipps, R. P. Evidence of Fibroblast Heterogeneity and the Role of Fibroblast Subpopulations in Fibrosis. *Clin. Immunol. Immunopathol.* **1994**, *72* (3), 283–292.

(107) Hinz, B.; Phan, S. H.; Thannickal, V. J.; Galli, A.; Bochaton-Piallat, M.-L.; Gabbiani, G. The Myofibroblast: One Function, Multiple Origins. *Am. J. Pathol.* **2007**, *170* (6), 1807–1816. https://doi.org/10.2353/ajpath.2007.070112.

(108) Chang, H. Y.; Chi, J.-T.; Dudoit, S.; Bondre, C.; van de Rijn, M.; Botstein, D.; Brown, P. O. Diversity, Topographic Differentiation, and Positional Memory in Human Fibroblasts. *Proc. Natl. Acad. Sci. U. S. A.* **2002**, *99* (20), 12877–12882. https://doi.org/10.1073/pnas.162488599.

(109) Hay, E. An Overview of Epithelio-Mesenchymal Transformation. *Cells Tissues Organs* **1995**, *154* (1), 8–20.

(110) Lawson, W. E.; Polosukhin, V. V.; Zoia, O.; Stathopoulos, G. T.; Han, W.; Plieth, D.; Loyd, J. E.; Neilson, E. G.; Blackwell, T. S. Characterization of Fibroblast-Specific Protein 1 in Pulmonary Fibrosis. *Am. J. Respir. Crit. Care Med.* **2005**, *171* (8), 899–907. https://doi.org/10.1164/rccm.200311-1535OC.

(111) Okada, H.; Danoff, T. M.; Kalluri, R.; Neilson, E. G. Early Role of Fsp1 in Epithelial-Mesenchymal Transformation. *Am. J. Physiol. - Ren. Physiol.* **1997**, *273* (4), F563.

(112) Komuro, T. Re-Evaluation of Fibroblasts and Fibroblast-like Cells. *Anat. Embryol. (Berl.)* **1990**, *182* (2), 103–112. https://doi.org/10.1007/BF00174011.

(113) Österreicher, C. H.; Penz-Österreicher, M.; Grivennikov, S. I.; Guma, M.; Koltsova, E. K.; Datz, C.; Sasik, R.; Hardiman, G.; Karin, M.; Brenner, D. A. Fibroblast-Specific Protein 1 Identifies an Inflammatory Subpopulation of Macrophages in the Liver. *Proc. Natl. Acad. Sci. U. S. A.* **2011**, *108* (1), 308–313. https://doi.org/10.1073/pnas.1017547108.

(114) Brisset, A. C.; Hao, H.; Camenzind, E.; Bacchetta, M.; Geinoz, A.; Sanchez, J.-C.; Chaponnier, C.; Gabbiani, G.; Bochaton-Piallat, M.-L. Intimal Smooth Muscle Cells of Porcine and Human Coronary Artery Express S100A4, a Marker of the Rhomboid Phenotype In Vitro. *Circ. Res.* **2007**, *100* (7), 1055. https://doi.org/10.1161/01.RES.0000262654.84810.6c.

(115) Iwano, M.; Plieth, D.; Danoff, T. M.; Xue, C.; Okada, H.; Neilson, E. G. Evidence That Fibroblasts Derive from Epithelium during Tissue Fibrosis. *J Clin Invest* **2002**, *110*.

(116) Kong, P.; Christia, P.; Saxena, A.; Su, Y.; Frangogiannis, N. G. Lack of Specificity of Fibroblast-Specific Protein 1 in Cardiac Remodeling and Fibrosis. *Am. J. Physiol. - Heart Circ. Physiol.* **2013**, *305* (9), H1363–H1372. https://doi.org/10.1152/ajpheart.00395.2013.

(117) Swonger, J. M.; Liu, J. S.; Ivey, M. J.; Tallquist, M. D. Genetic Tools for Identifying and Manipulating Fibroblasts in the Mouse. *Fibroblast Differ.* **2016**, *92* (3), 66–83. https://doi.org/10.1016/j.diff.2016.05.009.

(118) Rinn, J. L.; Bondre, C.; Gladstone, H. B.; Brown, P. O.; Chang, H. Y. Anatomic Demarcation by Positional Variation in Fibroblast Gene Expression Programs. *PLoS Genet.* **2006**, *2*. https://doi.org/10.1371/journal.pgen.0020119.

(119) Ivanov, N. A.; Tao, R.; Chenoweth, J. G.; Brandtjen, A.; Mighdoll, M. I.; Genova, J. D.; McKay, R. D.; Jia, Y.; Weinberger, D. R.; Kleinman, J. E.; Hyde, T. M.; Jaffe, A. E. Strong Components of Epigenetic Memory in Cultured Human Fibroblasts Related to Site of Origin and Donor Age. *PLoS Genet.* **2016**, *12* (2), e1005819. https://doi.org/10.1371/journal.pgen.1005819.

(120) Coolen, N. A.; Schouten, K. C.; Boekema, B. K.; Middelkoop, E.; Ulrich, M. M. Wound Healing in a Fetal, Adult, and Scar Tissue Model: A Comparative Study. *Wound Repair Regen.* **2010**, *18* (3), 291–301.

(121) Fang, Z.; Zhu, T.; Shen, W. L.; Tang, Q. M.; Chen, J. L.; Yin, Z.; Ji, J. F.; Heng, B. C.; Ouyang, H. W.; Chen, X. Transplantation of Fetal Instead of Adult Fibroblasts Reduces the Probability of Ectopic Ossification During Tendon Repair. *Tissue Eng. Part A* **2014**, *20* (13–14), 1815–1826. https://doi.org/10.1089/ten.tea.2013.0296.

(122) Moulin, V.; Tam, B. Y. Y.; Castilloux, G.; Auger, F. A.; O'Connor-McCourt, M. D.; Philip, A.; Germain, L. Fetal and Adult Human Skin Fibroblasts Display Intrinsic Differences in Contractile Capacity. *J. Cell. Physiol.* **2001**, *188* (2), 211–222. https://doi.org/10.1002/jcp.1110.

(123) Brink, H. E.; Bernstein, J.; Nicoll, S. B. Fetal Dermal Fibroblasts Exhibit Enhanced Growth and Collagen Production in Two- and Three-Dimensional Culture in Comparison to Adult Fibroblasts. *J. Tissue Eng. Regen. Med.* **2009**, *3* (8), 623–633. https://doi.org/10.1002/term.204.

(124) Baum, J.; Duffy, H. S. Fibroblasts and Myofibroblasts: What Are We Talking About? *J. Cardiovasc. Pharmacol.* **2011**, *57* (4), 376–379. https://doi.org/10.1097/FJC.0b013e3182116e39.

(125) Desmoulière, A.; Chaponnier, C.; Gabbiani, G. Perspective Article: Tissue Repair, Contraction, and the Myofibroblast. *Wound Repair Regen.* **2005**, *13* (1), 7–12. https://doi.org/10.1111/j.1067-1927.2005.130102.x.

(126) Gabbiani, G.; Hirschel, B. J.; Ryan, G. B.; Statkov, P. R.; Majno, G. GRANULATION TISSUE AS A CONTRACTILE ORGAN : A STUDY OF STRUCTURE AND FUNCTION. *J. Exp. Med.* **1972**, *135* (4), 719–734.

(127) Humphreys, B. D.; Lin, S.-L.; Kobayashi, A.; Hudson, T. E.; Nowlin, B. T.; Bonventre, J. V.; Valerius, M. T.; McMahon, A. P.; Duffield, J. S. Fate Tracing Reveals the Pericyte and Not Epithelial Origin of Myofibroblasts in Kidney Fibrosis. *Am. J. Pathol.* **2010**, *176* (1), 85–97. https://doi.org/10.2353/ajpath.2010.090517.

(128) Hashimoto, N.; Phan, S. H.; Imaizumi, K.; Matsuo, M.; Nakashima, H.; Kawabe, T.; Shimokata, K.; Hasegawa, Y. Endothelial–Mesenchymal Transition in Bleomycin-Induced Pulmonary Fibrosis. *Am. J. Respir. Cell Mol. Biol.* **2010**, *43* (2), 161–172. https://doi.org/10.1165/rcmb.2009-0031OC.

(129) Kim, K. K.; Kugler, M. C.; Wolters, P. J.; Robillard, L.; Galvez, M. G.; Brumwell, A. N.; Sheppard, D.; Chapman, H. A. Alveolar Epithelial Cell Mesenchymal Transition Develops in Vivo during Pulmonary Fibrosis and Is

Regulated by the Extracellular Matrix. *Proc. Natl. Acad. Sci. U. S. A.* **2006**, *103* (35), 13180–13185. https://doi.org/10.1073/pnas.0605669103.

(130) Tanjore, H.; Xu, X. C.; Polosukhin, V. V.; Degryse, A. L.; Li, B.; Han, W.; Sherrill, T. P.; Plieth, D.; Neilson, E. G.; Blackwell, T. S.; Lawson, W. E. Contribution of Epithelial-Derived Fibroblasts to Bleomycin-Induced Lung Fibrosis. *Am. J. Respir. Crit. Care Med.* **2009**, *180* (7), 657–665. https://doi.org/10.1164/rccm.200903-0322OC.

(131) Haudek, S. B.; Xia, Y.; Huebener, P.; Lee, J. M.; Carlson, S.; Crawford, J. R.; Pilling, D.; Gomer, R. H.; Trial, J.; Frangogiannis, N. G.; Entman, M. L. Bone Marrow-Derived Fibroblast Precursors Mediate Ischemic Cardiomyopathy in Mice. *Proc. Natl. Acad. Sci. U. S. A.* **2006**, *103* (48), 18284–18289. https://doi.org/10.1073/pnas.0608799103.

(132) Kisseleva, T.; Uchinami, H.; Feirt, N.; Quintana-Bustamante, O.; Segovia, J. C.; Schwabe, R. F.; Brenner, D. A. Bone Marrow-Derived Fibrocytes Participate in Pathogenesis of Liver Fibrosis. *J. Hepatol.* **2006**, *45* (3), 429–438. https://doi.org/10.1016/j.jhep.2006.04.014.

(133) Phillips, R. J.; Burdick, M. D.; Hong, K.; Lutz, M. A.; Murray, L. A.; Xue, Y. Y.; Belperio, J. A.; Keane, M. P.; Strieter, R. M. Circulating Fibrocytes Traffic to the Lungs in Response to CXCL12 and Mediate Fibrosis. *J. Clin. Invest.* **2004**, *114* (3), 438–446. https://doi.org/10.1172/JCI200420997.

(134) Suga, H.; Rennert, R. C.; Rodrigues, M.; Sorkin, M.; Glotzbach, J. P.; Januszyk, M.; Fujiwara, T.; Longaker, M. T.; Gurtner, G. C. Tracking the Elusive Fibrocyte: Identification and Characterization of Collagen-Producing Hematopoietic Lineage Cells During Murine Wound Healing. *Stem Cells* **2014**, *32* (5), 1347–1360.

(135) Chan, K.; Kan, Y. W. Nrf2 Is Essential for Protection against Acute Pulmonary Injury in Mice. *Proc Natl Acad Sci USA* **1999**, *96*. https://doi.org/10.1073/pnas.96.22.12731.

(136) Cho, H. Y.; Reddy, S. P.; Yamamoto, M.; Kleeberger, S. R. The Transcription Factor NRF2 Protects against Pulmonary Fibrosis. *FASEB J* **2004**, *18*.

(137) Kikuchi, N.; Ishii, Y.; Morishima, Y.; Yageta, Y.; Haraguchi, N.; Itoh, K.; Yamamoto, M.; Hizawa, N. Nrf2 Protects against Pulmonary Fibrosis by Regulating the Lung Oxidant Level and Th1/Th2 Balance. *Respir. Res.* **2010**, *11* (1), 31. https://doi.org/10.1186/1465-9921-11-31.

(138) Artaud-Macari, E.; Goven, D.; Brayer, S.; Hamimi, A.; Besnard, V.; Marchal-Somme, J.; Ali, Z. E.; Crestani, B.; Kerdine-Römer, S.; Boutten, A. Nuclear Factor Erythroid 2-Related Factor 2 Nuclear Translocation Induces Myofibroblastic Dedifferentiation in Idiopathic Pulmonary Fibrosis. *Antioxid. Redox Signal.* **2013**, *18* (1), 66–79.

(139) Ortega, N.; Behonick, D. J.; Werb, Z. Matrix Remodeling during Endochondral Ossification. *Trends Cell Biol.* **2004**, *14* (2), 86–93.

(140) Hernandez, M. R. The Optic Nerve Head in Glaucoma: Role of Astrocytes in Tissue Remodeling. *Prog. Retin. Eye Res.* **2000**, *19* (3), 297–321.
(141) Davis, G. E.; Senger, D. R. Endothelial Extracellular Matrix. *Circ. Res.* **2005**, *97* (11), 1093–1107.
(142) Shapiro, S. D.; Senior, R. M. Matrix Metalloproteinases: Matrix Degradation and More. *Am. J. Respir. Cell Mol. Biol.* **1999**, *20* (6), 1100–1102.
(143) Underly, R. G.; Levy, M.; Hartmann, D. A.; Grant, R. I.; Watson, A. N.; Shih, A. Y. Pericytes as Inducers of Rapid, Matrix Metalloproteinase-9 Dependent Capillary Damage during Ischemia. *J. Neurosci.* **2016**. https://doi.org/10.1523/JNEUROSCI.2891-16.2016.
(144) Wessels, A.; van den Hoff, M. J.; Adamo, R. F.; Phelps, A. L.; Lockhart, M. M.; Sauls, K.; Briggs, L. E.; Norris, R. A.; van Wijk, B.; Perez-Pomares, J. M. Epicardially Derived Fibroblasts Preferentially Contribute to the Parietal Leaflets of the Atrioventricular Valves in the Murine Heart. *Dev. Biol.* **2012**, *366* (2), 111–124.
(145) Gomez, I. G.; Duffield, J. S. The FOXD1 Lineage of Kidney Perivascular Cells and Myofibroblasts: Functions and Responses to Injury. *Kidney Int. Suppl.* **2014**, *4* (1), 26–33. https://doi.org/10.1038/kisup.2014.6.
(146) Lo, C.-M.; Wang, H.-B.; Dembo, M.; Wang, Y. Cell Movement Is Guided by the Rigidity of the Substrate. *Biophys. J.* **2000**, *79* (1), 144–152.
(147) Hadjipanayi, E.; Mudera, V.; Brown, R. Close Dependence of Fibroblast Proliferation on Collagen Scaffold Matrix Stiffness. *J. Tissue Eng. Regen. Med.* **2009**, *3* (2), 77.
(148) Schrader, J.; Gordon-Walker, T. T.; Aucott, R. L.; van Deemter, M.; Quaas, A.; Walsh, S.; Benten, D.; Forbes, S. J.; Wells, R. G.; Iredale, J. P. Matrix Stiffness Modulates Proliferation, Chemotherapeutic Response, and Dormancy in Hepatocellular Carcinoma Cells. *Hepatology* **2011**, *53* (4), 1192–1205.
(149) Wipff, P.-J.; Rifkin, D. B.; Meister, J.-J.; Hinz, B. Myofibroblast Contraction Activates Latent TGF-B1 from the Extracellular Matrix. *J. Cell Biol.* **2007**, *179* (6), 1311–1323.
(150) Engler, A. J.; Sen, S.; Sweeney, H. L.; Discher, D. E. Matrix Elasticity Directs Stem Cell Lineage Specification. *Cell* **2006**, *126* (4), 677–689. https://doi.org/10.1016/j.cell.2006.06.044.
(151) Goffin, J. M.; Pittet, P.; Csucs, G.; Lussi, J. W.; Meister, J.-J.; Hinz, B. Focal Adhesion Size Controls Tension-Dependent Recruitment of α-Smooth Muscle Actin to Stress Fibers. *J. Cell Biol.* **2006**, *172* (2), 259–268.
(152) Huang, X.; Yang, N.; Fiore, V. F.; Barker, T. H.; Sun, Y.; Morris, S. W.; Ding, Q.; Thannickal, V. J.; Zhou, Y. Matrix Stiffness–Induced Myofibroblast Differentiation Is Mediated by Intrinsic Mechanotransduction. *Am. J. Respir. Cell Mol. Biol.* **2012**, *47* (3), 340–348.
(153) Lodish, H. F. *Molecular Cell Biology*; W.H. Freeman and Co.: New York, 2013.

(154) Kalluri, R. The Biology and Function of Fibroblasts in Cancer. *Nat. Rev. Cancer* **2016**, *16* (9), 582–598.
(155) Ciobanasu, C.; Faivre, B.; Le Clainche, C. Integrating Actin Dynamics, Mechanotransduction and Integrin Activation: The Multiple Functions of Actin Binding Proteins in Focal Adhesions. *SPP 1464Actin Dyn. – Part I* **2013**, *92* (10–11), 339–348. https://doi.org/10.1016/j.ejcb.2013.10.009.
(156) Geiger, B.; Spatz, J. P.; Bershadsky, A. D. Environmental Sensing through Focal Adhesions. *Nat Rev Mol Cell Biol* **2009**, *10* (1), 21–33. https://doi.org/10.1038/nrm2593.
(157) Plow, E. F.; Haas, T. A.; Zhang, L.; Loftus, J.; Smith, J. W. Ligand Binding to Integrins. *J. Biol. Chem.* **2000**, *275* (29), 21785–21788. https://doi.org/10.1074/jbc.R000003200.
(158) Ivaska, J.; Reunanen, H.; Westermarck, J.; Koivisto, L.; Kähäri, V.-M.; Heino, J. Integrin A2β1 Mediates Isoform-Specific Activation of P38 and Upregulation of Collagen Gene Transcription by a Mechanism Involving the A2 Cytoplasmic Tail. *J. Cell Biol.* **1999**, *147* (2), 401–416.
(159) Schiller, H. B.; Hermann, M.-R.; Polleux, J.; Vignaud, T.; Zanivan, S.; Friedel, C. C.; Sun, Z.; Raducanu, A.; Gottschalk, K.-E.; Théry, M. B1-and Av-Class Integrins Cooperate to Regulate Myosin II during Rigidity Sensing of Fibronectin-Based Microenvironments. *Nat. Cell Biol.* **2013**, *15* (6), 625–636.
(160) Arnaout, M. A.; Mahalingam, B.; Xiong, J.-P. INTEGRIN STRUCTURE, ALLOSTERY, AND BIDIRECTIONAL SIGNALING. *Annu. Rev. Cell Dev. Biol.* **2005**, *21* (1), 381–410. https://doi.org/10.1146/annurev.cellbio.21.090704.151217.
(161) Tomasek, J. J.; Gabbiani, G.; Hinz, B.; Chaponnier, C.; Brown, R. A. Myofibroblasts and Mechano-Regulation of Connective Tissue Remodelling. *Nat Rev Mol Cell Biol* **2002**, *3* (5), 349–363. https://doi.org/10.1038/nrm809.
(162) Winograd-Katz, S. E.; Fässler, R.; Geiger, B.; Legate, K. R. The Integrin Adhesome: From Genes and Proteins to Human Disease. *Nat Rev Mol Cell Biol* **2014**, *15* (4), 273–288.
(163) Burridge, K.; Wittchen, E. S. The Tension Mounts: Stress Fibers as Force-Generating Mechanotransducers. *J Cell Biol* **2013**, *200* (1), 9–19.
(164) Creemers, E. E.; Pinto, Y. M. Molecular Mechanisms That Control Interstitial Fibrosis in the Pressure-Overloaded Heart. *Cardiovasc. Res.* **2011**, *89* (2), 265–272. https://doi.org/10.1093/cvr/cvq308.
(165) Small, E. M.; Thatcher, J. E.; Sutherland, L. B.; Kinoshita, H.; Gerard, R. D.; Richardson, J. A.; DiMaio, J. M.; Sadek, H.; Kuwahara, K.; Olson, E. N. Myocardin-Related Transcription Factor-A Controls Myofibroblast Activation and Fibrosis in Response to Myocardial Infarction. *Circ. Res.* **2010**, *107* (2), 294. https://doi.org/10.1161/CIRCRESAHA.110.223172.
(166) Acharya, A.; Baek, S. T.; Huang, G.; Eskiocak, B.; Goetsch, S.; Sung, C. Y.; Banfi, S.; Sauer, M. F.; Olsen, G. S.; Duffield, J. S. The BHLH Transcription

Factor Tcf21 Is Required for Lineage-Specific EMT of Cardiac Fibroblast Progenitors. *Development* **2012**, *139* (12), 2139–2149.

(167) Balestrini, J. L.; Chaudhry, S.; Sarrazy, V.; Koehler, A.; Hinz, B. The Mechanical Memory of Lung Myofibroblasts. *Integr. Biol.* **2012**, *4* (4), 410–421.

(168) Hinz, B.; Phan, S. H.; Thannickal, V. J.; Prunotto, M.; Desmouliere, A.; Varga, J.; De Wever, O.; Mareel, M.; Gabbiani, G. Recent Developments in Myofibroblast Biology: Paradigms for Connective Tissue Remodeling. *Am J Pathol* **2012**, *180*. https://doi.org/10.1016/j.ajpath.2012.02.004.

(169) Zunder, E. R.; Finck, R.; Behbehani, G. K.; Amir, E. D.; Krishnaswamy, S.; Gonzalez, V. D.; Lorang, C. G.; Bjornson, Z.; Spitzer, M. H.; Bodenmiller, B.; Fantl, W. J.; Pe'er, D.; Nolan, G. P. Palladium-Based Mass Tag Cell Barcoding with a Doublet-Filtering Scheme and Single-Cell Deconvolution Algorithm. *Nat Protoc.* **2015**, *10* (2), 316–333.

(170) Frei, A. P.; Bava, F.-A.; Zunder, E. R.; Hsieh, E. W.; Chen, S.-Y.; Nolan, G. P.; Gherardini, P. F. Highly Multiplexed Simultaneous Detection of RNAs and Proteins in Single Cells. *Nat. Methods* **2016**.

(171) Mosser, D. M.; Edwards, J. P. Exploring the Full Spectrum of Macrophage Activation. *Nat. Rev. Immunol.* **2008**, *8* (12), 958–969. https://doi.org/10.1038/nri2448.

(172) Martin, K. S.; Virgilio, K. M.; Peirce, S. M.; Blemker, S. S. Computational Modeling of Muscle Regeneration and Adaptation to Advance Muscle Tissue Regeneration Strategies. *Cells Tissues Organs* **2015**, *202* (3–4), 250–266.

(173) Martin, K. S.; Kegelman, C. D.; Virgilio, K. M.; Passipieri, J. A.; Christ, G. J.; Blemker, S. S.; Peirce, S. M. In Silico and In Vivo Experiments Reveal M-CSF Injections Accelerate Regeneration Following Muscle Laceration. *Ann. Biomed. Eng.* **2017**, *45* (3), 747–760. https://doi.org/10.1007/s10439-016-1707-2.

(174) Martin, K. S.; Blemker, S. S.; Peirce, S. M. Agent-Based Computational Model Investigates Muscle-Specific Responses to Disuse-Induced Atrophy. *J. Appl. Physiol.* **2015**, *118* (10), 1299–1309. https://doi.org/10.1152/japplphysiol.01150.2014.

(175) Brown, B. N.; Price, I. M.; Toapanta, F. R.; DeAlmeida, D. R.; Wiley, C. A.; Ross, T. M.; Oury, T. D.; Vodovotz, Y. An Agent-Based Model of Inflammation and Fibrosis Following Particulate Exposure in the Lung. *Math. Biosci.* **2011**, *231* (2), 186–196. https://doi.org/10.1016/j.mbs.2011.03.005.

(176) Voit, E. O. Mesoscopic Modeling as a Starting Point for Computational Analyses of Cystic Fibrosis as a Systemic Disease. *Comput. Proteomics Syst. Biol. Clin. Implic.* **2014**, *1844* (1, Part B), 258–270. https://doi.org/10.1016/j.bbapap.2013.03.023.

(177) Dutta-Moscato, J.; Solovyev, A.; Mi, Q.; Nishikawa, T.; Soto-Gutierrez, A.; Fox, I. J.; Vodovotz, Y. A Multiscale Agent-Based in Silico Model of Liver Fibrosis Progression. *Front. Bioeng. Biotechnol.* **2014**, *2*, 18. https://doi.org/10.3389/fbioe.2014.00018.

(178) Hao, W.; Rovin, B. H.; Friedman, A. Mathematical Model of Renal Interstitial Fibrosis. *Proc. Natl. Acad. Sci.* **2014**, *111* (39), 14193–14198. https://doi.org/10.1073/pnas.1413970111.

(179) Zeigler, A. C.; Richardson, W. J.; Holmes, J. W.; Saucerman, J. J. Computational Modeling of Cardiac Fibroblasts and Fibrosis. *J. Mol. Cell. Cardiol.* **2016**, *93*, 73–83. https://doi.org/10.1016/j.yjmcc.2015.11.020.

(180) Janes, K. A.; Wang, C.-C.; Holmberg, K. J.; Cabral, K.; Brugge, J. S. Identifying Single-Cell Molecular Programs by Stochastic Profiling. *Nat Meth* **2010**, *7* (4), 311–317. https://doi.org/10.1038/nmeth.1442.

(181) Nakamura, Y.; Suda, T. Idiopathic Pulmonary Fibrosis: Diagnosis and Clinical Manifestations. *Clin. Med. Insights Circ. Respir. Pulm. Med.* **2016**, *9* (Suppl 1), 163–171. https://doi.org/10.4137/CCRPM.S39897.

(182) Organ, L. A.; Duggan, A.-M. R.; Oballa, E.; Taggart, S. C.; Simpson, J. K.; Kang'ombe, A. R.; Braybrooke, R.; Molyneaux, P. L.; North, B.; Karkera, Y.; Leeming, D. J.; Karsdal, M. A.; Nanthakumar, C. B.; Fahy, W. A.; Marshall, R. P.; Jenkins, R. G.; Maher, T. M. Biomarkers of Collagen Synthesis Predict Progression in the PROFILE Idiopathic Pulmonary Fibrosis Cohort. *Respir. Res.* **2019**, *20* (1), 148. https://doi.org/10.1186/s12931-019-1118-7.

(183) Todd, J. L.; Neely, M. L.; Overton, R.; Durham, K.; Gulati, M.; Huang, H.; Roman, J.; Newby, L. K.; Flaherty, K. R.; Vinisko, R.; Liu, Y.; Roy, J.; Schmid, R.; Strobel, B.; Hesslinger, C.; Leonard, T. B.; Noth, I.; Belperio, J. A.; Palmer, S. M.; Asi, W.; Baker, A.; Beegle, S.; Belperio, J. A.; Condos, R.; Cordova, F.; Culver, D. A.; de Andrade, J. A. M.; Dilling, D.; Flaherty, K. R.; Glassberg, M.; Gulati, M.; Guntupalli, K.; Gupta, N.; Case, A. H.; Hotchkin, D.; Huie, T.; Kaner, R.; Kim, H.; Kreider, M.; Lancaster, L.; Lasky, J.; Lederer, D.; Lee, D.; Liesching, T.; Lipchik, R.; Lobo, J.; Mageto, Y.; Menon, P.; Morrison, L.; Namen, A.; Oldham, J.; Raj, R.; Ramaswamy, M.; Russell, T.; Sachs, P.; Safdar, Z.; Sigal, B.; Silhan, L.; Strek, M.; Suliman, S.; Tabak, J.; Walia, R.; Whelan, T. P.; on behalf of the IPF-PRO Registry investigators. Peripheral Blood Proteomic Profiling of Idiopathic Pulmonary Fibrosis Biomarkers in the Multicentre IPF-PRO Registry. *Respir. Res.* **2019**, *20* (1), 227. https://doi.org/10.1186/s12931-019-1190-z.

(184) Gu, B.-H.; Madison, M. C.; Corry, D.; Kheradmand, F. Matrix Remodeling in Chronic Lung Diseases. *Matrix Biol.* **2018**, *73*, 52–63. https://doi.org/10.1016/j.matbio.2018.03.012.

(185) Ricard-Blum, S.; Baffet, G.; Théret, N. Molecular and Tissue Alterations of Collagens in Fibrosis. *Matrix Biol.* **2018**, *68–69*, 122–149. https://doi.org/10.1016/j.matbio.2018.02.004.

(186) Bitterman, P. B. Pathogenesis of Fibrosis in Acute Lung Injury. *Am. J. Med.* **1992**, *92* (6, Supplement 1), S39–S43. https://doi.org/10.1016/0002-9343(92)90606-C.

(187) Hannan, R. T.; Peirce, S. M.; Barker, T. H. Fibroblasts: Diverse Cells Critical to Biomaterials Integration. *ACS Biomater. Sci. Eng.* **2018**, *4* (4), 1223–1232. https://doi.org/10.1021/acsbiomaterials.7b00244.

(188) Alam, J.; Musiime, M.; Romaine, A.; Sawant, M.; Melleby, A. O.; Lu, N.; Eckes, B.; Christensen, G.; Gullberg, D. Generation of a Novel Mouse Strain with Fibroblast-Specific Expression of Cre Recombinase. *Matrix Biol. Plus* **2020**, 100045. https://doi.org/10.1016/j.mbplus.2020.100045.

(189) Avery, D.; Govindaraju, P.; Jacob, M.; Todd, L.; Monslow, J.; Puré, E. Extracellular Matrix Directs Phenotypic Heterogeneity of Activated Fibroblasts. *Matrix Biol.* **2018**, *67*, 90–106. https://doi.org/10.1016/j.matbio.2017.12.003.

(190) Soliman, H.; Rossi, F. M. V. Cardiac Fibroblast Diversity in Health and Disease. *Matrix Biol.* **2020**, *91–92*, 75–91. https://doi.org/10.1016/j.matbio.2020.05.003.

(191) Riccetti, M.; Gokey, J. J.; Aronow, B.; Perl, A.-K. T. The Elephant in the Lung: Integrating Lineage-Tracing, Molecular Markers, and Single Cell Sequencing Data to Identify Distinct Fibroblast Populations during Lung Development and Regeneration. *Matrix Biol.* **2020**, *91–92*, 51–74. https://doi.org/10.1016/j.matbio.2020.05.002.

(192) Kelly-Goss, M. R.; Sweat, R. S.; Stapor, P. C.; Peirce, S. M.; Murfee, W. L. Targeting Pericytes for Angiogenic Therapies. *Microcirculation* **2014**, *21* (4), 345–357. https://doi.org/10.1111/micc.12107.

(193) Tigges, U.; Welser-Alves, J. V.; Boroujerdi, A.; Milner, R. A Novel and Simple Method for Culturing Pericytes from Mouse Brain. *Microvasc. Res.* **2012**, *84* (1), 74–80. https://doi.org/10.1016/j.mvr.2012.03.008.

(194) Barron, L.; Gharib, S. A.; Duffield, J. S. Lung Pericytes and Resident Fibroblasts: Busy Multitaskers. *Am. J. Pathol.* **2016**, *186* (10), 2519–2531. https://doi.org/10.1016/j.ajpath.2016.07.004.

(195) Gomez, I. G.; Duffield, J. S. The FOXD1 Lineage of Kidney Perivascular Cells and Myofibroblasts: Functions and Responses to Injury. *Kidney Int. Suppl.* **2014**, *4* (1), 26–33. https://doi.org/10.1038/kisup.2014.6.

(196) Humphreys, B. D.; Lin, S.-L.; Kobayashi, A.; Hudson, T. E.; Nowlin, B. T.; Bonventre, J. V.; Valerius, M. T.; McMahon, A. P.; Duffield, J. S. Fate Tracing Reveals the Pericyte and Not Epithelial Origin of Myofibroblasts in Kidney Fibrosis. *Am. J. Pathol.* **2010**, *176* (1), 85–97. https://doi.org/10.2353/ajpath.2010.090517.

(197) Shankman, L. S.; Gomez, D.; Cherepanova, O. A.; Salmon, M.; Alencar, G. F.; Haskins, R. M.; Swiatlowska, P.; Newman, A. A. C.; Greene, E. S.; Straub, A. C.; Isakson, B.; Randolph, G. J.; Owens, G. K. KLF4-Dependent Phenotypic Modulation of Smooth Muscle Cells Has a Key Role in Atherosclerotic Plaque Pathogenesis. *Nat. Med.* **2015**, *21* (6), 628–637. https://doi.org/10.1038/nm.3866.

(198) Sun, Z.; Guo, S. S.; Fässler, R. Integrin-Mediated Mechanotransduction. *J. Cell Biol.* **2016**, *215* (4), 445–456. https://doi.org/10.1083/jcb.201609037.

(199) Fiore, V. F.; Strane, P. W.; Bryksin, A. V.; White, E. S.; Hagood, J. S.; Barker, T. H. Conformational Coupling of Integrin and Thy-1 Regulates Fyn Priming and Fibroblast Mechanotransduction. *J Cell Biol* **2015**, *211* (1), 173–190.

(200) Fiore, V. F.; Wong, S. S.; Tran, C.; Tan, C.; Xu, W.; Sulchek, T.; White, E. S.; Hagood, J. S.; Barker, T. H. $\boldsymbol{\alpha_v\beta_3}$ Integrin Drives Fibroblast Contraction and Strain Stiffening of Soft Provisional Matrix during Progressive Fibrosis. *JCI Insight* **2018**, *3* (20). https://doi.org/10.1172/jci.insight.97597.

(201) Hagood, J. S.; Prabhakaran, P.; Kumbla, P.; Salazar, L.; MacEwen, M. W.; Barker, T. H.; Ortiz, L. A.; Schoeb, T.; Siegal, G. P.; Alexander, C. B.; Pardo, A.; Selman, M. Loss of Fibroblast Thy-1 Expression Correlates with Lung Fibrogenesis. *Am. J. Pathol.* **2005**, *167* (2), 365–379.

(202) Brown, A. C.; Fiore, V. F.; Sulchek, T. A.; Barker, T. H. Physical and Chemical Microenvironmental Cues Orthogonally Control the Degree and Duration of Fibrosis-Associated Epithelial-to-Mesenchymal Transitions. *J. Pathol.* **2013**, *229* (1), 25–35. https://doi.org/10.1002/path.4114.

(203) Lenselink, E. A. Role of Fibronectin in Normal Wound Healing. *Int. Wound J.* **2015**, *12* (3), 313–316. https://doi.org/10.1111/iwj.12109.

(204) Markowski, M. C.; Brown, A. C.; Barker, T. H. Directing Epithelial to Mesenchymal Transition through Engineered Microenvironments Displaying Orthogonal Adhesive and Mechanical Cues. *J. Biomed. Mater. Res. A* **2012**, *100* (8), 2119–2127. https://doi.org/10.1002/jbm.a.34068.

(205) Muro, A. F.; Moretti, F. A.; Moore, B. B.; Yan, M.; Atrasz, R. G.; Wilke, C. A.; Flaherty, K. R.; Martinez, F. J.; Tsui, J. L.; Sheppard, D.; Baralle, F. E.; Toews, G. B.; White, E. S. An Essential Role for Fibronectin Extra Type III Domain A in Pulmonary Fibrosis. *Am. J. Respir. Crit. Care Med.* **2008**, *177* (6), 638–645. https://doi.org/10.1164/rccm.200708-1291OC.

(206) Torr, E. E.; Ngam, C. R.; Bernau, K.; Tomasini-Johansson, B.; Acton, B.; Sandbo, N. Myofibroblasts Exhibit Enhanced Fibronectin Assembly That Is Intrinsic to Their Contractile Phenotype. *J. Biol. Chem.* **2015**, *290* (11), 6951–6961. https://doi.org/10.1074/jbc.M114.606186.

(207) Viquez, O. M.; Yazlovitskaya, E. M.; Tu, T.; Mernaugh, G.; Secades, P.; McKee, K. K.; Quaranta, V.; Yurchenco, P.; Gewin, L. C.; Sonnenberg, A.; Pozzi, A.; Zent, R. Integrin Alpha6 Maintains the Structural Integrity of the Kidney Collecting System. *Matrix Biol. J. Int. Soc. Matrix Biol.* **2017**, *57–58*, 244–257. https://doi.org/10.1016/j.matbio.2016.12.003.

(208) Humphries, J. D.; Byron, A.; Humphries, M. J. Integrin Ligands at a Glance. *J. Cell Sci.* **2006**, *119* (19), 3901–3903. https://doi.org/10.1242/jcs.03098.

(209) Kim, K. K.; Kugler, M. C.; Wolters, P. J.; Robillard, L.; Galvez, M. G.; Brumwell, A. N.; Sheppard, D.; Chapman, H. A. Alveolar Epithelial Cell Mesenchymal Transition Develops in Vivo during Pulmonary Fibrosis and Is Regulated by the Extracellular Matrix. *Proc. Natl. Acad. Sci. U. S. A.* **2006**, *103* (35), 13180–13185. https://doi.org/10.1073/pnas.0605669103.

(210) Henderson, N. C.; Arnold, T. D.; Katamura, Y.; Giacomini, M. M.; Rodriguez, J. D.; McCarty, J. H.; Pellicoro, A.; Raschperger, E.; Betsholtz, C.; Ruminski, P. G.; Griggs, D. W.; Prinsen, M. J.; Maher, J. J.; Iredale, J. P.; Lacy-Hulbert, A.; Adams, R. H.; Sheppard, D. Targeting of Av Integrin Identifies a Core Molecular Pathway That Regulates Fibrosis in Several Organs. *Nat. Med.* **2013**, *19* (12), 1617–1624. https://doi.org/10.1038/nm.3282.

(211) Crnkovic, S.; Marsh, L. M.; El Agha, E.; Voswinckel, R.; Ghanim, B.; Klepetko, W.; Stacher-Priehse, E.; Olschewski, H.; Bloch, W.; Bellusci, S.; Olschewski, A.; Kwapiszewska, G. Resident Cell Lineages Are Preserved in Pulmonary Vascular Remodeling. *J. Pathol.* **2018**, *244* (4), 485–498. https://doi.org/10.1002/path.5044.

(212) Haskins, R. M.; Nguyen, A. T.; Alencar, G. F.; Billaud, M.; Kelly-Goss, M. R.; Good, M. E.; Bottermann, K.; Klibanov, A. L.; French, B. A.; Harris, T. E.; Peirce, S. M.; Isakson, B. E.; Owens, G. K. Klf4 Has an Unexpected Protective Role in Perivascular Cells within the Microvasculature. *Am. J. Physiol.-Heart Circ. Physiol.* **2018**, *315* (2), H402–H414. https://doi.org/10.1152/ajpheart.00084.2018.

(213) Hess, D. L.; Kelly-Goss, M. R.; Cherepanova, O. A.; Nguyen, A. T.; Baylis, R. A.; Tkachenko, S.; Annex, B. H.; Peirce, S. M.; Owens, G. K. Perivascular Cell-Specific Knockout of the Stem Cell Pluripotency Gene Oct4 Inhibits Angiogenesis. *Nat. Commun.* **2019**, *10* (1), 1–15. https://doi.org/10.1038/s41467-019-08811-z.

(214) Corliss, B. A.; Ray, H. C.; Doty, R. W.; Mathews, C.; Sheybani, N.; Fitzgerald, K.; Prince, R.; Kelly-Goss, M. R.; Murfee, W. L.; Chappell, J.; Owens, G. K.; Yates, P. A.; Peirce, S. M. Pericyte Bridges in Homeostasis and Hyperglycemia. *Diabetes* **2020**, *69* (7), 1503. https://doi.org/10.2337/db19-0471.

(215) Adamson, I. Y. R.; Bowden, D. H. The Pathogenesis of Bleomycin-Induced Pulmonary Fibrosis in Mice. *Am J Pathol* **1974**, *77*.

(216) Akamatsu, T.; Arai, Y.; Kosugi, I.; Kawasaki, H.; Meguro, S.; Sakao, M.; Shibata, K.; Suda, T.; Chida, K.; Iwashita, T. Direct Isolation of Myofibroblasts and Fibroblasts from Bleomycin-Injured Lungs Reveals Their Functional Similarities and Differences. *Fibrogenesis Tissue Repair* **2013**, *6* (1), 15. https://doi.org/10.1186/1755-1536-6-15.

(217) Xie, T.; Liang, J.; Liu, N.; Huan, C.; Zhang, Y.; Liu, W.; Kumar, M.; Xiao, R.; D'Armiento, J.; Metzger, D.; Chambon, P.; Papaioannou, V. E.; Stripp, B. R.; Jiang, D.; Noble, P. W. Transcription Factor TBX4 Regulates Myofibroblast Accumulation and Lung Fibrosis. *J. Clin. Invest. 126* (8), 3063–3079. https://doi.org/10.1172/JCI85328.

(218) Lin, S.-L.; Kisseleva, T.; Brenner, D. A.; Duffield, J. S. Pericytes and Perivascular Fibroblasts Are the Primary Source of Collagen-Producing Cells in Obstructive Fibrosis of the Kidney. *Am. J. Pathol.* **2008**, *173* (6), 1617–1627. https://doi.org/10.2353/ajpath.2008.080433.

(219) Ashburner, M.; Ball, C. A.; Blake, J. A.; Botstein, D.; Butler, H.; Cherry, J. M.; Davis, A. P.; Dolinski, K.; Dwight, S. S.; Eppig, J. T.; Harris, M. A.; Hill, D. P.; Issel-Tarver, L.; Kasarskis, A.; Lewis, S.; Matese, J. C.; Richardson, J. E.; Ringwald, M.; Rubin, G. M.; Sherlock, G. Gene Ontology: Tool for the Unification of Biology. *Nat. Genet.* **2000**, *25* (1), 25–29. https://doi.org/10.1038/75556.

(220) The Gene Ontology Resource: 20 Years and Still GOing Strong. *Nucleic Acids Res.* **2019**, *47* (D1), D330–D338. https://doi.org/10.1093/nar/gky1055.

(221) Naba, A.; Clauser, K. R.; Hoersch, S.; Liu, H.; Carr, S. A.; Hynes, R. O. The Matrisome: In Silico Definition and in Vivo Characterization by Proteomics of Normal and Tumor Extracellular Matrices. *Mol. Cell. Proteomics MCP* **2012**, *11* (4), M111.014647. https://doi.org/10.1074/mcp.M111.014647.

(222) Cao, L.; Nicosia, J.; Larouche, J.; Zhang, Y.; Bachman, H.; Brown, A. C.; Holmgren, L.; Barker, T. H. Detection of an Integrin-Binding Mechanoswitch within Fibronectin during Tissue Formation and Fibrosis. *ACS Nano* **2017**, *11* (7), 7110–7117. https://doi.org/10.1021/acsnano.7b02755.

(223) Reynolds, L. E.; D'Amico, G.; Lechertier, T.; Papachristodoulou, A.; Muñoz-Félix, J. M.; De Arcangelis, A.; Baker, M.; Serrels, B.; Hodivala-Dilke, K. M. Dual Role of Pericyte A6β1-Integrin in Tumour Blood Vessels. *J. Cell Sci.* **2017**, *130* (9), 1583–1595. https://doi.org/10.1242/jcs.197848.

(224) Kapp, T. G.; Rechenmacher, F.; Neubauer, S.; Maltsev, O. V.; Cavalcanti-Adam, E. A.; Zarka, R.; Reuning, U.; Notni, J.; Wester, H.-J.; Mas-Moruno, C.; Spatz, J.; Geiger, B.; Kessler, H. A Comprehensive Evaluation of the Activity and Selectivity Profile of Ligands for RGD-Binding Integrins. *Sci. Rep.* **2017**, *7*. https://doi.org/10.1038/srep39805.

(225) Hung, C.; Linn, G.; Chow, Y.-H.; Kobayashi, A.; Mittelsteadt, K.; Altemeier, W. A.; Gharib, S. A.; Schnapp, L. M.; Duffield, J. S. Role of Lung Pericytes and Resident Fibroblasts in the Pathogenesis of Pulmonary Fibrosis. *Am. J. Respir. Crit. Care Med.* **2013**, *188* (7), 820–830.

(226) Birbrair, A.; Zhang, T.; Wang, Z.-M.; Messi, M. L.; Mintz, A.; Delbono, O. Pericytes at the Intersection between Tissue Regeneration and Pathology. *Clin. Sci. Lond. Engl. 1979* **2015**, *128* (2), 81–93. https://doi.org/10.1042/CS20140278.

(227) Chang, F.-C.; Chou, Y.-H.; Chen, Y.-T.; Lin, S.-L. Novel Insights into Pericyte–Myofibroblast Transition and Therapeutic Targets in Renal Fibrosis. *J. Formos. Med. Assoc.* **2012**, *111* (11), 589–598.

(228) Dulauroy, S.; Di Carlo, S. E.; Langa, F.; Eberl, G.; Peduto, L. Lineage Tracing and Genetic Ablation of ADAM12(+) Perivascular Cells Identify a Major Source of Profibrotic Cells during Acute Tissue Injury. *Nat Med* **2012**, *18*.

(229) Bingham, G.; Lee, F.; Naba, A.; Barker, T. H. Spatial-Omics: Novel Approaches to Probe Cell Heterogeneity and ECM Biology. *Matrix Biol.* No. Special Edition: Fibroblasts: The Arbiters of Matrix Remodeling.

(230) Ciobanasu, C.; Faivre, B.; Le Clainche, C. Integrating Actin Dynamics, Mechanotransduction and Integrin Activation: The Multiple Functions of Actin Binding Proteins in Focal Adhesions. *SPP 1464Actin Dyn. – Part I* **2013**, *92* (10–11), 339–348. https://doi.org/10.1016/j.ejcb.2013.10.009.

(231) Ito, J. T.; Lourenço, J. D.; Righetti, R. F.; Tibério, I. F. L. C.; Prado, C. M.; Lopes, F. D. T. Q. S. Extracellular Matrix Component Remodeling in Respiratory Diseases: What Has Been Found in Clinical and Experimental Studies? *Cells* **2019**, *8* (4). https://doi.org/10.3390/cells8040342.

(232) White, E. S. Lung Extracellular Matrix and Fibroblast Function. *Ann. Am. Thorac. Soc.* **2015**, *12* (Suppl 1), S30–S33. https://doi.org/10.1513/AnnalsATS.201406-240MG.

(233) Sun, Y.; Fang, M.; Wang, J.; Cooper, C. R.; Pienta, K. J.; Taichman, R. S. Expression and Activation of Avβ3 Integrins by SDF-1/CXC12 Increases the Aggressiveness of Prostate Cancer Cells. *The Prostate* **2007**, *67* (1), 61–73.

(234) Gomez, D.; Shankman, L. S.; Nguyen, A. T.; Owens, G. K. Detection of Histone Modifications at Specific Gene Loci in Single Cells in Histological Sections. *Nat. Methods* **2013**, *10* (2), 171.

(235) Alencar Gabriel F.; Owsiany Katherine M.; K Santosh; Sukhavasi Katyayani; Mocci Giuseppe; Nguyen Anh; Williams Corey M.; Shamsuzzaman Sohel; Mokry Michal; Henderson Christopher A.; Haskins Ryan; Baylis Richard A.; Finn Aloke V.; McNamara Coleen A.; Zunder Eli R.; Venkata Vamsidhar; Pasterkamp Gerard; Björkegren Johan; Bekiranov Stefan; Owens Gary K. The Stem Cell Pluripotency Genes Klf4 and Oct4 Regulate Complex SMC Phenotypic Changes Critical in Late-Stage Atherosclerotic Lesion Pathogenesis. *Circulation 0* (0). https://doi.org/10.1161/CIRCULATIONAHA.120.046672.

(236) Kumar, A.; D'Souza, S. S.; Moskvin, O. V.; Toh, H.; Wang, B.; Zhang, J.; Swanson, S.; Guo, L.-W.; Thomson, J. A.; Slukvin, I. I. Specification and Diversification of Pericytes and Smooth Muscle Cells from Mesenchymoangioblasts. *Cell Rep.* **2017**, *19* (9), 1902–1916. https://doi.org/10.1016/j.celrep.2017.05.019.

(237) Hanumegowda, C.; Farkas, L.; Kolb, M. Angiogenesis in Pulmonary Fibrosis: Too Much or Not Enough? *CHEST J.* **2012**, *142* (1), 200–207.

(238) Scotton, C. J.; Chambers, R. C. Bleomycin Revisited: Towards a More Representative Model of IPF? *Am J Physiol Lung Cell Mol Physiol* **2010**, *299*. https://doi.org/10.1152/ajplung.00258.2010.

(239) Fletcher, A. L.; Malhotra, D.; Acton, S. E.; Lukacs-Kornek, V.; Bellemare-Pelletier, A.; Curry, M.; Armant, M.; Turley, S. J. Reproducible Isolation of Lymph Node Stromal Cells Reveals Site-Dependent Differences in Fibroblastic Reticular Cells. *Front. Immunol.* **2011**, *2*. https://doi.org/10.3389/fimmu.2011.00035.

(240) Liu, F.; Lagares, D.; Choi, K. M.; Stopfer, L.; Marinković, A.; Vrbanac, V.; Probst, C. K.; Hiemer, S. E.; Sisson, T. H.; Horowitz, J. C.; Rosas, I. O.;

Fredenburgh, L. E.; Feghali-Bostwick, C.; Varelas, X.; Tager, A. M.; Tschumperlin, D. J. Mechanosignaling through YAP and TAZ Drives Fibroblast Activation and Fibrosis. *Am. J. Physiol.-Lung Cell. Mol. Physiol.* **2014**, *308* (4), L344–L357. https://doi.org/10.1152/ajplung.00300.2014.

(241) Kramann, R.; Wongboonsin, J.; Chang-Panesso, M.; Machado, F. G.; Humphreys, B. D. Gli1+ Pericyte Loss Induces Capillary Rarefaction and Proximal Tubular Injury. *J. Am. Soc. Nephrol.* **2017**, *28* (3), 776–784. https://doi.org/10.1681/ASN.2016030297.

(242) Gui, Y.; Li, J.; Lu, Q.; Feng, Y.; Wang, M.; He, W.; Yang, J.; Dai, C. Yap/Taz Mediates MTORC2-Stimulated Fibroblast Activation and Kidney Fibrosis. *J. Biol. Chem.* **2018**, *293* (42), 16364–16375. https://doi.org/10.1074/jbc.RA118.004073.

(243) Hinz, B.; Gabbiani, G. Cell-Matrix and Cell-Cell Contacts of Myofibroblasts: Role in Connective Tissue Remodeling. *Thromb. Haemost.* **2003**, *90* (12), 993–1002. https://doi.org/10.1160/TH03-05-0328.

(244) Schindelin, J.; Arganda-Carreras, I.; Frise, E.; Kaynig, V.; Longair, M.; Pietzsch, T.; Preibisch, S.; Rueden, C.; Saalfeld, S.; Schmid, B.; Tinevez, J.-Y.; White, D. J.; Hartenstein, V.; Eliceiri, K.; Tomancak, P.; Cardona, A. Fiji: An Open-Source Platform for Biological-Image Analysis. *Nat. Methods* **2012**, *9* (7), 676–682. https://doi.org/10.1038/nmeth.2019.

(245) Babraham Bioinformatics - Trim Galore! https://www.bioinformatics.babraham.ac.uk/projects/trim_galore/ (accessed Nov 9, 2020).

(246) Babraham Bioinformatics - FastQC A Quality Control tool for High Throughput Sequence Data https://www.bioinformatics.babraham.ac.uk/projects/fastqc/ (accessed Nov 9, 2020).

(247) Pertea, M.; Kim, D.; Pertea, G. M.; Leek, J. T.; Salzberg, S. L. Transcript-Level Expression Analysis of RNA-Seq Experiments with HISAT, StringTie and Ballgown. *Nat. Protoc.* **2016**, *11* (9), 1650–1667. https://doi.org/10.1038/nprot.2016.095.

(248) Kim, D.; Langmead, B.; Salzberg, S. L. HISAT: A Fast Spliced Aligner with Low Memory Requirements. *Nat. Methods* **2015**, *12* (4), 357–360. https://doi.org/10.1038/nmeth.3317.

(249) Pertea, M.; Pertea, G. M.; Antonescu, C. M.; Chang, T.-C.; Mendell, J. T.; Salzberg, S. L. StringTie Enables Improved Reconstruction of a Transcriptome from RNA-Seq Reads. *Nat. Biotechnol.* **2015**, *33* (3), 290–295. https://doi.org/10.1038/nbt.3122.

(250) Love, M. I.; Huber, W.; Anders, S. Moderated Estimation of Fold Change and Dispersion for RNA-Seq Data with DESeq2. *Genome Biol.* **2014**, *15* (12), 550. https://doi.org/10.1186/s13059-014-0550-8.

(251) Ge-Lab http://ge-lab.org/#/data (accessed Nov 9, 2020).

(252) Subramanian, A.; Tamayo, P.; Mootha, V. K.; Mukherjee, S.; Ebert, B. L.; Gillette, M. A.; Paulovich, A.; Pomeroy, S. L.; Golub, T. R.; Lander, E. S.; Mesirov, J. P. Gene Set Enrichment Analysis: A Knowledge-Based Approach for Interpreting Genome-Wide Expression Profiles. *Proc. Natl. Acad. Sci. U. S. A.* **2005**, *102* (43), 15545–15550. https://doi.org/10.1073/pnas.0506580102.

(253) Birbrair, A.; Zhang, T.; Wang, Z. M.; Messi, M. L.; Enikolopov, G. N.; Mintz, A.; Delbono, O. Role of Pericytes in Skeletal Muscle Regeneration and Fat Accumulation. *Stem Cells Dev* **2013**, *22*.

(254) Dar, A.; Domev, H.; Ben-Yosef, O.; Tzukerman, M.; Zeevi-Levin, N.; Novak, A.; Germanguz, I.; Amit, M.; Itskovitz-Eldor, J. Multipotent Vasculogenic Pericytes from Human Pluripotent Stem Cells Promote Recovery of Murine Ischemic Limb. *Circulation* **2012**, *125*.

(255) Dore-Duffy, P.; Katychev, A.; Wang, X.; Van Buren, E. CNS Microvascular Pericytes Exhibit Multipotential Stem Cell Activity. *J Cereb Blood Flow Metab* **2006**, *26*.

(256) Chen, W. C. W.; Baily, J. E.; Corselli, M.; Díaz, M. E.; Sun, B.; Xiang, G.; Gray, G. A.; Huard, J.; Péault, B. Human Myocardial Pericytes: Multipotent Mesodermal Precursors Exhibiting Cardiac Specificity. *STEM CELLS* **2015**, *33* (2), 557–573. https://doi.org/10.1002/stem.1868.

(257) Guimarães-Camboa, N.; Cattaneo, P.; Sun, Y.; Moore-Morris, T.; Gu, Y.; Dalton, N. D.; Rockenstein, E.; Masliah, E.; Peterson, K. L.; Stallcup, W. B.; Chen, J.; Evans, S. M. Pericytes of Multiple Organs Do Not Behave as Mesenchymal Stem Cells In Vivo. *Cell Stem Cell* **2017**, *20* (3), 345-359.e5. https://doi.org/10.1016/j.stem.2016.12.006.

(258) Hosein, A. N.; Huang, H.; Wang, Z.; Parmar, K.; Du, W.; Huang, J.; Maitra, A.; Olson, E.; Verma, U.; Brekken, R. A. Cellular Heterogeneity during Mouse Pancreatic Ductal Adenocarcinoma Progression at Single-Cell Resolution. *JCI Insight* **2019**, *4* (16).

(259) Zunder, E. R.; Finck, R.; Behbehani, G. K.; Amir, E. D.; Krishnaswamy, S.; Gonzalez, V. D.; Lorang, C. G.; Bjornson, Z.; Spitzer, M. H.; Bodenmiller, B.; Fantl, W. J.; Pe'er, D.; Nolan, G. P. Palladium-Based Mass Tag Cell Barcoding with a Doublet-Filtering Scheme and Single-Cell Deconvolution Algorithm. *Nat Protoc.* **2015**, *10* (2), 316–333.

(260) Uccelli, A.; Moretta, L.; Pistoia, V. Mesenchymal Stem Cells in Health and Disease. *Nat. Rev. Immunol.* **2008**, *8* (9), 726–736.

(261) Gimble, J. M.; Katz, A. J.; Bunnell, B. A. Adipose-Derived Stem Cells for Regenerative Medicine. *Circ. Res.* **2007**, *100* (9), 1249–1260.

(262) Jin, H. J.; Kwon, J. H.; Kim, M.; Bae, Y. K.; Choi, S. J.; Oh, W.; Yang, Y. S.; Jeon, H. B. Downregulation of Melanoma Cell Adhesion Molecule (MCAM/CD146) Accelerates Cellular Senescence in Human Umbilical Cord Blood-Derived Mesenchymal Stem Cells. *Stem Cells Transl. Med.* **2016**, *5* (4), 427–439.

(263) Wangler, S.; Menzel, U.; Li, Z.; Ma, J.; Hoppe, S.; Benneker, L. M.; Alini, M.; Grad, S.; Peroglio, M. CD146/MCAM Distinguishes Stem Cell Subpopulations with Distinct Migration and Regenerative Potential in Degenerative Intervertebral Discs. *Osteoarthritis Cartilage* **2019**, *27* (7), 1094–1105.

(264) Liu, W.-F.; Ji, S.-R.; Sun, J.-J.; Zhang, Y.; Liu, Z.-Y.; Liang, A.-B.; Zeng, H.-Z. CD146 Expression Correlates with Epithelial-Mesenchymal Transition Markers and a Poor Prognosis in Gastric Cancer. *Int. J. Mol. Sci.* **2012**, *13* (5), 6399–6406.

(265) Paduano, F.; Marrelli, M.; Palmieri, F.; Tatullo, M. CD146 Expression Influences Periapical Cyst Mesenchymal Stem Cell Properties. *Stem Cell Rev. Rep.* **2016**, *12* (5), 592–603.

(266) Wang, J.; Zhou, J.; Huang, F.; Zhang, L.; He, Q.; Qian, H.; Lai, H. GLI2 Induces PDGFRB Expression and Modulates Cancer Stem Cell Properties of Gastric Cancer. *Eur Rev Med Pharmacol Sci* **2017**, *21* (17), 3857–3865.

(267) Olson, L. E.; Soriano, P. PDGFRbeta Signaling Regulates Mural Cell Plasticity and Inhibits Fat Development. *Dev Cell* **2011**, *20*.

(268) Steller, E. J.; Raats, D. A.; Koster, J.; Rutten, B.; Govaert, K. M.; Emmink, B. L.; Snoeren, N.; van Hooff, S. R.; Holstege, F. C.; Maas, C. PDGFRB Promotes Liver Metastasis Formation of Mesenchymal-like Colorectal Tumor Cells. *Neoplasia* **2013**, *15* (2), 204-IN30.

(269) Periasamy, R.; Elshaer, S. L.; Gangaraju, R. CD140b (PDGFRβ) Signaling in Adipose-Derived Stem Cells Mediates Angiogenic Behavior of Retinal Endothelial Cells. *Regen. Eng. Transl. Med.* **2019**, *5* (1), 1–9.

(270) Ray, H. C.; Corliss, B. A.; Bruce, A. C.; Kesting, S.; Dey, P.; Mansour, J.; Seaman, S. A.; Smolko, C. M.; Mathews, C.; Dey, B. K.; Owens, G. K.; Peirce, S. M.; Yates, P. A. Myh11+ Microvascular Mural Cells and Derived Mesenchymal Stem Cells Promote Retinal Fibrosis. *Sci. Rep.* **2020**, *10* (1), 15808. https://doi.org/10.1038/s41598-020-72875-x.

(271) Takahashi, K.; Yamanaka, S. Induction of Pluripotent Stem Cells from Mouse Embryonic and Adult Fibroblast Cultures by Defined Factors. *cell* **2006**, *126* (4), 663–676.

(272) Davis-Dusenbery, B. N.; Chan, M. C.; Reno, K. E.; Weisman, A. S.; Layne, M. D.; Lagna, G.; Hata, A. Downregulation of KLF4 by MIR-143/145 Is Critical for Modulation of Vascular Smooth Muscle Cell Phenotype by TGF-β and BMP. *J. Biol. Chem.* **2011**. https://doi.org/10.1074/jbc.M111.236950.

(273) Qin, S.; Zou, Y.; Zhang, C.-L. Cross-Talk between KLF4 and STAT3 Regulates Axon Regeneration. *Nat. Commun.* **2013**, *4*, 2633.

(274) Yu, F.; Li, J.; Chen, H.; Fu, J.; Ray, S.; Huang, S.; Zheng, H.; Ai, W. Kruppel-like Factor 4 (KLF4) Is Required for Maintenance of Breast Cancer Stem Cells and for Cell Migration and Invasion. *Oncogene* **2011**, *30* (18), 2161–2172.

(275) Riverso, M.; Montagnani, V.; Stecca, B. KLF4 Is Regulated by RAS/RAF/MEK/ERK Signaling through E2F1 and Promotes Melanoma Cell Growth. *Oncogene* **2017**.

(276) Jung, J.-S.; Volk, C.; Marga, C.; Navarrete Santos, A.; Jung, M.; Rujescu, D.; Navarrete Santos, A. Adipose-Derived Stem/Stromal Cells Recapitulate Aging Biomarkers and Show Reduced Stem Cell Plasticity Affecting Their Adipogenic Differentiation Capacity. *Cell. Reprogramming* **2019**, *21* (4), 187–199. https://doi.org/10.1089/cell.2019.0010.

(277) Yin, M.; Zhou, H. J.; Lin, C.; Long, L.; Yang, X.; Zhang, H.; Taylor, H.; Min, W. CD34+KLF4+ Stromal Stem Cells Contribute to Endometrial Regeneration and Repair. *Cell Rep.* **2019**, *27* (9), 2709-2724.e3. https://doi.org/10.1016/j.celrep.2019.04.088.

(278) Melnik, S.; Werth, N.; Boeuf, S.; Hahn, E.-M.; Gotterbarm, T.; Anton, M.; Richter, W. Impact of C-MYC Expression on Proliferation, Differentiation, and Risk of Neoplastic Transformation of Human Mesenchymal Stromal Cells. *Stem Cell Res. Ther.* **2019**, *10* (1), 73. https://doi.org/10.1186/s13287-019-1187-z.

(279) Guo, X.; Tang, Y.; Zhang, P.; Li, S.; Chen, Y.; Qian, B.; Shen, H.; Zhao, N. Effect of Ectopic High Expression of Transcription Factor OCT4 on the "Stemness" Characteristics of Human Bone Marrow-Derived Mesenchymal Stromal Cells. *Stem Cell Res. Ther.* **2019**, *10* (1), 160. https://doi.org/10.1186/s13287-019-1263-4.

(280) Lee, Y.-M.; Kim, T.-H.; Lee, J.-H.; Lee, W.-J.; Jeon, R.-H.; Jang, S.-J.; Ock, S.-A.; Lee, S.-L.; Park, B.-W.; Rho, G.-J. Overexpression of Oct4 in Porcine Ovarian Stem/Stromal Cells Enhances Differentiation of Oocyte-like Cells in Vitro and Ovarian Follicular Formation in Vivo. *J. Ovarian Res.* **2016**, *9*, 24. https://doi.org/10.1186/s13048-016-0233-z.

(281) Mildmay-White, A.; Khan, W. Cell Surface Markers on Adipose-Derived Stem Cells: A Systematic Review. *Curr. Stem Cell Res. Ther.* **2017**, *12* (6), 484–492. https://doi.org/10.2174/1574888X11666160429122133.

(282) Yannarelli, G.; Pacienza, N.; Montanari, S.; Santa-Cruz, D.; Viswanathan, S.; Keating, A. OCT4 Expression Mediates Partial Cardiomyocyte Reprogramming of Mesenchymal Stromal Cells. *PloS One* **2017**, *12* (12), e0189131. https://doi.org/10.1371/journal.pone.0189131.

(283) Yan, W.; Wu, X.; Zhou, W.; Fong, M. Y.; Cao, M.; Liu, J.; Liu, X.; Chen, C.-H.; Fadare, O.; Pizzo, D. P.; Wu, J.; Liu, L.; Liu, X.; Chin, A. R.; Ren, X.; Chen, Y.; Locasale, J. W.; Wang, S. E. Cancer-Cell-Secreted Exosomal MiR-105 Promotes Tumour Growth through the MYC-Dependent Metabolic Reprogramming of Stromal Cells. *Nat. Cell Biol.* **2018**, *20* (5), 597–609. https://doi.org/10.1038/s41556-018-0083-6.

(284) Cherepanova, O. A.; Gomez, D.; Shankman, L. S.; Swiatlowska, P.; Williams, J.; Sarmento, O. F.; Alencar, G. F.; Hess, D. L.; Bevard, M. H.; Greene, E. S.; Murgai, M.; Turner, S. D.; Geng, Y.-J.; Bekiranov, S.; Connelly, J. J.; Tomilin, A.; Owens, G. K. Activation of the ESC Pluripotency Factor OCT4 in Smooth Muscle Cells Is Atheroprotective. *Nat. Med.* **2016**, *22* (6), 657–665. https://doi.org/10.1038/nm.4109.

(285) Geevarghese, A.; Herman, I. M. Pericyte-Endothelial Cross-Talk: Implications and Opportunities for Advanced Cellular Therapies. *Transl. Res. J. Lab. Clin. Med.* **2014**, *163* (4), 296–306. https://doi.org/10.1016/j.trsl.2014.01.011.

(286) Cleary, M. A.; Narcisi, R.; Focke, K.; van der Linden, R.; Brama, P. A. J.; van Osch, G. J. V. M. Expression of CD105 on Expanded Mesenchymal Stem Cells Does Not Predict Their Chondrogenic Potential. *Osteoarthritis Cartilage* **2016**, *24* (5), 868–872. https://doi.org/10.1016/j.joca.2015.11.018.

(287) Takagi, H.; King, G. L.; Aiello, L. P. Identification and Characterization of Vascular Endothelial Growth Factor Receptor (Flt) in Bovine Retinal Pericytes. *Diabetes* **1996**, *45* (8), 1016–1023. https://doi.org/10.2337/diab.45.8.1016.

(288) Witmer, A. N.; Dai, J.; Weich, H. A.; Vrensen, G. F. J. M.; Schlingemann, R. O. Expression of Vascular Endothelial Growth Factor Receptors 1, 2, and 3 in Quiescent Endothelia. *J. Histochem. Cytochem.* **2002**, *50* (6), 767–777. https://doi.org/10.1177/002215540205000603.

(289) Cao, R.; Xue, Y.; Hedlund, E.-M.; Zhong, Z.; Tritsaris, K.; Tondelli, B.; Lucchini, F.; Zhu, Z.; Dissing, S.; Cao, Y. VEGFR1-Mediated Pericyte Ablation Links VEGF and PIGF to Cancer-Associated Retinopathy. *Proc. Natl. Acad. Sci. U. S. A.* **2010**, *107*, 856–861. https://doi.org/10.1073/pnas.0911661107.

(290) Dejana, E.; Lampugnani, M. G. Endothelial Cell Transitions. *Science* **2018**, *362* (6416), 746–747. https://doi.org/10.1126/science.aas9432.

(291) Dejana, E.; Hirschi, K. K.; Simons, M. The Molecular Basis of Endothelial Cell Plasticity. *Nat. Commun.* **2017**, *8* (1), 14361. https://doi.org/10.1038/ncomms14361.

(292) Evrard, S. M.; Lecce, L.; Michelis, K. C.; Nomura-Kitabayashi, A.; Pandey, G.; Purushothaman, K.-R.; d'Escamard, V.; Li, J. R.; Hadri, L.; Fujitani, K.; Moreno, P. R.; Benard, L.; Rimmele, P.; Cohain, A.; Mecham, B.; Randolph, G. J.; Nabel, E. G.; Hajjar, R.; Fuster, V.; Boehm, M.; Kovacic, J. C. Endothelial to Mesenchymal Transition Is Common in Atherosclerotic Lesions and Is Associated with Plaque Instability. *Nat. Commun.* **2016**, *7*, 11853. https://doi.org/10.1038/ncomms11853.

(293) Chen, P.-Y.; Qin, L.; Baeyens, N.; Li, G.; Afolabi, T.; Budatha, M.; Tellides, G.; Schwartz, M. A.; Simons, M. Endothelial-to-Mesenchymal Transition Drives Atherosclerosis Progression. *J. Clin. Invest.* **2015**, *125* (12), 4514–4528. https://doi.org/10.1172/JCI82719.

(294) Anderberg, C.; Cunha, S. I.; Zhai, Z.; Cortez, E.; Pardali, E.; Johnson, J. R.; Franco, M.; Páez-Ribes, M.; Cordiner, R.; Fuxe, J.; Johansson, B. R.; Goumans, M.-J.; Casanovas, O.; ten Dijke, P.; Arthur, H. M.; Pietras, K. Deficiency for Endoglin in Tumor Vasculature Weakens the Endothelial Barrier to Metastatic Dissemination. *J. Exp. Med.* **2013**, *210* (3), 563–579. https://doi.org/10.1084/jem.20120662.

(295) Choi, K. J.; Nam, J.-K.; Kim, J.-H.; Choi, S.-H.; Lee, Y.-J. Endothelial-to-Mesenchymal Transition in Anticancer Therapy and Normal Tissue Damage.

Exp. Mol. Med. **2020**, *52* (5), 781–792. https://doi.org/10.1038/s12276-020-0439-4.

(296) Choi, S.-H.; Kim, A.-R.; Nam, J.-K.; Kim, J.-M.; Kim, J.-Y.; Seo, H. R.; Lee, H.-J.; Cho, J.; Lee, Y.-J. Tumour-Vasculature Development via Endothelial-to-Mesenchymal Transition after Radiotherapy Controls CD44v6 + Cancer Cell and Macrophage Polarization. *Nat. Commun.* **2018**, *9* (1), 5108. https://doi.org/10.1038/s41467-018-07470-w.

(297) Fong, D. S.; Aiello, L.; Gardner, T. W.; King, G. L.; Blankenship, G.; Cavallerano, J. D.; Ferris, F. L.; Klein, R. Retinopathy in Diabetes. *Diabetes Care* **2004**, *27* (suppl 1), s84–s87. https://doi.org/10.2337/diacare.27.2007.S84.

(298) He, L.; Mäe, M. A.; Sun, Y.; Muhl, L.; Nahar, K.; Liébanas, E. V.; Fagerlund, M. J.; Oldner, A.; Liu, J.; Genové, G.; Pietilä, R.; Zhang, L.; Xie, Y.; Leptidis, S.; Mocci, G.; Stritt, S.; Osman, A.; Anisimov, A.; Hemanthakumar, K. A.; Räsenen, M.; Björkegren, J.; Vanlandewijck, M.; Blomgren, K.; Hansson, E.; Mäkinen, T.; Peng, X.-R.; Arnold, T. D.; Alitalo, K.; Eriksson, L. I.; Lendahl, U.; Betsholtz, C. Pericyte-Specific Vascular Expression of SARS-CoV-2 Receptor ACE2 – Implications for Microvascular Inflammation and Hypercoagulopathy in COVID-19 Patients. *bioRxiv* **2020**, 2020.05.11.088500. https://doi.org/10.1101/2020.05.11.088500.

(299) Kolde, R. Pheatmap: Pretty Heatmaps. *R Package Version* **2012**, *1* (2).

(300) Fogg, K. C.; Miller, A. E.; Li, Y.; Flanigan, W.; Walker, A.; O'Shea, A.; Kendziorski, C.; Kreeger, P. K. Ovarian Cancer Cells Direct Monocyte Differentiation through a Non-Canonical Pathway. *BMC Cancer* **2020**, *20* (1), 1008. https://doi.org/10.1186/s12885-020-07513-w.

(301) Makarev, E.; Izumchenko, E.; Aihara, F.; Wysocki, P. T.; Zhu, Q.; Buzdin, A.; Sidransky, D.; Zhavoronkov, A.; Atala, A. Common Pathway Signature in Lung and Liver Fibrosis. *Cell Cycle* **2016**, *15* (13), 1667–1673. https://doi.org/10.1080/15384101.2016.1152435.

(302) Nangaku, M. Chronic Hypoxia and Tubulointerstitial Injury: A Final Common Pathway to End-Stage Renal Failure. *J. Am. Soc. Nephrol.* **2006**, *17* (1), 17–25.

(303) Vancheri, C. Common Pathways in Idiopathic Pulmonary Fibrosis and Cancer. *Eur. Respir. Rev.* **2013**, *22* (129), 265–272. https://doi.org/10.1183/09059180.00003613.

(304) Weber, K. T. Fibrosis, a Common Pathway to Organ Failure: Angiotensin II and Tissue Repair.; 1997; Vol. 17, p 467.

(305) Park, T. I.-H.; Feisst, V.; Brooks, A. E. S.; Rustenhoven, J.; Monzo, H. J.; Feng, S. X.; Mee, E. W.; Bergin, P. S.; Oldfield, R.; Graham, E. S.; Curtis, M. A.; Faull, R. L. M.; Dunbar, P. R.; Dragunow, M. Cultured Pericytes from Human Brain Show Phenotypic and Functional Differences Associated with Differential CD90 Expression. *Sci. Rep.* **2016**, *6*, 26587.

(306) Adams, T. S.; Schupp, J. C.; Poli, S.; Ayaub, E. A.; Neumark, N.; Ahangari, F.; Chu, S. G.; Raby, B. A.; DeIuliis, G.; Januszyk, M.; Duan, Q.; Arnett, H. A.;

Siddiqui, A.; Washko, G. R.; Homer, R.; Yan, X.; Rosas, I. O.; Kaminski, N. Single-Cell RNA-Seq Reveals Ectopic and Aberrant Lung-Resident Cell Populations in Idiopathic Pulmonary Fibrosis. *Sci. Adv.* **2020**, *6* (28), eaba1983. https://doi.org/10.1126/sciadv.aba1983.

(307) Kimmel, J. C.; Penland, L.; Rubinstein, N. D.; Hendrickson, D. G.; Kelley, D. R.; Rosenthal, A. Z. Murine Single-Cell RNA-Seq Reveals Cell-Identity- and Tissue-Specific Trajectories of Aging. *Genome Res.* **2019**, *29* (12), 2088–2103. https://doi.org/10.1101/gr.253880.119.

(308) Li, S.; Wan, C.; Zheng, R.; Fan, J.; Dong, X.; Meyer, C. A.; Liu, X. S. Cistrome-GO: A Web Server for Functional Enrichment Analysis of Transcription Factor ChIP-Seq Peaks. *Nucleic Acids Res.* **2019**, *47* (W1), W206–W211. https://doi.org/10.1093/nar/gkz332.

(309) GEO Accession viewer https://www.ncbi.nlm.nih.gov/geo/query/acc.cgi?acc=GSE107641 (accessed Dec 4, 2020).

(310) Avsec, Ž.; Weilert, M.; Shrikumar, A.; Krueger, S.; Alexandari, A.; Dalal, K.; Fropf, R.; McAnany, C.; Gagneur, J.; Kundaje, A.; Zeitlinger, J. Deep Learning at Base-Resolution Reveals Cis-Regulatory Motif Syntax. *bioRxiv* **2020**, 737981. https://doi.org/10.1101/737981.

(311) GEO Accession viewer https://www.ncbi.nlm.nih.gov/geo/query/acc.cgi?acc=GSM4072779 (accessed Dec 4, 2020).

(312) Nintedanib: From Discovery to the Clinic | Journal of Medicinal Chemistry https://pubs.acs.org/doi/abs/10.1021/jm501562a (accessed Feb 11, 2020).

(313) Hilberg, F.; Roth, G. J.; Krssak, M.; Kautschitsch, S.; Sommergruber, W.; Tontsch-Grunt, U.; Garin-Chesa, P.; Bader, G.; Zoephel, A.; Quant, J. BIBF 1120: Triple Angiokinase Inhibitor with Sustained Receptor Blockade and Good Antitumor Efficacy. *Cancer Res.* **2008**, *68* (12), 4774–4782.

(314) Liu, Y.; Lu, F.; Kang, L.; Wang, Z.; Wang, Y. Pirfenidone Attenuates Bleomycin-Induced Pulmonary Fibrosis in Mice by Regulating Nrf2/Bach1 Equilibrium. *BMC Pulm. Med.* **2017**, *17*. https://doi.org/10.1186/s12890-017-0405-7.

(315) Ackermann, M.; Kim, Y. O.; Wagner, W. L.; Schuppan, D.; Valenzuela, C. D.; Mentzer, S. J.; Kreuz, S.; Stiller, D.; Wollin, L.; Konerding, M. A. Effects of Nintedanib on the Microvascular Architecture in a Lung Fibrosis Model. *Angiogenesis* **2017**, *20* (3), 359–372. https://doi.org/10.1007/s10456-017-9543-z.

(316) Hu, H.-H.; Chen, D.-Q.; Wang, Y.-N.; Feng, Y.-L.; Cao, G.; Vaziri, N. D.; Zhao, Y.-Y. New Insights into TGF-β/Smad Signaling in Tissue Fibrosis. *Chem. Biol. Interact.* **2018**, *292*, 76–83.

(317) Wu, C.-F.; Chiang, W.-C.; Lai, C.-F.; Chang, F.-C.; Chen, Y.-T.; Chou, Y.-H.; Wu, T.-H.; Linn, G. R.; Ling, H.; Wu, K.-D.; Tsai, T.-J.; Chen, Y.-M.; Duffield, J. S.; Lin, S.-L. Transforming Growth Factor β-1 Stimulates Profibrotic Epithelial

Signaling to Activate Pericyte-Myofibroblast Transition in Obstructive Kidney Fibrosis. *Am. J. Pathol.* **2013**, *182* (1), 118–131. https://doi.org/10.1016/j.ajpath.2012.09.009.

(318) Flanders, K. C.; Heger, C. D.; Conway, C.; Tang, B.; Sato, M.; Dengler, S. L.; Goldsmith, P. K.; Hewitt, S. M.; Wakefield, L. M. Brightfield Proximity Ligation Assay Reveals Both Canonical and Mixed Transforming Growth Factor-β/Bone Morphogenetic Protein Smad Signaling Complexes in Tissue Sections. *J. Histochem. Cytochem.* **2014**, *62* (12), 846–863. https://doi.org/10.1369/0022155414550163.

(319) Mendez, R.; Banerjee, S. Proximal Ligation Assay (PLA) on Lung Tissue and Cultured Macrophages to Demonstrate Protein-Protein Interaction. *Bio-Protoc.* **2017**, *7* (21). https://doi.org/10.21769/BioProtoc.2602.

(320) Ashcroft, T.; Simpson, J. M.; Timbrell, V. Simple Method of Estimating Severity of Pulmonary Fibrosis on a Numerical Scale. *J Clin Pathol* **1988**, *41*. https://doi.org/10.1136/jcp.41.4.467.

(321) Tammela, T.; Enholm, B.; Alitalo, K.; Paavonen, K. The Biology of Vascular Endothelial Growth Factors. *Cardiovasc. Res.* **2005**, *65* (3), 550–563. https://doi.org/10.1016/j.cardiores.2004.12.002.

(322) Olofsson, B.; Korpelainen, E.; Pepper, M. S.; Mandriota, S. J.; Aase, K.; Kumar, V.; Gunji, Y.; Jeltsch, M. M.; Shibuya, M.; Alitalo, K. Vascular Endothelial Growth Factor B (VEGF-B) Binds to VEGF Receptor-1 and Regulates Plasminogen Activator Activity in Endothelial Cells. *Proc. Natl. Acad. Sci.* **1998**, *95* (20), 11709–11714.

(323) Olofsson, B.; Pajusola, K.; Kaipainen, A.; Von Euler, G.; Joukov, V.; Saksela, O.; Orpana, A.; Pettersson, R. F.; Alitalo, K.; Eriksson, U. Vascular Endothelial Growth Factor B, a Novel Growth Factor for Endothelial Cells. *Proc. Natl. Acad. Sci.* **1996**, *93* (6), 2576–2581.

(324) Zhang, F.; Tang, Z.; Hou, X.; Lennartsson, J.; Li, Y.; Koch, A. W.; Scotney, P.; Lee, C.; Arjunan, P.; Dong, L.; Kumar, A.; Rissanen, T. T.; Wang, B.; Nagai, N.; Fons, P.; Fariss, R.; Zhang, Y.; Wawrousek, E.; Tansey, G.; Raber, J.; Fong, G.-H.; Ding, H.; Greenberg, D. A.; Becker, K. G.; Herbert, J.-M.; Nash, A.; Yla-Herttuala, S.; Cao, Y.; Watts, R. J.; Li, X. VEGF-B Is Dispensable for Blood Vessel Growth but Critical for Their Survival, and VEGF-B Targeting Inhibits Pathological Angiogenesis. *Proc. Natl. Acad. Sci. U. S. A.* **2009**, *106* (15), 6152–6157. https://doi.org/10.1073/pnas.0813061106.

(325) Yang, X.; Zhang, Y.; Hosaka, K.; Andersson, P.; Wang, J.; Tholander, F.; Cao, Z.; Morikawa, H.; Tegnér, J.; Yang, Y.; Iwamoto, H.; Lim, S.; Cao, Y. VEGF-B Promotes Cancer Metastasis through a VEGF-A–Independent Mechanism and Serves as a Marker of Poor Prognosis for Cancer Patients. *Proc. Natl. Acad. Sci. U. S. A.* **2015**, *112* (22), E2900–E2909. https://doi.org/10.1073/pnas.1503500112.

(326) Wietecha, M. S.; DiPietro, L. A. Therapeutic Approaches to the Regulation of Wound Angiogenesis. *Adv. Wound Care* **2013**, *2* (3), 81–86. https://doi.org/10.1089/wound.2011.0348.

(327) Corliss, B. A.; Mathews, C.; Doty, R.; Rohde, G.; Peirce, S. M. Methods to Label, Image, and Analyze the Complex Structural Architectures of Microvascular Networks. *Microcirculation* **2019**, *26* (5), e12520. https://doi.org/10.1111/micc.12520.

(328) Cai, J.; Kehoe, O.; Smith, G. M.; Hykin, P.; Boulton, M. E. The Angiopoietin/Tie-2 System Regulates Pericyte Survival and Recruitment in Diabetic Retinopathy. *Invest. Ophthalmol. Vis. Sci.* **2008**, *49* (5), 2163–2171. https://doi.org/10.1167/iovs.07-1206.